UNIVERSITY OF
BIRMINGHAM

The Role of Rheology in the Flow and Mixing of Complex Fluids

by

Sara Ghorbanian Farah Abadi

A thesis submitted to
The University of Birmingham
for the degree of
MASTER OF PHILOSOPHY

School of Chemical Engineering
College of Engineering and Physical Sciences
The University of Birmingham
November 2016

ABSTRACT

Mixing of fluids with complex rheology is encountered more and more frequently in industries. Nonetheless, mixing behaviour of such fluids is still poorly understood due to the complexity of their rheological behaviour. This study aims to enhance fundamental understanding of the flow and mixing of rheologically complex fluids such as thixotropic, shear-thinning and viscoelastic fluids. The objectives of this study were to investigate within stirred vessels the effects of thixotropy and viscoelasticity, separately, in the absence of other rheological behaviours for the fluids examined. To achieve these aims the rheological behaviour of the fluid examined is isolated by using a fluid that exhibits only one of these behaviours of interest at a time. The Particle Image Velocimetry (PIV) technique was employed to characterize the flow fields of fluids. The flow pattern, normalized mean velocity and cavern growth in the vessel were characterized during the mixing for both thixotropic and viscoelastic fluids. The results were compared to the reference fluids under laminar and transition regimes. Three different types of impeller were investigated: Rushton turbine (RTD), and Pitch Blade Turbine (PBT) in up pumping mode (PBTU) and in down pumping mode (PBTD). Additional work was conducted using th Planar Laser Induced Fluorescence (PLIF) visualization technique to investigate in more detail the evolution of mixing in a cavern with time for a thixotropic fluid. The mixing efficiency of the impellers was analyzed in terms of impeller pumping efficiency and size and growth of a cavern.

Dedicated To My Beloved Parents

ACKNOWLEDGEMENTS

Firstly, I would like to thank my supervisor Professor M. Barigou for his guidance during the course of my research. I would like to express my gratitude towards Professor Mark Simmons for valuable advice and support throughout this work.

I would like to thank the following people: Dr. Andreas Tsoligkas for his first training with PIV experiments, and Dr. Federico Alberini for his guidance in using PIV and PLIF techniques; Dr. Asja Portsch, Dr. Taghi Miri, and Dr. James Bowen for the introduction and advice on using a Rheometer; Dr. Hamed Rowshandel for his valuable advice in Matlab, and Dr. Halina Murasiewicz and Dr.Artur Majewski for their generous support through this research.

In addition, I would like to express my appreciation, for their valuable help concerning the experimental setup, to David Boylin, Thomas Eddleston and Steven Williams from the workshop team.

I would also like to thank all the great people from the General Office, especially Lynn Draper, for their friendship and continuous support. I want to thank Zainab Alsharify, Shahad Al-Najjar Dr. Li Liu for their friendship and support.

I have to also thank the student services team, especially Julie Kendall and Laura Salkeld, for their understanding and support.

Last but not least, I would like to thank my family: my beloved parents, lovely sister, supportive brother, and sweet grandmother for their encouragement and infinite understanding and support. I have to also thank my husband for his understanding and supports.

TABLE OF CONTENTS

Chapter 1: INTRODUCTION 1
1.1 Motivation 1
1.2 Objectives 3
1.3 Thesis layout 4

Chapter 2: LITERATURE REVIEW 5
2.1 Mixing Systems 5
2.1.1 Mechanically Agitated Vessels 6
2.1.2 Flow Regime 7
2.1.2.1 Laminar and Transitional Flow Regimes 9
2.1.2.2 Turbulent Regime 11
2.1.3 Impeller selection and resulting flow patterns 12
2.1.4 Unconventional Geometry 18
2.1.5 Mixing Times 19
2.2 Fluid Rheology 21
2.1.1 Newtonian and non-Newtonian Fluids 21
2.2.1 Viscoelastic Fluid 23
2.2.2 Viscoplastic Fluid 26
2.1.2 Thixotropic Fluid 28
2.3 Visualization Techniques 30
2.3.1 Hot Wire Anemometry (HWA) 31
2.3.2 Laser Doppler Velocimetry/Anemometry (LDV/A) 32
2.3.3 Planar laser Induced Fluorescence (PLIF) 34
2.3.4 Particle Image Velocimetry (PIV) 35
2.3.5 Positron Emission Particle Tracking (PEPT) 37

Chapter 3: EXPERIMENTAL TECHNIQUE AND THEORETICAL ANALYSIS 40
3.1 Apparatus 40
3.2 Particle Image Velocimetry (PIV) 43
3.3 Planar Laser Induced Fluorescence (PLIF) 45
3.4 Flow Number 47

Chapter 4: EFFECT OF THIXOTROPY ON FLUID MIXING IN A STIRRED TANK 50
4.1 Introduction 51
4.2 Material and Experimental Design 53
4.2.1 Rheology of Test Fluids 53
4.2.1.1 Time Dependent Fluids (Thixotropy) 53
4.2.1.2 Time Independent Fluids 54
4.2.2 Rheology Results 54
4.2.2.1 Hysteresis Loop Test 56
4.2.2.2 Steady State Shear Viscosity 57
4.2.3 Experimental Design 61
4.2.4 Experimental Techniques 61

4.3 Results and Discussion 62
4.3.1 Flow Fields 63
4.3.1.1 *Re* = 158 63
4.3.1.2 *Re* = 61 72
4.3.1.3 *Re* = 7 72
4.3.2 Cavern Growth 76
4.3.3 Effect of Non-standard Configurations 80
4.3.3.1 Un-baffled Vessel 80
4.3.3.2 Off-bottom Clearance Effects 89
4.4 Conclusions 94

Chapter 5: THE EFFECT OF VISCOELASTICITY IN A STIRRED TANK 97
5.1 Introduction 97
5.2 Rheology and Material Characterization 100
5.2.1 Test fluids 100
5.2.1.1 Viscoelastic Fluid (Boger Fluid) 100
5.2.1.2 Newtonian Fluid 101
5.2.1.3 Shear-thinning Inelastic Fluid 101
5.2.2 Rheology of Test Fluids 102
5.3 Experimental Setup 108
5.4 Results and Discussion 108
5.4.1 Newtonian Fluid (N93, N95) 109
5.4.1.1 *Re* = 80 109
5.4.1.2 *Re* = 45 113
5.4.1.3 *Re* = 7 114
5.4.1.4 Shear-thinning Inelastic Fluid 115
5.4.2 Low viscoelastic Boger Fluids (100PAA) 116
5.4.2.1 RTD Configuration 116
5.4.2.2 PBTU Configuration 119
5.4.2.3 PBTD Configuration 122
5.4.3 High viscoelastic Boger Fluid (300PAA) 123
5.4.4 Pseudo-Caverns 128
5.4.5 Conclusions 129

Chapter 6: CONCLUSIONS AND FUTURE WORK 131
6.1 Conclusions 131
6.2 Future work 133

REFERENCES 135

LIST OF FIGURES

Figure 2.1. Schematic representation of a typical mechanically agitated vessel (Edwards et al., 1997).....7

Figure 2.2. Typical predicted 2D flow patterns for a fully baffled vessel with (a) axial flow and (b) radial flow impeller (Edwards et al., 1997).....13

Figure 2.3. Schematic illustration of 2D flow patterns around a radial flow impeller in a viscoelastic fluid, (a) low EI, (b) intermediate EI, (c) high EI (Özcan-Taskin and Nienow, 1995) 15

Figure 2.4. (a) Three-blade propeller, (b) Six-blade disc turbine, (c) Simple paddle, (d) Anchor impeller and (e) Helical ribbon (Edwards et al., 1997).....17

Figure 2.5. Mixing time measurement (Edwards et al., 1997).....20

Figure 2.6. Rheological properties of Newtonian and non-Newtonian fluids (Paul et al., 2004) 22

Figure 2.7. Stress components around a rotating coaxial cylinder (Özcan-Taskin, 1993) 24

Figure 2.8. Breakdown of a 3D thixotropic structure (Barnes, 1997).....30

Figure 2.9. A typical LDV experimental set up, 1: laser; 2: fiber-optical module; 3: transmitting/receiving optics; 4: stirred vessel; 5: photomultipliers; 6: flow velocity analyser; 7: oscilloscope; 8: computer; 9: intersection of the two laser beams (Guida, 2010) 32

Figure 2.10. Simplified PLIF experimental facility. 35

Figure 2.11. Simplified, typical PIV set-up, Image taken from (Guida, 2010).....36

Figure 2.12. Schematic illustration of a PEPT experimental set-up showing positron annihilation and γ-ray detection by the PEPT camera, Image taken from (Guida, 2010) 38

Figure 3.1. The layout of the stirred vessel configurations, equipped with impeller, as used in this work. (a) baffled, (b) un-baffled. 41

Figure 3.2. Impeller geometries used in the experiments, a) PBT, b) RTD.....42

Figure 3.3. Schematic of various off-bottom clearance configurations studied in this work 43

Figure 3.4. Experimental setup for PIV measurements 44

Figure 3.5. Pixel greyscale versus tracer concentration.....46

Figure 3.6. Experiment setup for PLIF experiments.....46

Figure 3.7. Schematic diagram of flow rates for PBTD impeller taken from (Guida et al., 2010). 48

Figure 4.1. 2.2*w*% Laponite fluid under application of shearing followed by a recoveryperiod for three different shear rates…….. 55

Figure 4.2. Viscosity curve overlap in test runs. 56

Figure 4.3. (a) Full shear ramp experiment of 2.2*w*% Laponite fluid (six ramps),.....58

Figure 4.4. Schematic of steady shear flow tests; (a) few constant shear stress applied to the thixotropic fluid (b) response of shear rate at constant shear stress over a time of experiments. 59

Figure 4.5. Flow curves corresponding to different shearing times of 2.2*w*% Laponite. 59

Figure 4.6. Flow curve of 1*w*% Carbopol fluid at different shearing times.....60

Figure 4.7. The contour of normalized velocity magnitude of three impellers for 2.2*w*% Laponite at *Re* = 158. 65

Figure 4.8. Velocity vector on an axial-radial plane for a two flow regime at *Re* = 61 and *Re*=158 for both fluids mixed by the PBTD impeller. 66

Figure 4.9. The contour of normalized magnitude velocity for the three impellers at...68

Figure 4.10. Velocity vector on an axial-radial plane for two flow regimes *Re* = 61, *Re* =158 for both fluids mixed with the PBTU impeller. 69

Figure 4.11. Contour of shear strain rate plot for 2.2*w*% Laponite (at t_1 and t_3) and 1*w*% Carbopol fluid. 71

Figure 4.12. The contour of normalized magnitude velocity for three impellers for 2.2*w*% Laponite at *Re* = 61. 73

Figure 4.13. (a) Normalized magnitude velocity for three impellers at *Re*= 7 for 2.2*w*% Laponite fluid at t_3, (b) velocity field for three impellers at *Re* = 7 for 2.2*w*% Laponite fluid at t_3. 75

Figure 4.14. The changes of normalized cavern area % for the thixotropic fluid as a function of time for (a) *Re*= 158 and (b) *Re* = 61. 76

Figure 4.15. The cavern height and radius growth as a function of time for the thixotropic fluid at (a) *Re* =158, (b) *Re* = 61. 77

Figure 4.16. Schematic diagram of cavern growth while mixing for 2.2*w*% Laponite and 1*w*% Carbopol at *Re* = 61. 78

Figure 4.17. The cavern growth from PLIF experiments for both 1*w*% Carbopol and 2.2*w*% Laponite fluid at *Re* = 7..... 79

Figure 4.18. Variation of Power number as a function of Reynold number for viscoplastic fluid in the (a) baffled vessel and (b) un-baffled vessel. Image adopted from Hirata and Aoshima (1996)..... 81

Figure 4.19. The cavern shape and size for the thixotropic and viscoplastic fluids in the baffled and un-baffled vessel at *Re* = 158. 82

Figure 4.20. The contour of normalized magnitude velocity of three impellers at *Re* = 61 for 1 *w*% Carbopol. 84

Figure 4.21. The Normalized mean velocity component (radial and axial) at two axial positions for 1*w*% Carbopol and 2.2*w*% Laponite at *Re* =158 in a baffled and un-baffled tank. 85

Figure 4.22. The normalized mean velocity component (radial and axial) at three horizontal positions for 1*w*% Carbopol and 2.2*w*% Laponite at *Re* = 158 in a baffled and un-baffled tank. 86

Figure 4.23. The cavern size growth ratio for the thixotropic fluid during mixing in the baffled and un-baffled vessel at *Re* =158. 87

Figure 4.24. The contour of normalized magnitude velocity for three impellers at 88

Figure 4.25. The contour of normalized velocity magnitude plot of 2.2*w*% Laponite at t_3 and 1*w*% Carbopol for the PBTD impeller at *Re* = 158 and for four off bottom impeller clearances. 91

Figure 4.26. The contour of normalized magnitude velocity plot of 2.2*w*% Laponite at t_3 and 1*w*% Carbopol for the PBTU impeller at *Re*=158 and for four off bottom impeller clearances. 92

Figure 4.27. The cavern size growth ratio for 2.2*w*% Laponite as a function of time for four impeller clearance positions. 93

Figure 5.1. Steady shear properties for all tests fluids a), viscosity versus shear rate and b) shear stress versus shear rate. 104

Figure 5.2. First normal stress difference N_1 (Pa) of viscoelastic fluids as a function of shear rate (s^{-1}).....106

Figure 5.3. The contour of normalized velocity magnitude of three impellers for the Newtonian fluid N93, at three flow regimes: *Re* = 80, *Re* = 45, *Re* = 7 111

Figure 5.4. The contour of normalized velocity magnitude of three impellers for the Newtonian fluid N95, at three flow regimes: *Re* = 80, *Re* = 45, *Re* = 7. 112

Figure 5.5. The contour of normalized velocity magnitude of three impellers for the shear-thinning fluid 1.5*w*% CMC, at three flow regimes: *Re* = 80, *Re* = 45, *Re* = 7....117

Figure 5.6. a)The contour of normalized velocity magnitude and b) the streamline plots of the viscoelastic Boger fluid 100PAA for three impeller types at *Re* = 80.....118

Figure 5.7. Flow pattern observation for the RDT impeller in a baffled vessel: (a) low (*El*), (b) intermediate (*El*) and appearance of secondary reverse flow (1), (c) high *(El*). 119

Figure 5.8. Flow pattern observation for the PBTU impeller in a baffled vessel a) Newtonian fluid b) viscoelastic fluid with high (*El*), c) viscoelastic fluid with intermediate (*El*) : Note the reverse flow field in (1), the appearance of secondary counter-rotating ring vortex in (2), and the secondary reverse flow in (3). 120

Figure 5.9. a) The contour of normalized velocity magnitude and b) the streamline plot of three impellers for the viscoelastic Boger fluid 100PAA at *Re* = 45.....121

Figure 5.10. Flow pattern observation for the PBTD impeller in a baffled vessel: a) Newtonian fluid, b) viscoelastic fluid with low (*El*), c) viscoelastic fluid with intermediate (*El*), d) viscoelastic fluid with high (*El*); Note the reverse flow field in (1), the appearance of a secondary counter-rotating ring vortex in (2) and the growth of a secondary ring vortex in (3) 122

Figure 5.11. a)The contour of normalized velocity magnitude and b) the streamline plot of the three impellers for the viscoelastic Boger fluid 100PAA at *Re* = 7 124

Figure 5.12. The Contour of normalized velocity magnitude of three impellers for the 300PAA Boger fluid, at three flow regimes: *Re* = 80, *Re* = 45, *Re* = 7. 125

Figure 5.13. The streamline plots for all test fluids used in this study at *Re* = 80 under three impeller configurations. 126

Figure 5.14. The streamline plots for all test fluids used in this study at *Re* = 45 under three impeller configurations. 127

Figure 5.15. Pseudo-cavern boundaries for different impellers at three flow regimes: *Re* = 7, *Re* = 45, and *Re* = 80. 129

LIST OF TABLES

Table 2.1: Viscosity and speed relationship with impeller type. 16

Table 3.1. Dimensions of impellers used in experiments 42

Table 4.1. Rheology parameter of Herschel–Bulkley model for different shearing times during experiment 2.2*w*% Laponite fluid 60

Table 4.2. Different configurations used in this study; B: baffled vessel, U: un-baffled vessel 61

Table 4.3. Characterized parameters of flow for the PBTD impeller. 64

Table 4.4. Characterized parameters of flow for PBTU impeller. 67

Table 4.5.Characterized parameter of flow for RTD impeller. 67

Table 4.6. Characterized parameters of flow for thixotropic fluid in the un-baffled vessel. 82

Table 5.1: Composition and density of test fluids used 101

Table 5.2: Rheological properties of fluids used in the experiments. 105

Table 5.3: Dimensionless numbers over the range of impeller speed for the viscoelastic fluids used in the experiments. 107

Table 5.4: All experimental configurations and setup used in this study. 108

Table 5.5. Characteristic parameters of flow for the Newtonian fluid N93. 110

Table 5.6. Characteristic parameters of flow for the Newtonian fluid N95. 113

Table 5.7. Characterized parameter of flow for shear-thinning fluid 1.5*w*% CMC 115

Table 5.8. Ratio of pseudo-cavern area to tank area (A_C/A_T) % for the test fluids N93 and 100PAA 128

NOMENCLATURE

D	Impeller diameter	m
H	Vessel fill height	m
B	width of wall baffles	m
C	Off-bottom clearance	m
T	Diameter of vessel	m
N	Impeller rotational speed	s^{-1}
M	Image magnification	μm /pixel
Q	Impeller pumping rate	$m^3\ s^{-1}$
Q_a	Axial impeller pumping rate	$m^3\ s^{-1}$
Q_r	Radial pumping rate	$m^3\ s^{-1}$
L	characteristic length	m
L_{IA}	The length of the integration area	m
r	Radial distance	m
z	Axial distance	m
k_s	Metzner and Otto constant	-
k	Consistency index	$Pa\ s^n$
n	Flow behavior index	-
N_1	First normal stress difference	Pa
N_2	Second normal stress difference	Pa
A	Constant value	-
b	Constant value	-

u_{tip}	Impeller tip velocity	m s^{-1}
u_{rz}	mean radial axial velocity	m s^{-1}
u	The radial velocity component	m s^{-1}
v	The axial velocity component	m s^{-1}
A_C	Cavern area	m^2
A_T	Tank area	m^2
t	Time	s
d_f	Fringe spacing	M
f_D	Doppler frequency	Hz
v	Kinematic viscosity	m^2 s^{-1}

Greek symbols

μ	Viscosity	Pa s
μ_a	Apparent Viscosity	Pa s
η_B	Plastic viscosity	Pa s
ρ	Density	kgm^{-3}
τ	Shear Stress, N/m^2	Pa
$\dot{\gamma}$	Shear rate	s^{-1}
τ_y	Fluid yield stress	Pa
x y z	Cartesian coordinates	m
λ	Wavelength	m
ϑ	Azimuthal coordinate	rad
ψ	Normal stress difference coefficient	Pa s^2
Ø	Angle	°

Dimensionless Numbers

Re	Reynolds number

Re_{imp}	Impeller Reynolds number
Re_{PL}	Reynold number/ Power low model
Re_{HB}	Reynold number/Herschel-Bulkley
El	Elasticity number
Wi	Weissenberg number
Fl	Flow number

Abbreviations

PBT	Pitched blade turbine
PBTD	Down-pumping PBT
PBTU	Up-pumping PBT
RTD	Ruston disc turbine
PEPT	Positron emission particle tracking
PIV	Particle image velocimetry
PLIF	Planar laser induced fluorescence
LDV	Laser Doppler velocimetry

Chapter 1

INTRODUCTION

1.1 Motivation

The mixing of fluids in stirred vessels is by far one of the most common processes encountered throughout the industry in many different processes. Correct mixing is needed to ensure homogeneity of materials so as to achieve the desired product. Improving mixing efficiency plays a major role in attaining high-quality product in the industry.

Mixing of fluids with complex rheology is being incorporated more and more frequently in various industrial processes, such as in fermentation, pharmaceuticals, polymerization, personal and home care products and food products. However, an understanding of the mixing behaviour of such fluids is lacking (Collias and Prud'homme, 1985). The rheological complexities of non-Newtonian fluids can cause a plethora of difficulties in mixing. Shear-thinning liquids, for example, display different behaviour compared to Newtonian liquids during mixing, as increase in shear rate leads to significant decrease in viscosity. In addtion, for shear-thinning liquids different viscosities can be observed in various parts of the mixing vessel, so it is hard to set up the right operating conditions and equipment to maximize the mixing efficiency. The exact opposite behaviour is displayed by shear thickening fluids; the viscosity will be higher once the shear rate is increased. During the mixing of non-Newtonian fluids with a yield stress a cavern is formed, which is the region around the impeller where shear stresses are high.and hence the fluid is mobile. Oustside the cavern, in area away from impeller, shear stresses are small and as

such the liquid is stagnant. A pseudo-cavern can be observed in the case of mixing shear-thinning fluids or highly viscous Newtonian fluids. In the case of the pseudo-cavern the fluid beyond the cavern boundaries is in motion, however the velocities are small. An extensive investigation into the formation of caverns and pseudo-caverns developed during mixing of non-Newtonian fluids was done by Adams and Barigou (2007).

Furthermore, Thixotropy is one of the challenging rheological phenomena in non-Newtonian fluid science. Thixotropic fluids have extensive applications in natural systems but also in industry, with mixing of such fluids being widely used in the food, polymer and pharmaceutical industries. Nonetheless, thixotropy is still poorly understood due to the complexity of the microstructure of thixotropic fluids. Such fluids show a decrease in viscosity over time for a continuously applied shear stress, often with yield stress. Mixing of complex fluids with shear-thinning time dependency and yield stress is challenged in the mixing industry.

The mixing of viscoelastic fluids is commonly carried out in stirred tanks in many industrial processes. Viscoelastic fluids show varying flow patterns under different mixing conditions, often climbing the rotating shaft due to normal forces, and also affecting the power drawn (Collias and Prud'homme, 1985). Such fluids display other complex rheological properties, for example shear thinning behaviour. This behavior has been studied in the literature extensively however, the effect of viscoelasticity in a stirred vessel has not been properly addressed, due to the difficulty encountered in separating the effects of viscoelasticity from other rheological properties, and as such it is still poorly understood.

As such the motivation for this work came from the need for a better understanding of the role of non-Newtonian fluid behavior, especially thixotropy and viscoelasticity on fluid mixing in a stirred vessel.

1.2 Objectives

The objectives of this study are:

- This project aims to enhance fundamental understanding of a number of issues concerned with the flow and mixing of rheologically complex fluids, in particular the impact of different rheological behaviors on the fluid dynamics and mixing in stirred vessels.
- Ordinary fluids exhibit a combination of rheological behaviors, e.g. shear-thinning, elasticity, yield stress, thixotropy etc. The aim of this project is to try and isolate rheological behaviors one at a time by using model fluids that exhibit only one of these behaviors each time. As such, the effects of each rheological behavior can be separately studied and identified. Boger Fluid, one of the formulated fluids of this study, was used to investigate the effect of viscoelasticity in a stirred tank for it exhibits viscoelasticity in the absence of other complex rheological behaviors.
- Transparent, formulated fluids underwent classic characterization techniques such as rheology, and also new flow visualization techniques such as Particle Image Velocimetry (PIV) and Planar Laser Induced Fluorescence (PLIF) so as to improved scientific understanding of mixing of complex fluids in a stirred vessel.

1.3 Thesis layout

Following the current Introduction Chapter is a comprehensive review of existing literature on different aspects of single-phase fluid mixing in stirred tanks, an introduction to fluid rheology and non-Newtonian fluid behavior and a review of the existing flow visualization techniques, as presented in Chapter 2. The experimental procedures, experimental techniques and equipment used, and the theory for analysis of PIV data are given in Chapter 3.

Chapters 4 and 5 are results chapters. Details of materials, fluid rheology results and the experimental procedures are given in each of these chapters. Chapter 4 presents results regarding the effect of thixotropy on fluid mixing. Results for a thixotropic fluid are obtained from PIV and PLIF techniques and are discussed and compared with those of a time-independent fluid. A full study of thixotropic rheology is presented in this chapter. In addition, viscoplastic fluid behavior is similarly investigated. Subsequently, Chapter 5 explores the mixing of a viscoelastic fluid via use of PIV. The behaviour of a viscoelastic fluid during mixing is compared with that of a shear-thinning fluid and a Newtonian fluid. Please note that the test fluids rheology and results are discussed separately in each results chapter, in order to clarify ideology of fluid rheology behavior used in each chapter.

Finally, the conclusions from this work and suggestions for future work are presented in Chapter 6.

Notation and References sections that are used in each chapter have been grouped and are presented at the end of the thesis.

Chapter 2

LITERATURE REVIEW

Mixing operations are one of the most commonly employed processes in several industries, such as the pharmaceuticals, chemicals, food processing and mineral. In such industrial settings fluid mixing can take place in a range of different types of equipment. These include in-line static mixers, rotor-stator mixers and mechanically agitated vessels. Amongst the wide variety of mixers, mechanically agitated vessels have been considered to be the most commonly used mixing devices. The goal is to achieve a desired process result for the fluid mixed system, and ensure reduction of inhomogeneity and non-uniformity in the system. The process fluid used in mixing operations may exist either in a single phase or in multiple phases. Understanding mixing of complex fluids may be very tedious, as their complex rheological behaviour makes it very difficult to understand the results of their mixing studies. In addition, not much work has been done to understand the mixing behaviour of such fluids. This chapter provides a general description of the mixing phenomena along with describing flow regimes, flow patterns and several geometrical parameters. This review also focuses on the different fluid rheologies of non-Newtonian fluids, namely viscoelastic, shear-thinning and thixotropic fluids. Finally, a critical analysis of the different experimental techniques relevant to this work is provided.

2.1 Mixing Systems

Mixing is commonly defined as the reduction of inhomogeneity in order to achieve a desired process result. It plays a key role in a range of industries varying from fine chemicals and petrochemicals to food and biotechnology (Paul et al., 2004). Mixing

operations are generally classed depending upon the type of process materials. Examples of some commonly used process materials include viscous liquids, solid-liquid and gas-liquid systems. Based on the extensive research done within the field of chemical engineering, it is certain that the solid-liquid mixing process is the most commonly used and as such the most important one.

An enormous range of mixing equipment is currently commercially available, indicating to the wide range of mixing requirements typically needed in the chemical processing industry. To perform chemical mixing operations, numerous distinct types of mixers have been utilized. However, the most commonly reviewed mixers are the mechanically agitated vessels (Edwards et al., 1997).

2.1.1 Mechanically Agitated Vessels

Mechanically agitated vessels are the most common mixing equipment used in the chemical, pharmaceutical and pulp and paper industries. More than 50% of the world's chemical processes involve the use of mechanically agitated vessels for the production of high added value products (Paul et al., 2004). These vessels are used in the processing industry for blending miscible liquids, achieving gas dispersion or solid suspension in a liquid, and for carrying out efficient optimization of chemical reactions.

Figure 2.1 below is a simplified schematic representation of a typical mechanically agitated vessel. This figure serves to demonstrate the overall configuration and the main features of a baffled vessel, comprising of four baffles, a centrally located impeller shaft and an impeller. Energy transfer from the rotating impeller to the process fluid promotes fluid motion.

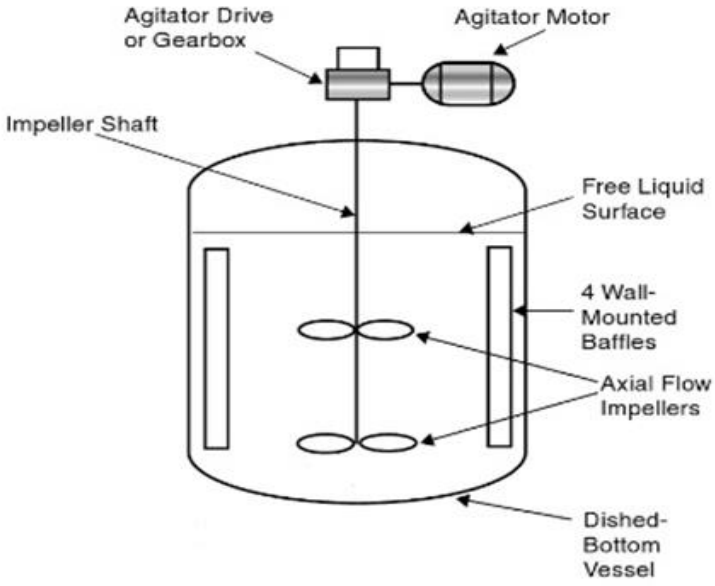

Figure 2.1. Schematic representation of a typical mechanically agitated vessel (Edwards et al., 1997)

The process fluid may exist as either a single phase or a multiple phase system. Examples of single phase fluids include viscous, Newtonian and Non-Newtonian materials, whereas examples of multiple phase fluids include two phase flows such as gas-liquid and solid-liquid systems. In some cases the presence of more than one phase can necessitate the treatment of interphase transfers of momentum and energy. Physical changes may also occur during the flow of water and steam or in processes leading to suspension and polymerisation (Thyagaraja et al., 1987).

2.1.2 Flow Regime

In fluid mechanics, the Reynolds number, *Re*, is extremely useful in characterizing fluid flows and describing fluid mixing. *Re* is a dimensionless number which gives a measure of the ratio of inertial forces to viscous forces and is traditionally defined as:

$$Re = \frac{\rho u L}{\mu} = \frac{u L}{v} \quad (1)$$

where u is the mean fluid velocity.

For mixing studies in stirred vessels, the impeller Reynolds number is denoted as Re_{imp} and is defined as:

$$Re_{imp} = \frac{\rho N D^2}{\mu} \tag{2}$$

The impeller Reynolds number is generally useful in characterising different flow regimes in mechanically agitated vessels. When $Re_{imp} < 10$ the fluid flow is in laminar regime, whereas when $Re_{imp} > 10^4$ the fluid flow is in turbulent regime. The transitional region lies between 10 to10^4 Re_{imp}. It is feasible and quite useful to describe mixing mechanisms under laminar or turbulent flow conditions, as they have evident differences (Edwards et al., 1997).

As Non-Newtonian fluids shear-thinning materials by definition do not have a constant viscosity, with their viscosity dropping as shear rate is increased. To represent the rheological behaviour of these non-Newtonian materials, the best approach is to use the power law model, shown below:

$$\tau = k\dot{\gamma}^n \tag{3}$$

The consistency factor provides a measure of fluid thickness while the flow behaviour index measures the strength of non-Newtonian fluid. The value of the flow behaviour index, n, for shear-thinning fluids lies between 0 and 1, being 1 for Newtonian fluids. Equation 3 cannot be used to describe non-Newtonian fluids as the viscosity of these materials is not constant. Therefore, the Metzner and Otto correlation needs to be applied in order to calculate the average shear rate which, in turn, can help in calculating the Reynolds number by the power law model as shown below:

$$Re_{PL} = \frac{\rho N^{2-n} D^2}{k k_s^{n-1}} \quad (4)$$

where k_s is the Metzner and Otto constant, and its value is dependent on the impeller type. For example, for a pitched blade turbine the k_s value is between 11 and 13 (Metzner and Otto, 1957).

Another type of non-Newtonian behaviour is shown by shear thickening materials, which behave in the opposite manner to shear-thinning fluids in that for shear thickening materials the viscosity increases with increase in the shear rate. Their rheological behaviour can also be represented by the power law model (Equation. 3), whereby the flow behaviour index being above unity. This is further discussed in section 2.2.3.

2.1.2.1 Laminar and Transitional Flow Regimes

Laminar regimes are mainly associated with high viscosity fluids. For a flow to be completely laminar at typical rates of energy input, the value of viscosity must be large enough to result in impeller Reynolds number less than 10. However, for fluids with such high viscosity values, the fluid rheology is often very complex.

Laminar or transitional regimes usually predominate in cases where efficient mixing of high viscosity fluids is difficult to achieve. Examples of such high viscosity fluids include pastes, creams and paints. Inertial forces reduce due to the action of high viscosities in laminar conditions. Therefore, to achieve adequate bulk motion, it is important for the rotating impellers to occupy a significant area of the vessel (Edwards et al., 1997). Large velocity gradients exist in the vicinity of these rotating impellers. These are known as laminar regions, with high shear rates capable of deforming and stretching fluid elements. Specifically, upon continuous shearing these fluid elements are thinned, elongated and

folded. Such mixing features are of high importance for mixing mechanisms in laminar flow regimes (Edwards et al., 1997; Alvarez et al., 2002; Zalc et al., 2001).

Non-Newtonian fluids are mainly high viscosity fluids and their complex fluid rheology causes their mixing features to be even more complicated. Such complications can arise from the fluid's viscosity dependence on shear time or its time dependent behaviour.

The power number, *Po* is a dimensionless variable that has been widely used as a function of the Reynolds number, $Re_{imp,}$ to evaluate mixing operations. The relationship between the two can be illustrated through a *Po* vs. Re_{imp} curve. Metzner et al (1961) discusses that for various types of impellers, the slope of this curve is found to be -1 in the laminar regime, however in the transitional regime *Po* and Re_{imp} have been found to have a complex relationship (Galindo and Nienow, 1992; Brito-de la Fuente et al., 1997; Aubin et al., 2000; Paul et al., 2004).

To summarise the above, it is evident that fluid mixing in stirred vessels possesses considerable complexity irrespective of flow regime. Fluid rheology has a major consequence on the flow patterns and mixing performances. As such, a good understanding of the rheological properties of all types of fluids can help in fluid mixing studies.

2.1.2.2 Turbulent Regime

In mixing vessels, fluid flow is classified as turbulent when the impeller Reynolds number should be higher than 10^4. The inertial force imparted by the rotating impeller is sufficient enough to circulate the fluid quickly throughout the vessel and back to the impeller again. In addition, during this circulation turbulent eddy diffusion takes place, leading to adequate mixing which is much more enhanced than mixing rates in laminar flows. In turbulent flow, numerous eddies of different length scales and intensities exist. The provoked motion of these turbulent eddies help in enhancing fluid mixing rates hence making the turbulent regime a desirable regime for efficient mixing in stirred vessels (Yianneskis et al, 1987). In laminar and transitional regions, lack of turbulent eddy dissipation causes less efficient mixing.

Wu and Patterson (1989) performed a study on mixing characteristics of viscous fluids and reported that the turbulence field in the turbulent regime exhibits three dimensional velocity fluctuations. Escudie and Line (2006) further explain the presence of anisotropic turbulence dissipations and periodic hydrodynamics exhibited by fluids under turbulent regimes. The strongest turbulent intensity is found close to the impeller as compared to other regions in a typical stirred vessel. Also, a large percentage of energy is dissipated close to the impeller region (Cutter, 1966), whereas fluctuations in turbulent trailing vortices are found behind the impeller blades (Yianneskis et al., 1987; Schäfer et al., 1998; Escudié et al., 2004).

The power number, *Po*, is found to be independent of the Reynolds number, Re_{imp}, in the turbulent regime (Metzner et al., 1961; Galindo and Nienow, 1992; Brito-de la Fuente et al., 1997; Aubin et al., 2000; Paul et al., 2004).

2.1.3 Impeller selection and resulting flow patterns

Flow patterns have been commonly studied as they characterize how well the system is mixed. In order to better understand the fluid mixing configuration, it is important to study and analyse the formation, shape and velocities of flow patterns. Literature reviews show that most of the work done has been performed on Newtonian fluids. This is because most non-Newtonian fluids are opaque and the commonly used visualisation techniques are optical, thus requiring transparent materials. In addition, as mentioned earlier, non-Newtonian materials have complex rheological properties (Maingonnat et al 2005).

As has been repeatedly reported in literature, flow patterns are highly dependent upon the type of impeller used in stirred vessels. Flow patterns help determine the existence of 'dead zones' in the vessel or whether all particles are suspended in the liquid. The two typical primary flow patterns that are formed in a baffled vessel with the standard configuration for a Newtonian fluid in the turbulent region are shown in **Figure 2.2**. An axial flow pattern for a propeller is shown in **Figure 2.2a**, while **Figure 2.2b** shows a radial flow pattern for a disc turbine. It is obvious that the velocities at any particular point will be unsteady and will show three dimensional characteristics (Edwards et al., 1997).

Presently, a wide range of impellers are used industrially, which can be simply categorised into three groups for use in a stirred vessel: radial impellers such as the Rushton Disc Turbine (RDT), axial impellers such as the marine propeller (MP) and mixed impellers such as the Pitched Blade Turbine (PBT). Briefly, RDT impellers discharge fluid radially towards the vessel walls, MP impellers discharge the fluid axially, upwards or downwards depending upon the direction of rotation and PBT impellers

consist of a blade pitch angle varying in the range of 10° to 90° from the horizontal plane, with 45° being the most commonly used.

Radial impellers are specifically used for gas dispersion due to their high shear characteristics. Mixed and axial impellers are generally used for inducing solid particle suspensions, due to their high pumping efficiencies (Lee and Yianneskis, 1998).

For a vessel with a radial flow pattern, the strong swirling flow is discharged rapidly from the impeller. This radial flow is then separated in two paths at the vessel walls. Four flow circulation loops - two below and two above the impeller plane - are formed. This flow pattern is usually recommended for gas dispersion and single phase operations. Radial flow impellers such as the 6-Blade, Rushton Disc Turbine (RDT) help form such flows. These impellers comprise of vertically straight or curved blades that are connected to a disc that prevents fluid pumping through the impeller.

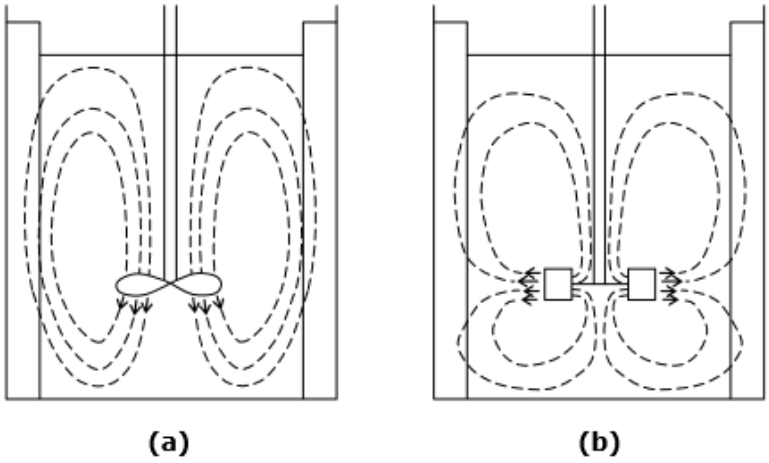

Figure 2.2. Typical predicted 2D flow patterns for a fully baffled vessel with (a) axial flow and (b) radial flow impeller (Edwards et al., 1997).

In an axial flow field the impellers move the fluid out in an axial direction. The fluid flow may be upwards or downwards, depending upon the rotation direction. The strong, downward discharge by the impeller is imposed on the vessel's bottom, after which it

rises along the vessel walls. This helps in adequate mixing by aiding in the suspension of solid particles. In axial flow two flow loops are formed, with the flow pumping through the impeller plane near the shaft.

Axial flow impellers make use of blades which are angled to the vertical plane and no disc is present such as in the case of the 6-Blade, Pitched Blade Turbine (PBT). Other typical examples of axial devices include marine propellers and hydrofoils. As mentioned above the flow pattern formed by an axial plane consists of a two loop structure, it the flow being either up-pumping or down-pumping. Up-pumping flow is increasingly popular for gas liquid operations and may also be applicable for solid-liquid systems. Down-pumping flow is applicable for use in suspending solids via utilization of the discharge near the shaft, which is assumed to help disperse the solids from the base of the vessel.

In general, power consumption and pumping effectiveness appear to be more favourable for a down-pumping PBT (Aubin et al., 2004). However, in terms of gas dispersion and energy dissipation, up-pumping PBT has been established to be very effective (Bujalski et al., 1990; Gabriele et al., 2009).

Mixed flow impellers are capable of discharging the flow in both axial and radial directions. Hall et al (2005b) and Chung (2008) have shown that mixed flows often occur for fluids with low to medium viscosities. They also found that for high transitional and turbulent regimes, the mixed flow generated by an up-pumping PBT (PBTU) resulted in a stronger lower circulation loop. However, if the impeller D/T ration is increased above 0.55, the PBTU becomes a radial flow impeller. This is due to prevailing centrifugal forces (Hemrajani and Tatterson, 2004).

This thesis focuses mainly on viscoelastic fluids, and as such **Figure 2.3** below shows the flow patterns generated around a radial flow impeller for a viscoelastic fluid.

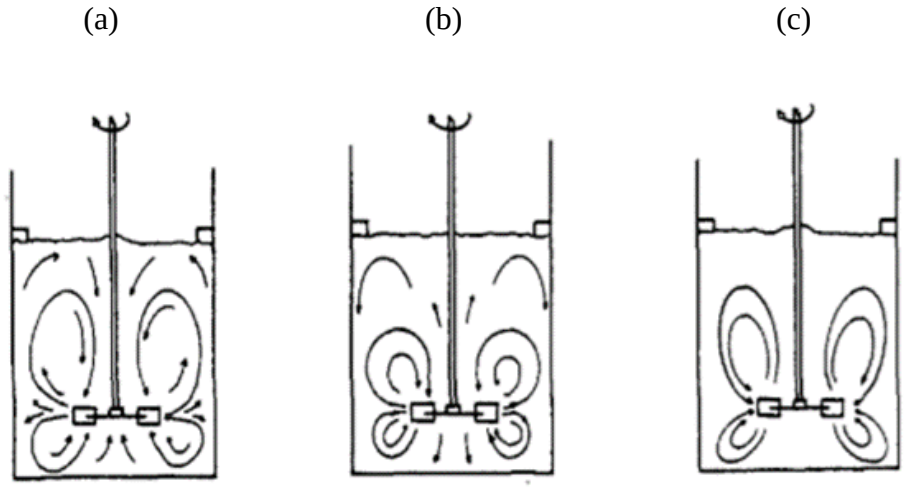

Figure 2.3. Schematic illustration of 2D flow patterns around a radial flow impeller in a viscoelastic fluid, (a) low EI, (b) intermediate EI, (c) high EI (Özcan-Taskin and Nienow, 1995)

Flow patterns of viscoelastic fluids are effected by the elasticity of the fluid. Flexural rigidity, EI, is defined as the ratio of elasticity of the fluid over fluid inertia. Three different flow patterns were generated for low to high EI, with couple flow reversal being observed for high EI values. It is extremely important to properly design and optimise mixing processes in order to comply with the standard safety operating procedures and prevent any possible hazards, and to meet process requirements. This immense need has encouraged numerous researchers to study the complex, local hydrodynamics inside stirred vessels. Consequently, several impeller designs have been developed which are often designed for a specific purpose (Zlokarnik, 2001).

Some of the commonly used impellers are shown in **Figure 2.4**. (a) Three-blade propeller, (b) Six-blade disc turbine, (c) Simple paddle, (d) Anchor impeller and (e) Helical ribbon

(Edwards et al., 1997).These are propellers, turbines, paddles, anchors, helical ribbons and screws. These impellers are usually attached to a central vertical shaft located inside a cylindrical vessel. The range of applications of each of these impellers depends greatly upon the fluid viscosity in the stirred vessel. Table 2.1 below summarizes the capacity of these different types of impeller. It can be seen that propellers, turbines and paddles are usually used in operations concerning the mixing of low viscosity fluids while operating at high rotational speeds (Edwards et al., 1997).

Other types of impellers, such as anchors, helical ribbon and helical screw are strong enough to be generally used for laminar mixing of very viscous materials. They can sweep the entire volume of the vessel and therefore operate at much slower speeds, depending upon their size and power consumption.

Peters and Smith (1962) have performed an in-depth study on the viscous flow in an anchor agitated vessel. Their study has shown that an anchor impeller is capable of promoting rapid fluid motion near the vessels walls but is unable to induce any motion near the shaft. Therefore, the liquid in the area near the shaft may be relatively stagnant.

Table 2.1.Viscosity and speed relationship with impeller type (Edwards et al., 1997)

Impeller	**Viscosity**		
Propeller	< 2kg/ms		
Turbine	< 50 kg/ms		
Paddle	< 1000 kg/ms		
Anchor	-		
Helical ribbon	-		
Helical screw	-		

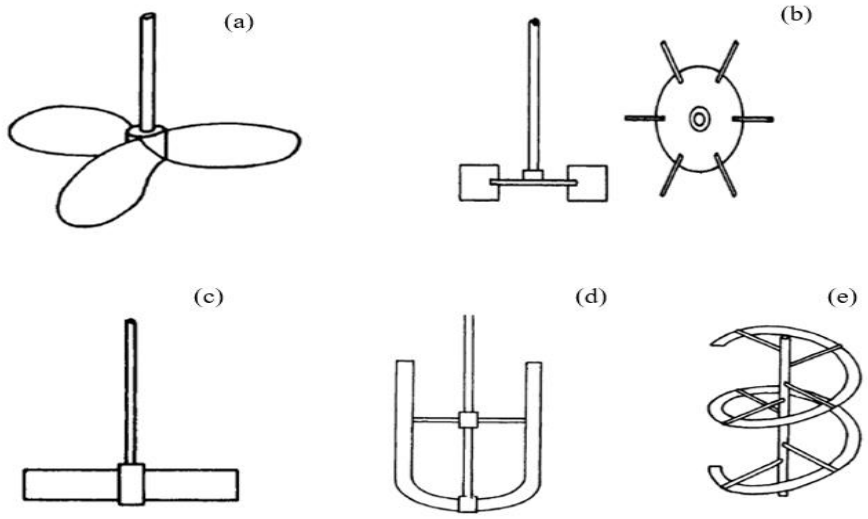

Figure 2.4. (a) Three-blade propeller, (b) Six-blade disc turbine, (c) Simple paddle, (d) Anchor impeller and (e) Helical ribbon (Edwards et al., 1997).

Moreover, there is less top-to-bottom turnover in an anchor agitated vessel. To overcome such an issue the use of a helical ribbon impeller and a helical screw together, has been proposed by Edwards et al (1997). These impellers can be added to the vertical shaft in order to also achieve fluid flow in the central regions of the vessel. This impeller combination of both helical ribbon and helical screw would mean that the ribbon would pump flow upwards near the vessel walls through the help of the screw, while the twisted portion of the ribbon helps in pumping the flow downwards near the shaft (Edwards et al., 1997).

The past few years have seen a rapid increase in numerous new impeller designs that have been introduced with significant developments and improvements. These have proven to result in excellent fluid turnover in mechanically agitated vessels at lower power consumptions. Such innovations can be valuable for performing mixing duties for moderate viscosity materials along with aiding in blending of viscous materials and ensuring adequate solid suspension.

2.1.4 Unconventional Geometry

In terms of vessel configuration, the shape of the vessel, impeller type and geometry play a crucial role in achieving several mixing operations. Impeller bottom clearance refers to the distance from the base of the vessel to the impeller central line. This parameter has been extensively studied as it has a significant effect on the mixing of various fluids. Studies revealed that a better flow pattern could be generated if the impeller position is moved from its standard point (i.e. T/3) to a higher position (T/2), where T is the tank diameter. This change can also induce larger fluid motion, allowing the fluid to sweep across the vessel volume and aiding in the mixing of highly viscous fluids (Jaworski et al., 1991; Kresta and Wood, 1993; Amannullah et al., 1997; Fangary et al., 2000; Ochieng et al., 2008; Ein-Mozaffari and Upreti, 2009). In contrast, some studies showed that placing the impeller in a lower position can result in more efficient operations for solid-liquid suspensions mixed with the RDT. This is due to the greater energy transfer to solid particles, allowing the RDT to elevate particles from the bottom of the vessel in the suspensions (Nienow, A. W., 1968; Armenante and Nagamine, 1998; Montante et al., 1999).

Additional studies have stated that geometrical parameters relating to the impeller, such as impeller diameter, blade width and thickness, and the number of impeller blades, have been reported to majorly affect fluid mixing operations (Rutherford et al., 1996; Prajapati and Ein-Mozaffari, 2009; Ein-Mozaffari and Upreti, 2009; Ameur et al., 2011; Ameur and Bouzit, 2012).

Baffled tanks have been more commonly used for fluid mixing as compared to unbaffled tanks. Baffles are employed in stirred vessels to break the solid body rotation which would

otherwise occur without them. Solid body rotation occurs where the fluid velocity field is dominated by a tangential swirling component moving with the impeller. To prevent poor mixing and the formation of a central vortex due to minimal interchange or eddying within the flow, it is recommended to use baffles in turbulent flow regimes. Baffles also promote fluid mixing in the axial direction. If baffles are not employed, most of the turbulent kinetic energy imparted by the impeller remains in the impeller region. Little mixing occurs elsewhere in the vessel, particularly near the top. Therefore, vortexing may also be observed (Paul et al., 2004).

Eccentric agitation can be used to improve mixing in stirred vessels if baffles cannot be used. In addition the impeller shaft can be moved away from the vessel axis, however this is not likely to work well in bigger tanks as there is extra strain on the shaft and motor bearings (Paul et al., 2004).

Unbaffled tanks are used in cases where mixing of highly viscous fluids is required and where vortexing seldom occurs. Baffles are also not employed when helical ribbon, helical screw and anchor impellers are used (Paul et al., 2004).

It is evident that the flow patterns of a fluid flow depend typically upon the impeller, vessel and baffle geometry along with fluid rheology. Therefore, understanding the effect of these geometrical parameters on mixing performances is extremely important. Finally, while designing stirred vessels, the designer must ensure to select the appropriate combination of equipment that will result in desirable flow patterns.

2.1.5 Mixing Times

Mixing time refers to the time it takes for a volume of fluid to achieve the same concentration in all regions of the vessel. To elaborate, mixing or blending times provide a measurement of the time required to achieve homogeneity within a vessel due to

convective mixing. Mixing times can also provide a measure of the non-ideality of a mixing system, since for an ideally perfect back-mixed system, the mixing time would equal to zero.

Figure 2.5 shows an illustration of a mixing time experiment where a stirred vessel contains a single-phase liquid, to which a volume of tracer particle is added. The mixing time here is represented as the time measured from the moment the tracer particle is added until all vessel contents have achieved a specific level of uniformity. At this stage the system is identified to be 'mixed'.

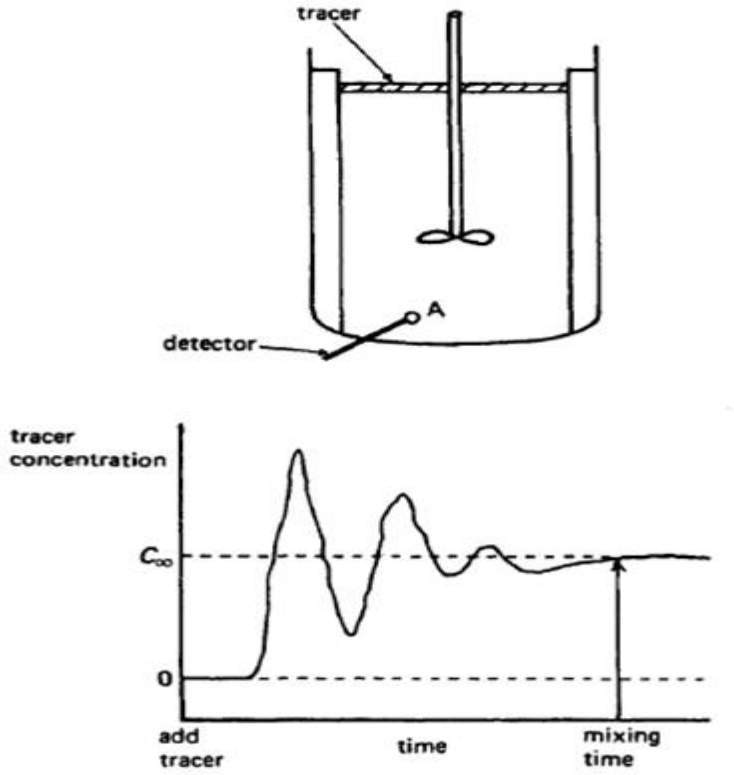

Figure 2.5. Mixing time measurement (Edwards et al., 1997)

Mixing time can also be used to monitor mixing quality and to check chemical reaction performances. Numerous techniques are available for the measurement of mixing time. Two of the most commonly used techniques are dye injection and acid-base colourization-decolourization (Cronin et al., 1994). Each of these techniques is capable

of providing accurate results for mixing time. They also allow for visual observation of the mixing flow patterns and indicate the position of any dead zones in the vessel. However, they cannot be used for industrial purposes as they are restricted to use in clear vessels. This can be overcome by using an image processing technique such as Planar Laser Induced Fluorescence (PLIF) (Chung et al., 2007; 2009) or by using the colorimetric method (Cabaret et al., 2007).

2.2 Fluid Rheology

Fluid rheology governs several factors in mixing within a stirred vessel, such as local hydrodynamics and phase distribution. Fluids can be described with a rheological model that would explain fluid deformation under applied forces. Rheology refers to the study of deformation and flow of matter at specified conditions.

This chapter aims to focus on fluid rheology of various fluids with different flow behaviour relevant to mixing processes and intends to briefly introduce the experimental aspects of the work of this thesis.

2.1.1 Newtonian and non-Newtonian Fluids

Fluids can be described as Newtonian or non-Newtonian. A fluid that has a constant viscosity at all shear rates under constant temperature and pressures, and can be described by a one-parameter rheological model is known as Newtonian fluid. As shown in **Figure 2.6**, a Newtonian material is characterised by a straight line through the origin of a shear stress against shear rate plot.

The rheological model for a Newtonian fluid is shown below:

$$\tau = \mu\dot{\gamma} \tag{5}$$

where μ is the viscosity of the Newtonian fluid and is also the constant proportionality factor.

This model also provides a definition for the fluid viscosity, the ratio of the shear stress to the shear rate. The Reynolds number for a Newtonian fluid in a stirred vessel is defined in section 2.1.2.

Fluids used in several industries such as food, oil and mining exhibit non-Newtonian rheological properties such as plasticity, elasticity, yield stress and thixotropy. Fluid mixing in stirred vessel becomes complex with an increase in a fluid's non-Newtonian behaviour. Non-Newtonian fluids with viscosities dependent on shear rate but independent of time are the most commonly used fluids in industry.

Non-Newtonian fluids can be generally characterized into three different categories (Skelland, 1967), based on fluid viscosity and shear rate: These categories are time independent fluids, time dependent fluids and viscoelastic fluids.

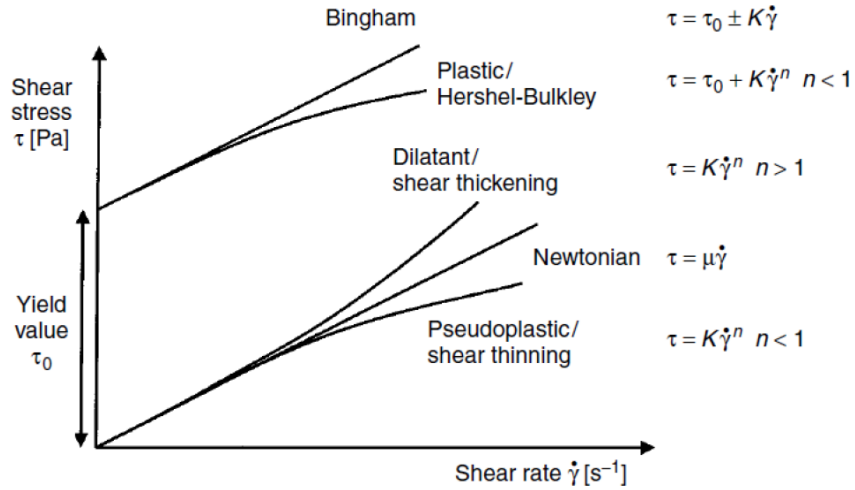

Figure 2.6. Rheological properties of non-Newtonian and Newtonian fluids (Paul et al., 2004)

Thixotropic, shear-thinning and viscoelastic fluids are most relevant to this thesis, therefore their rheological characteristics are discussed in more detail below.

2.2.1 Viscoelastic Fluid

Viscoelastic fluids are a common type of non-Newtonian fluid. They possess both, elastic solid and viscous fluid properties. Generally, Hookean and Newtonian materials show an immediate response upon stress or strain addition whereas viscoelastic materials do not respond immediately upon stress input. Viscoelastic fluids show slow partial elastic recovery upon removal of deforming shear stress. This behaviour is referred to as creep. Creep studies can be helpful in determining yield stresses of different materials. To do so, a series of creep and recovery tests could be carried out in incremental stress levels.

Usually, viscoelastic fluids are macromolecular in nature, comprising of materials of high molecular weight. Common viscoelastic fluids include polymeric fluids (melts and solutions) used for making plastic articles, food systems such as dough making for bread, and biological fluids such as synovial fluids found in joints (Baird, 2001).

Dynamic testing is generally feasible for measuring viscoelastic changes in fluids. Such tests are useful in providing an assessment of product applicability along with establishing causal relationships in problem solving efforts. Although the behaviour of viscoelastic fluids is rheologically complex, modern rheometers are capable of easily measuring viscoelastic responses.

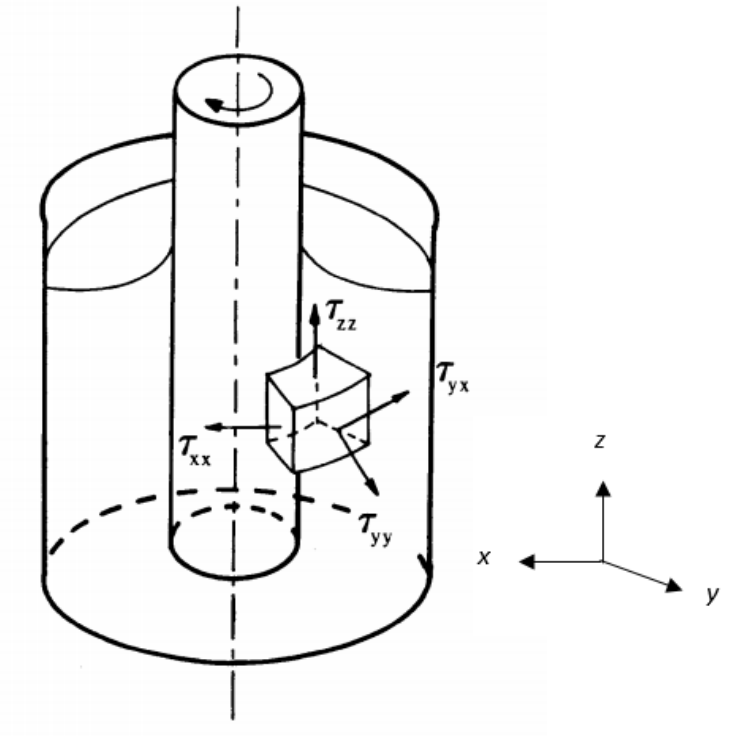

Figure 2.7. Stress components around a rotating coaxial cylinder (Özcan-Taskin, 1993)

Figure 2.7 shows the normal stresses generated under simple shear flow. These are, τ_{xx}, τ_{yy}, and τ_{zz}. The magnitude of these normal stresses is observed to vary with shear rate. A convenient way of analysing such systems is to work in terms of normal stress differences, as shown below:

$$\tau_{xx} - \tau_{yy} = N_1(\dot{\gamma}) \tag{6a}$$

$$\tau_{yy} - \tau_{zz} = N_2(\dot{\gamma}) \tag{6b}$$

where N_1 is the first and N_2 is the second normal stress difference, in Pascals (Pa) (Özcan-Taskin, 1993).

Non-zero normal stress differences are generated in cases of viscoelastic fluids, whereas in Newtonian fluids these two normal stress differences are null.

The first and second normal stress difference coefficients ψ_1 and ψ_2 (Pa.s^2) respectively are described as:

$$\psi_1 = \frac{N_1}{\dot{\gamma}^2} \tag{7a}$$

and

$$\psi_2 = \frac{N_2}{\dot{\gamma}^2} \tag{7b}$$

Similar to the shear stress and shear rate relationship, the first normal stress difference can also be easily related to the shear rate with a power law:

$$N_1 = A\dot{\gamma}^b \tag{8}$$

where the typical range of b is $1<b \leq 2$ (Özcan-Taskin, 1993).

Furthermore the Weissenberg number, (*Wi*), is a dimensionless number that can be used to compare the magnitude of elastic stresses to shear stresses, shown below:

$$Wi = \frac{N_1}{\tau} \tag{9}$$

Since the viscosity of a non-Newtonian fluid is a function of shear rate, it is referred to as apparent viscosity and is denoted as:

$$\mu_a = \frac{\tau}{\dot{\gamma}} \tag{10}$$

Rearranging Equation 7a gives:

$$N_1 = \psi_1 \dot{\gamma}^2 \tag{11}$$

Therefore substituting for both parameters, N_1 and τ gives:

$$Wi = \frac{N_1}{\tau} = \frac{\psi_1 \dot{\gamma}^2}{\mu_a \dot{\gamma}} \tag{12}$$

Barnes et al (1988) proved that second normal stress differences are considered much smaller than N_1 and are negative in value. According to Weissenberg's (1948) hypothesis, N_2 was presumed to be zero however lately it has been made possible with the use of modern rheometers to measure non-zero N_2 values with a good degree of accuracy. Even though in some cases N_2 has proven to be very crucial, for several other applications, such as mixing, it has little practical significance and therefore is considered negligible (Ulbrecht and Carreau, 1985).

The generation of non-zero normal stress differences is extraordinarily significant in analysing the role of viscoelasticity in stirred vessels. Normal stress differences are usually linked with non-linear viscoelastic effects and can be quantified as the viscoelastic fluid property (Özcan-Taskin, 1993). Another expression of viscoelasticity is defined by elongational viscosity, which usually shows a different behaviour as compared to shear viscosity. This is seen in polymer solutions, which show a decrease in viscosity as shear rate increases (shear-thinning behaviour), and show an increase in elongational viscosity with an increase in elongational rate (Barnes et al., 1988).

2.2.2 Viscoplastic Fluid

Viscoplastic materials are another common type of non-Newtonian fluids. Apparent yield stress is a useful parameter to describe such viscoplastic fluids. For a viscoplastic fluid to flow, the shear stress of the material must be higher than the apparent yield stress. The material behaves like a solid if the shear stress is below the apparent yield stress. The Bingham plastic model shown below is a simple rheological model used for describing viscoplastic fluids.

$$\tau = \tau_y + \eta_B \dot{\gamma} \quad for\ \tau > \tau_y$$
$$\dot{\gamma} = 0 \quad for\ < \tau_y \tag{13}$$

The apparent viscosity of Bingham plastic materials is found to decrease as shear rate increases, behaviour that is similar to shear-thinning fluids. Seeing as it is difficult to measure shear stresses at very small shear rates, the yield stress is usually calculated by extrapolating the shear stress vs shear rate plot back to zero. In this case the yield stress is known as the apparent yield stress.

Another common type of viscoplastic model is a combination of the power law and Bingham plastic model, known as the Herschel-Bulkley model:

$$\tau = \tau_y + k\dot{\gamma}^n \quad for\ \tau > \tau_y$$
$$\dot{\gamma} = 0 \quad for \quad \tau < \tau_y \tag{14}$$

The Herschel-Bulkey model shown above includes the flow behaviour index (*n*) as compared to the Bingham model. The fluid is represented as Bingham if n is 1, and is referred to as Herschel-Bulkley if n is less than 1.

Adams (2009) states that viscoplastic fluids show mixing properties alike to shear-thinning fluids, when fluid mixing is restricted near to vicinity of the impeller. However, due to apparent yield stress, there is a fixed boundary for viscoplastic fluids whereby no fluid motion beyond the cavern boundary is observed (Galindo and Nienow, 1992; Adams and Barigou, 2007, Adams, 2009).

As mentioned above, the standard Reynolds number is not applicable to the power law model, and as such the Metzner and Otto correlation needs to be used to describe the Reynolds number for a Bingham fluid:

$$Re_{HB} = \frac{\rho k_s N^2 D^2}{\tau_y + \eta_B k_s N} \tag{15}$$

2.1.2 Thixotropic Fluid

Time-dependent fluids have a memory, or a relaxation time, which is quite long compared to the experimental time. As shear stress is applied on such materials, they experience changes in their physical structures. This results in the effective viscosity of the material to change with time (Barnes, 1997).

Thixotropic fluids are one of the types of time-dependent fluids that exhibit shear-thinning behaviour over large timescales. Upon shear stress input, the viscosity of a thixotropic fluid decreases gradually until stress removal, after which a gradual recovery is expected. Examples include block co-polymers and self-assembling, surfactant-based systems (Barnes, 1997).

Another type of time dependent fluid are Rheopectic materials, which display opposite behaviour to thixotropic materials. They exhibit shear-thickening behaviour over large timescales and show a gradual increase in viscosity upon shear stress input, followed by recovery upon stress removal. Examples include wood pulp and high fibre systems. The analysis of such materials is extremely complex. Nonetheless, thixotropy fluids will be discussed briefly in this section.

In general addition of mechanical response to stress or strain on a structured fluid causes a varying level of viscoelasticity in the system. The microstructure may either react in a linear way, where it does not change itself, or in a nonlinear way, where the microstructure does change but reversibly. Complications arise in thixotropic studies because this reversible microstructural change takes a very long time to recover, due to the local spatial rearrangement of components. Such a long time-response makes thixotropic studies one of the main challenges facing rheologists today, as determining

accurate experimental characterisation and adequate theoretical description becomes extremely difficult and complex (Barnes, 1997).

Thixotropic materials gradually collapse upon shearing and slowly recover and rebuild at rest. This causes difficulties in mixing and handling of such structures. In addition, the time required to break the microstructure may take minutes but the rebuilding recovery stage may take up to several hours. The thixotropy phenomena still needs to be understood, and thus the need for an up-to-date review.

Early within the research on thixotropy, Scott-Blair (1943) gave a few examples of thixotropic materials. These included clays, soil suspensions, creams, flour doughs and suspensions, paints, and starch pastes. He was also able to define the preliminary instruments, known as thixotrometers, specifically used to characterise thixotropy phenomena. Another point of interest which arose was whether thixotropy should be studied at constant shear rate or constant stress input. Furthermore, Scott-Blair showed an easier flow in small tubes was due to thixotropy, whereas Pryce-Jones (1934, 1936, and 1943) stated that thixotropy was more pronounced in systems containing non-spherical particles.

Figure 2.8 depict an illustration of the breakdown and recovery process in a typical 3D thixotropic material.

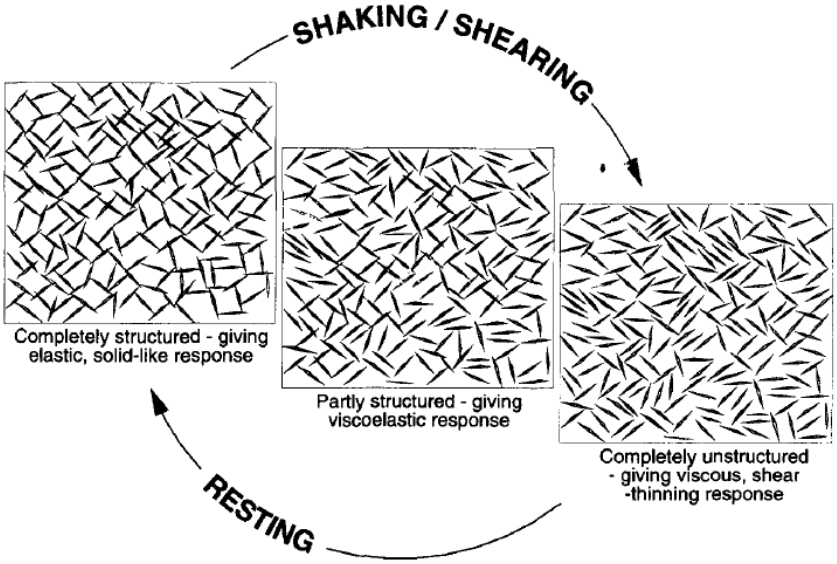

Figure 2.8. Breakdown of a 3D thixotropic structure (Barnes, 1997)

There are numerous definitions of thixotropy provided in literature. These several definitions attempt to provide a reflection on whether thixotropy is desirable or not (Barnes, 1997). Amongst the several definitions, this thesis accepts the definition mentioned in Polymer Technology Dictionary, "Thixotropy: A term used in rheology which means that the viscosity of a material decreases significantly with the time of shearing and then, increases significantly when the force inducing the flow is removed" (Whelan, 1994)

2.3 Visualization Techniques

A large number of experimental measurement techniques have been used to quantify mixing processes. In this section, the experimental techniques most relevant to work in this thesis are briefly introduced. This section describes the optical techniques of Laser Doppler Velocimetry (LDV) and Particle Image Velocimetry (PIV) for single and planar

flow fields. The section concisely defines the invasive technique Hot Wire Anemometry (HWA), which can be applied to opaque fluids. It also provides a description of Planar Laser Induced Fluorescence (PLIF) and Positron Emission Particle Tracking (PEPT) techniques, for quantifying and tracking tracer local concentration.

2.3.1 Hot Wire Anemometry (HWA)

Hot Wire Anemometry (HWA) is an intrusive probe technique that makes use of one to three separate wires. When the flow passes through the probe wires, a voltage pulse is recorded which is then further translated into velocity. This technique provides a measurement of instantaneous velocities and temperature at any instantaneous point in a flow.

Hot wire anemometry is an ideal tool for measuring velocity fluctuations in a time domain for turbulent flows. Gunkel and Weber (1975) made use of the HWA technique to measure the flow of air in a baffled vessel. The technique also enabled them to measure the pumping capacity of a six-bladed disc turbine. The technique is also capable of providing measurements in two phase flows containing a continuous turbulent phase and distributed bubbles.

However, since the technique is intrusive there is a risk of modification of local flow field. As a result, the readings cannot be trusted to be entirely accurate. Moreover, the technique is insensitive to reversal of flow direction, causing rectification error. Furthermore, contamination is caused due to deposition of impurities on the sensor from the flow, hence altering the calibration characteristics and reducing frequency response.

2.3.2 Laser Doppler Velocimetry/Anemometry (LDV/A)

Laser Doppler Velocimetry (LDV) is a non-intrusive optical technique for measuring velocities at any point in a fluid flow. The technique uses two argon-ion laser beams that are made to pinpoint a particular location in the vessel that is under investigation. The intersection of two coherent laser beams forms a small volume. Small reflective particles of neutral buoyancy pass through the small volume and scatter the laser light. The scattering is detected and is used to calculate the fluid velocity at that particular location. Overall flow fields can be estimated by taking measurements at multiple locations.

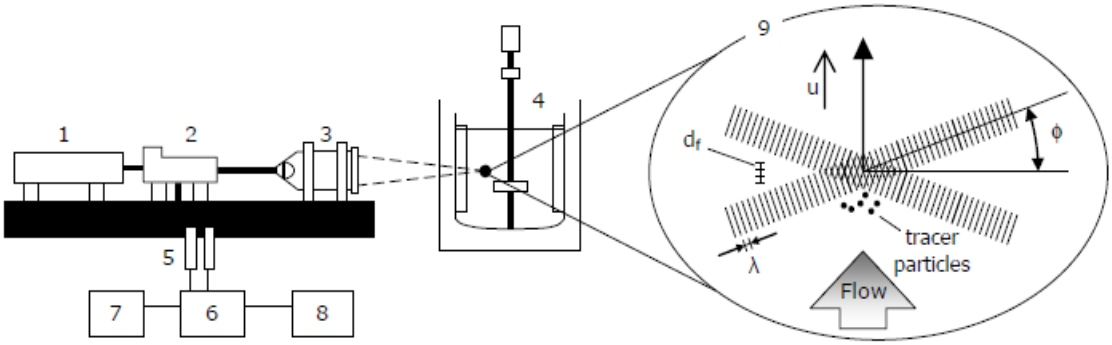

Figure 2.9. A typical LDV experimental set up, 1: laser; 2: fiber-optical module; 3: transmitting/receiving optics; 4: stirred vessel; 5: photomultipliers; 6: flow velocity analyser; 7: oscilloscope; 8: computer; 9: intersection of the two laser beams (Guida, 2010)

Measurements are made at the crossover of the two laser beams, as shown in **Figure 2.9**. The two laser beams with wavelength, λ, produce an interference fringe pattern of alternating light and dark planes. The fringe spacing, d_f is a geometric function of λ and the angle, Φ, (Papadopoulos and Arik, 2004). This is shown below as:

$$d_f = \frac{\lambda}{2sin\phi} \tag{16}$$

A scatter light signal (burst) is generated every time a particle passes through the measuring region. This signal is collected by the receiving optics system and further forwarded to the photodetector. The frequency of the light signal is known as the Doppler

frequency, f_D and is the inverse of the time required to cross a pair of consecutive fringes. Therefore,

$$u = f_D d_f \tag{17}$$

where u is the vertical velocity component.

A pair of beam is only able to detect one vertical velocity component, as shown in **Figure 2.9**. Therefore, Mavros et al. (1996; 1998) explained the possibility of determining two or three velocity vector components by using a combination of two or three sets of double laser beams. In addition, Armenante et al. (1997) proposed the installation of optical equipment on a traversing system, which would then allow the laser beam intersection to be traced at various different points. This would help in the determination of accurate velocities at various locations.

LDV can be performed on forward or back scattered light. Data received from forward scattering has a better signal to noise ratio, which can benefit the measurement of high speed flows and flows with very little turbulence intensities. Back scattering LDV is quite a simple approach, where all units belong to a common housing thus saving time required to align separate units.

Although LDV is an accurate technique for measuring flow patterns and velocities, data acquisition takes very long as data needs to be collected at every location individually. Also, since this is an optical technique, only transparent fluids can be used. This is the major drawback of the LDV, since real mixing processes involve partially or entirely opaque fluids. Furthermore, Galletti et al (2005) measured the flow instabilities in stirred vessels and observed that they vary greatly from one point to another.

2.3.3 Planar laser Induced Fluorescence (PLIF)

Planar Laser Induced Fluorescence (PLIF) is another non-invasive optical technique used to measure flow patterns and mixing times in stirred vessels (Sano and Usui, 1985; Nienow, 1997a; Guillard et al., 2000). This technique allows mapping of concentration as a function of time over a full flow plane and consists of instantaneous concentration data in a transparent system. PLIF has also been successfully used to describe mixing structures in various mixing devices (Adams and Barigou, 2007; Alvarez-Hernández et al., 2002).

The PLIF technique works by recording the distribution of the fluorescent dye as a function of time (Szalai et al. 2004). A thin laser sheet is made to pass through a stirred vessel, which in turn illuminates the fluorescent dye. A CCD camera, located in a plane perpendicular to the laser sheet, captures the process of tracer distribution. This is shown in the **Figure 2.10** below.

It has been reported in the literature that PLIF was used for measuring species concentration, temperature and velocity in 2D and 3D. However, it must be noted that PLIF measures concentration of a certain species at a certain energy state. Therefore, the population in these states depends upon the species concentration and temperature (Seitzman and Hanson, 1993).

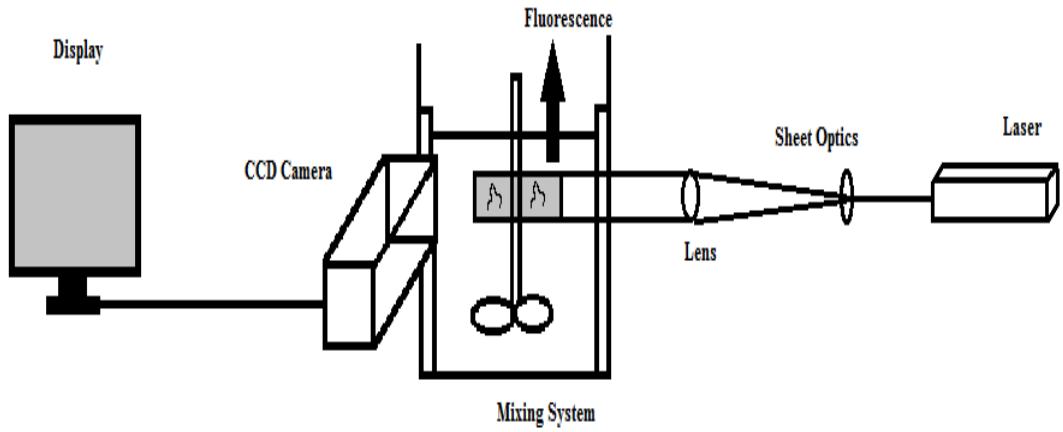

Figure 2.10. Simplified PLIF experimental facility.

Bakker and Van den Akker (1996) made use of the PLIF technique to measure the yield of a reactor system operating in a turbulent flow. Guillard et al. (2000) performed a study on turbulent flows in a stirred vessel and showed that PLIF is capable of revealing the presence of coherent mixing structures and detecting strong tangential flows in the impeller stream. PLIF has also been used to measure flow structures in stirred vessels with disc impellers (Fountain et al., 2000), to study flow patterns in the laminar regime for a variety of impellers (Alvarez-Hernández et al., 2002, and Szalai et al., 2004) and to investigate eccentric agitation in small, unbaffled vessels (Hall et al., 2005a).

Whereras PLIF has several benefits, it must be noted that it is unable to measure velocities. In addition, as in the case of LDV, this technique can only be used on transparent fluids.

2.3.4 Particle Image Velocimetry (PIV)

Particle Image Velocimetry (PIV) is a well-known, non-invasive, optical Eulerian technique used for measuring instantaneous flow in translucent systems. It is capable of

providing 2D Eulerian data by measuring velocities on a laser plane. The technique has made major contribution to the research of complex hydrodynamics in stirred vessels. A number of researchers have listed the principles of PIV such as Lourenco et al. (1989), Adrian (1991), and Willert and Gharib (1991).

The PIV set-up comprises of a laser emission unit and a camera for recording images, as shown in **Figure 2.11**. Both of these are controlled by a synchronizer. The laser emission unit illuminates a cross-section of the seeded flow field. The recording camera is located in a plane perpendicular to the light sheet and a data processor is used for analysing images. A small quantity of seeding tracer particles are suspended in a transparent fluid. Tracer particles are illuminated by a pulsing, thin plane of laser sheet and seeding particles are located by image recording. These images are then divided into several small interrogation areas (IA). Fast Fourier Transform (FFT) cross correlation helps determine the displacement of seeding tracer particles in the IA.

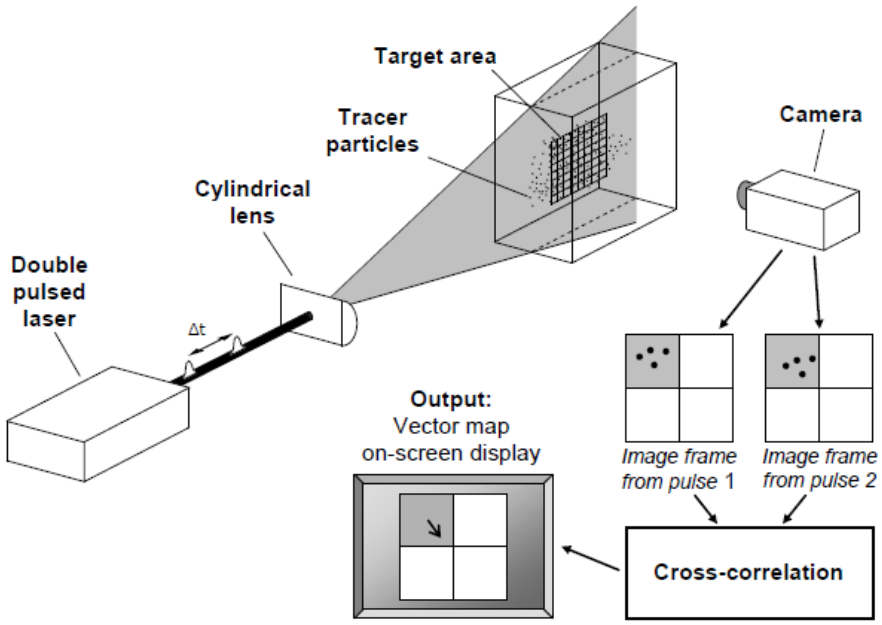

Figure 2.11. Simplified, typical PIV set-up, Image taken from (Guida, 2010)

PIV measurements have provided extensive information on single phase flow fields in stirred vessels (Bakker et al., 1996; Sheng et al., 1998; Zalc et al, 2001; Kukura et al., 2002; Aubin et al., 2004). Moreover, factors such as local energy dissipation rate and trailing vortices have also been reported in literature via use of PIV (Zhou and Kresta, 1996; Sharp and Adrian, 2001; Khan et al., 2006; Baldi and Yianneskis, 2003; Khan et al., 2004; Chung et al., 2007).

Among the numerous flow visualisation techniques, PIV is the most employed technique to examine the complex nature of flow in stirred vessels. However, the vessels and fluids used in a PIV experiment are required to be optically transparent. Therefore, PIV cannot be applied to opaque fluids and slurries (Micheletti and Yianneskis, 2004; Unadkat et al., 2009; Montante et al., 2012).

2.3.5 Positron Emission Particle Tracking (PEPT)

Positron Emission Particle Tracking (PEPT) is a non-invasive radioactive tracer technique, widely used to measure flow fields unobtrusively in not only translucent, but also in opaque systems (Barigou, 2004).

PEPT is one of the most powerful imaging techniques and is able to accurately track the position of a positron emitting particle over time. It can be used in an opaque vessel, a high solid fraction solid-liquid pipe flow (Fairhurst et al., 2001) or for examining flow of a non-Newtonian fluid in a stirred tank (Fangary et al., 2000). Other uses include measuring flow patterns and velocities for mixing of two shear-thinning materials or for the mixing of a shear thickening slurry and a paper pulp suspension.

The PEPT set-up consists of two gamma camera-heads facing each other. The operating system is mounted amid the gamma detectors, as shown in **Figure 2.12**. Each gamma

detector contains of a single sodium iodide crystal. A single positron-emitting, radioactive tracer particle is introduced into the fluid to track fluid flow. Upon the release of a positron from the nuclide, the positron is annihilated with an electron. This annihilation results in the release of energy in the form of two back-to-back 511 keV γ-rays. Each gamma detector captures incident γ-rays over a large rectangular active area. The two incident γ-rays are simultaneously detected by both detectors, producing scintillations in the crystals present in the gamma detectors. The photomultipliers produce position signals, which help obtain the two 2D centroids. The position of the tracer particle is located at the intersection of the photon trajectories. The local algorithm helps in calculating the time-space location of the tracer particle (Parker et al., 1993).

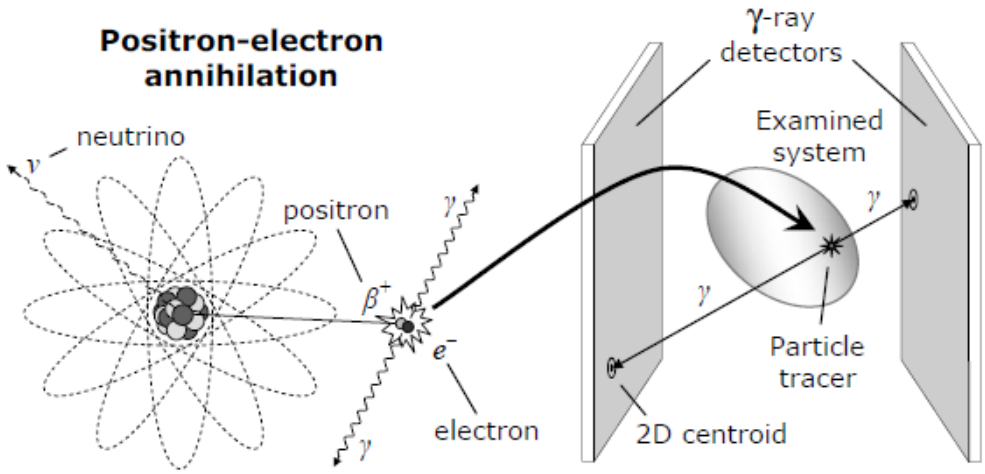

Figure 2.12. Schematic illustration of a PEPT experimental set-up showing positron annihilation and γ-ray detection by the PEPT camera, Image taken from (Guida, 2010)

PEPT data is received in three Cartesian coordinates, x, y, z, of the radioactive tracer at the location time. The data can be studied in either a Lagrangian analysis method, where factors such as residence time, circulation time and trajectory length distributions are used, or the data can be converted to extract local Eulerian quantities of the flow.

PEPT has been employed widely to study flows in several different situations. Pianko-Oprych et al. (2009) compared the use of PEPT with PIV for measurement of turbulent water flow in a stirred vessel and found that the results obtained by PEPT were accurate and reliable. Fangary et al. (1999, 2000, and 2002) used PEPT data for studying the agitation of non-Newtonian fluids in a stirred vessel. They were able to obtain particle trajectory-length distribution and to estimate fluid circulation time. Eulerian data for shear-thinning and visco-plastic fluids from PEPT measurements was analysed by Adams et al. (2008, 2009). PEPT has also been used to study solid-liquid flows in stirred vessels (Barigou et al., 2009) and multiphase flows to map fluid flow (Parker et al., 2002; Barigou, 2004).

Chapter 3

Experimental Techniques and Theoretical Analysis

Stirred vessels are the most common mixing equipment used in the industries, for example they are used in the processing industry for blending miscible liquids. This chapter presents a description of the equipment used, followed by a description of the experimental techniques. Particle Image Velocimetry (PIV) is a non-intrusive visualisation technique applied for measuring instantaneous flow velocity and to thus improve studies of fluid with complex rheology mixed in stirred vessels. 2D Eulerian data can be obtained by PIV by measuring the flow velocities of the fluid present on a laser plane going through the stirred tank. The Planer Laser Induced Fuorescence (PLIF) visualisation technique was also was employed in this study to invistigate flow behaviour of non-Newtonian fluids over mixing time. Theoretical analysis of 2D data measurements obtained from PIV is discussed later in this chapter. The material of test fluids used in this work and the rheology of these fluids is discussed in each results chapter separately.

3.1 Apparatus

One rig was used for both the PIV and PLIF experiments conducted in this study for all fluids. The cylindrical glass stirred vessel used in this work contained a flat-base of diameter $T=115$ mm. In order to reduce light distortion, the stirred vessel was placed inside a water-filled square glass tank. Four wall baffles of width $B = 0.1T$ were equally spaced within the vessel, as shown in **Figure 3.1a**.

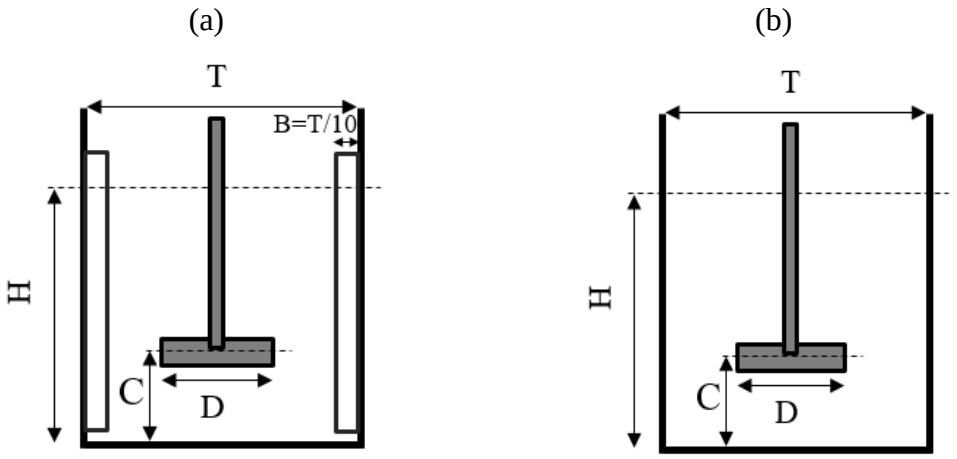

Figure 3.1. The layout of the stirred vessel configurations, equipped with impeller, as used in this work. (a) baffled, (b) un-baffled.

Three different impellers were used for the experiments, all having the same diameter: a Pitched Blade Turbine with down pumping (PBTD), one with up pumping (PBTU) and a Ruston Disk Turbine (RTD). The dimensions of the three different impellers are illustrated in **Figure 3.2** and are summarized in Table 3.1, where D_{Hub} is the hub diameter, D_{Shaft} is the shaft diameter and W is the hub height. Two configurations of stirred vessel were used, namely a fully baffled vessel (B), and an un-baffled vessel (U), as shown **Figure 3.1b**. The off-bottom clearance of the impeller configuration was also studied for C = T/4, C = T/3, C = T/2 and C = 3T/4 impeller positions. The stirred vessel was filled with the fluid under investigation to a height H = T for all configurations (see **Figure 3.3**).

Table 3.1. Dimensions of impellers used in experiments

Impeller	*D(mm)*	D_{Shaft} *(mm)*	D_{Hub} *(mm)*	Blade width *W(mm)*	Blade Thickness*(mm)*
6-PBTD	60 0.52T	7	14.45	12.5	1.67
6-RTD	62 0.54T	7	46.58	12.5	1.70
6- PBTU	60 0.52T	7	14.45	12.5	1.67

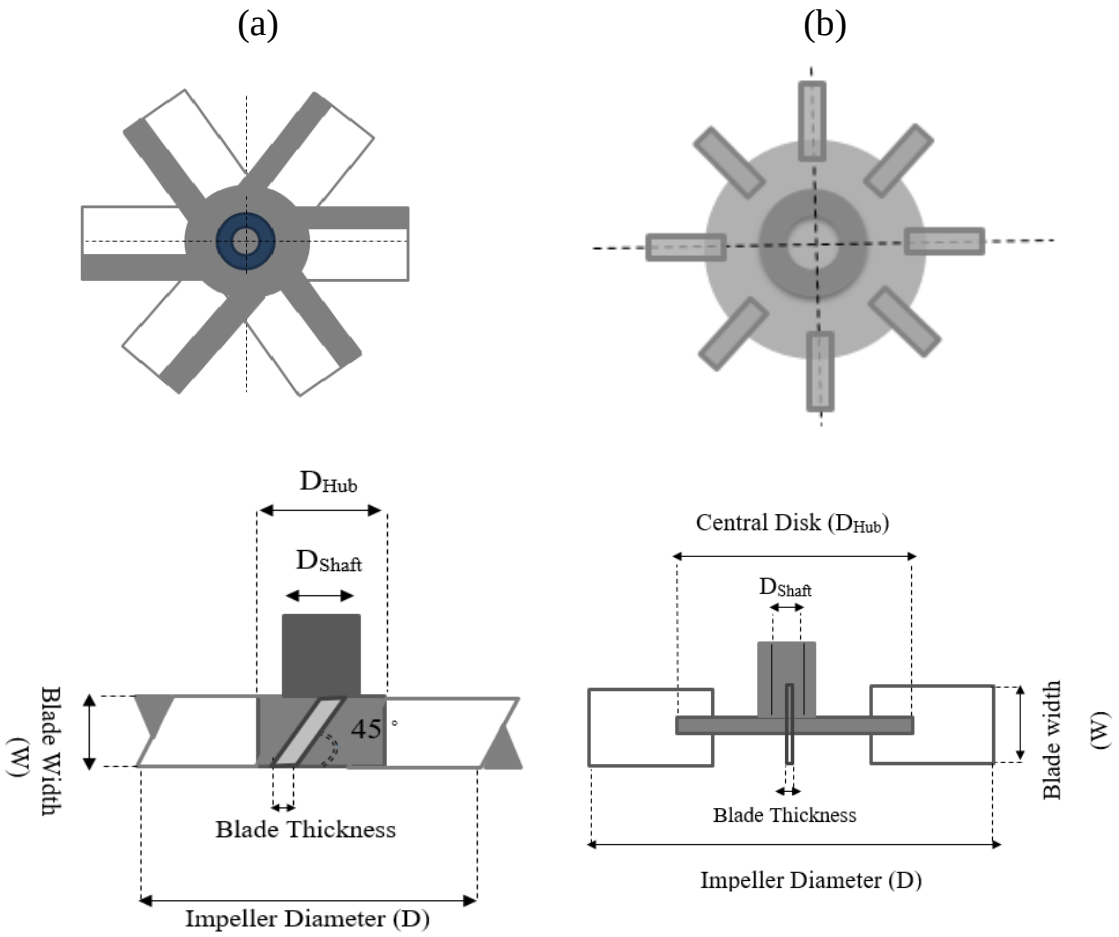

Figure 3.2. Impeller geometries used in the experiments, a) PBT, b) RTD

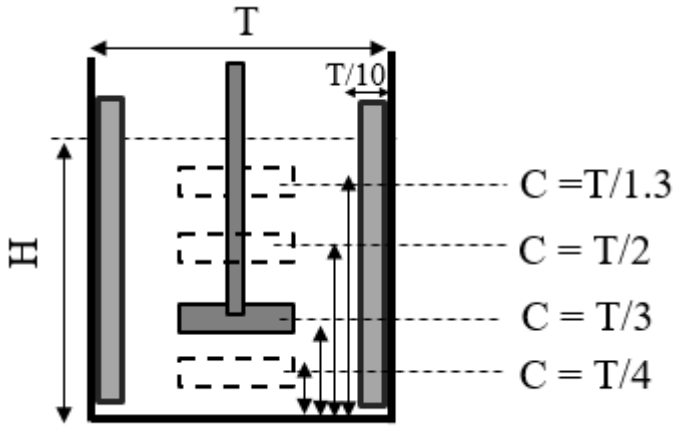

Figure 3.3. Schematic of various off-bottom clearance configurations studied in this work

3.2 Particle Image Velocimetry (PIV)

The set-up for 2D particle image velocimetry (PIV) is depicted in **Figure 3.4**, and the technique was employed in all experiments. The system comprised of a 532 nm Nd-Yag laser (type New Wave Solo III), pulsing from 0.5 to 14 Hz. A CCD camera (Power View Plus, TSI Inc, USA) was used for capturing high resolution images (2048×2048 pixels). Camera frame and laser sequencing were synchronized by use of a TSI Laser pulse 610035 synchronizer. In order to perform fluid velocity measurements, silver coated hollow glass particles of 10 µm diameter (Dantec Dynamics Ltd, Bristol) were seeded into the vessel and a 1 mm thick laser sheet was used to illuminate these particles.-Each frame produced an image pair, A & B, which is separated by a time interval dT. The maximum time interval, dT_{max} is calculated as a function of the magnification of the image and maximum velocity present in the system, which is equal to the velocity of the impeller blade tip (U_{tip}). Fast Fourier Transform (FFT) cross-correlation was used on each image pair. The image pairs were sectioned into small interrogation areas (IA).

Owing to the fact that in both laminar and transition regions the velocity hardly approaches half of the tip speed, 0.5 U_{tip} was used to calculate the maximum time interval (Chung, K.H.K. 2008):

$$dT_{max} = \frac{0.25\ L_{IA}\ M}{0.5\ U_{tip}} \tag{1}$$

where M is image magnification (in this case 64.5 μm /pixel), and L_{IA} is the length of the integration area *(IA*). The flow field in the vessel was analysed in a plane in front of the baffles, offset by 5°.

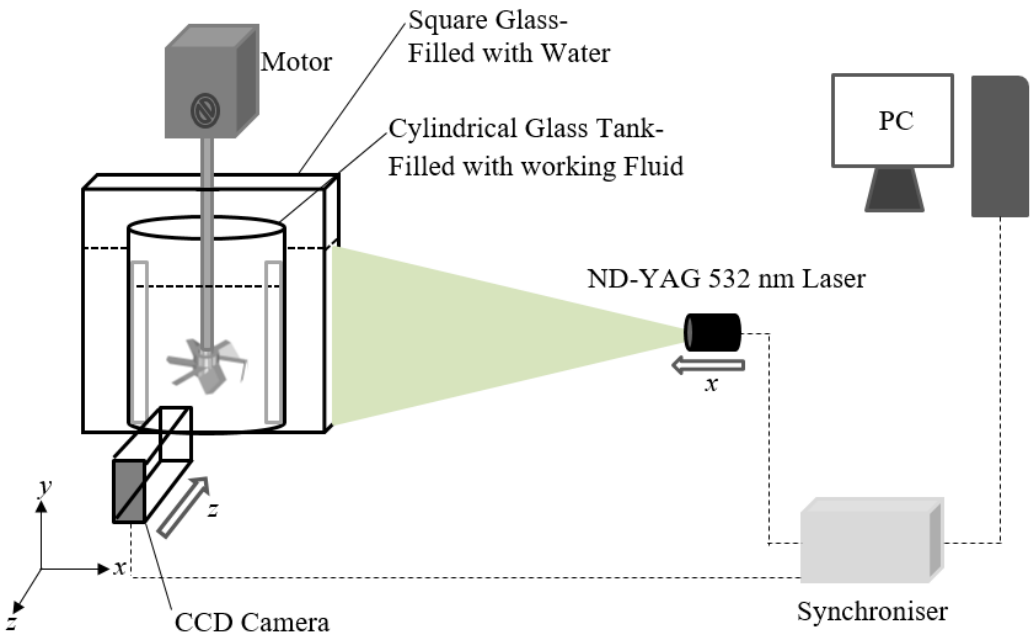

Figure 3.4. Experimental setup for PIV measurements

To prepare a fluid for PIV measurements it must be first transferred into an experimental tank and then the mixer motor, laser and camera should be turned on in the aforementioned order. The process for capturing is different for each test fluid and as such further details can be found in the relevant result chapters. During the PIV process 500

image pairs were captured by the camera. These images were then processed using TSI Insight 4G software, which uses a cursive Nyquist grid of an IA of 32x32 pixels in the first pass and 16x16 pixels in the second pass. The spatial resolution of the PIV measurements was fixed at 1.03 ×1.03 mm. The time-averaged flow field velocity was calculated using Tecplot Focus 2013R1 software. MATLAB (R2012a) software was also used for further analysis and data visualization.

3.3 Planar Laser Induced Fluorescence (PLIF)

A TSI PIV system was used to perform 2D Planar Laser Induced Fluorescence (PLIF). To eliminate reflection from excessive laser light the camera was equipped with a 545 nm filter that allowed for only the fluorescent light in the measurement plane to be captured in the image. In order to calibrate the system, the tank was filled with different concentrations of Rhodamine 6G dye solution, ranging from 0.1 to 1 mg/L, at the same laser power. Each individual pixel was analyzed using a dedicated MATLAB routine to obtain a grayscale value at each concentration of dye. The grayscale values were plotted against dye concentration. A linear equation relationship is produced, as shown in **Figure 3.5**. Based on the result from **Figure 3.5**, a dye concentration of 0.6 mg/l was chosen to ensure all measurements remain within the linear range. A small volume(5ml) of Rhodamine 6G dye was injected above one of the impeller blades (**Figure 3.6**) via syringe, to ensure that the dye began to propagate inside the cavern. The camera begins to capture one frame per second until the dye stops propagating through the fluid.

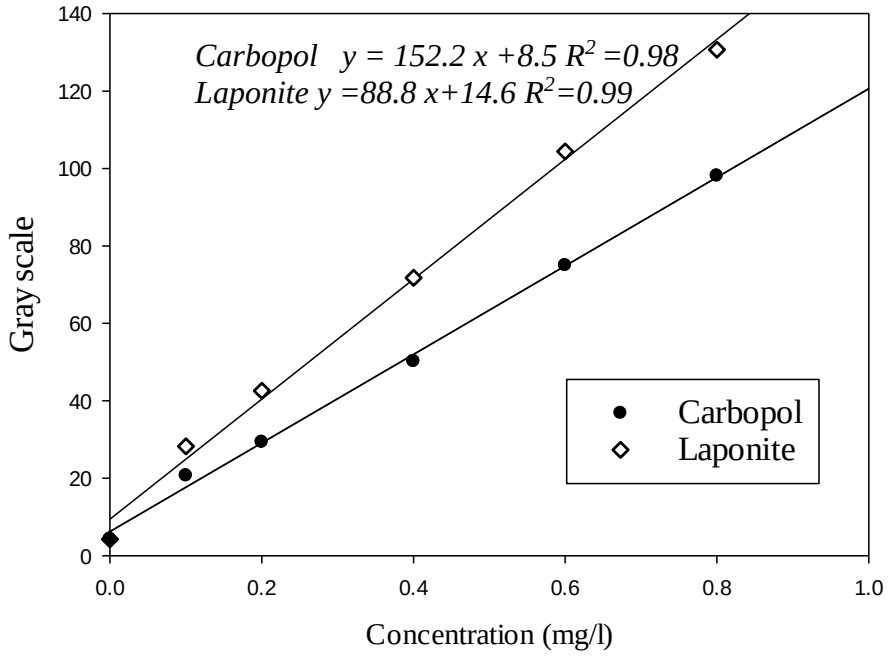

Figure 3.5. Pixel greyscale versus tracer concentration

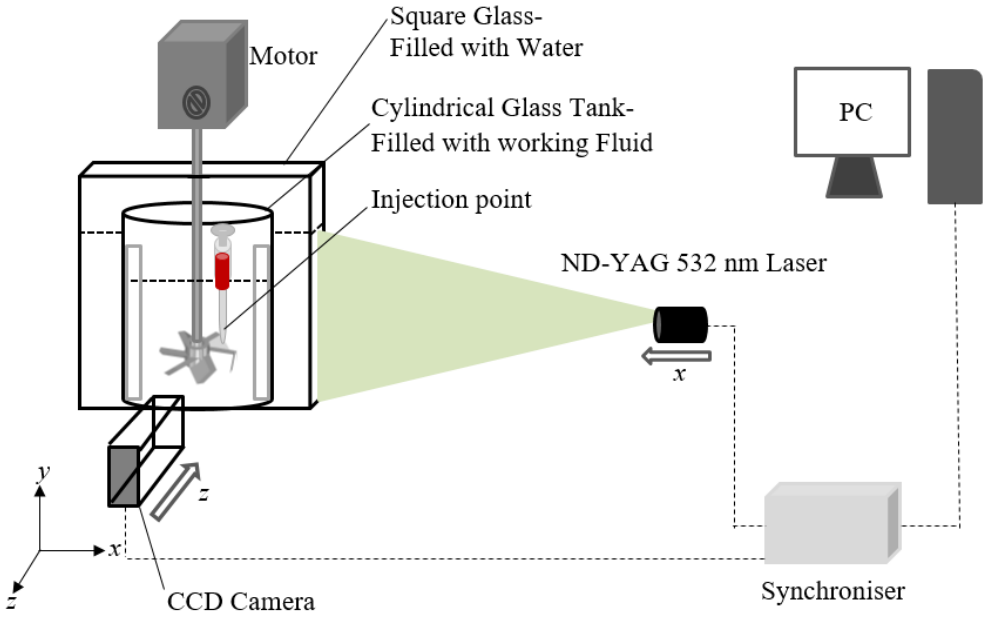

Figure 3.6. Experiment setup for PLIF experiments

3.4 Flow Number

The pumping efficiency of the impeller is measured by the dimensionless parameter Flow number, Fl. This value is usually defined as the normalized, net volumetric flow rate of fluid passing through the boundaries of an impeller:

$$Fl = \frac{Q}{ND^3} \tag{2}$$

where Q is net volumetric flow rate (m^3s^{-1}). The plane at which the flow field measurements are taken depends on the direction of the major flow discharge. For an axial flow impeller, as shown in **Figure 3.7**, the axial pumping rates of impeller Q_1, and Q_2 in directions z_1 and z_2 respectively can be calculated using (Khan, 2005, Guida et al., 2010):

$$Q_1 = 2\pi r \int_{\vartheta=0}^{\vartheta=2\pi} \int_{r=0}^{r=\frac{D}{2}} u(\vartheta, r, z_1) r d\vartheta \, dz \tag{3}$$

$$Q_2 = 2\pi r \int_{\vartheta=0}^{\vartheta=2\pi} \int_{r=0}^{r=\frac{D}{2}} u(\vartheta, r, z_2) r d\vartheta \, dz \tag{4}$$

where z_1 and z_2 denote the height at the bottom and top of the impeller blade respectively and u is the time-averaged axial velocity at an axial coordinate z. The radial pumping rates of impeller Q_3 in radial directions can be defined as:

$$Q_3 = \frac{D}{2} \int_{\vartheta=0}^{\vartheta=2\pi} \int_{Z=z_2}^{Z=z_1} v\left(\vartheta, \frac{D}{2}, z\right) d\vartheta \, dz \tag{5}$$

where v is time-averaged radial velocity at a radial coordinate r. PIV data is available only on a single vertical plane and as such axial symmetry is presumed. Consequently, the mean velocity components are independent of the angular position ϑ of the measurement plane, therefore the results are multiplied by 2π and integration for ϑ angle over the 0 to 2π radian range is omitted in Equation (3) to (5).

In the case of a PBT impeller, where flow discharge is anticipated in both the axial and radial directions (see **Figure 3.7**), the net flow rate and flow number may be given as (Guida et al., 2010):

for PBTD: $Q = Q_2 + Q_3$ $\qquad Fl = \frac{Q_2+Q_3}{ND^3}$ (6)

for PBTU: $Q = Q_1 + Q_3$ $\qquad Fl = \frac{Q_1+Q_3}{ND^3}$ (7)

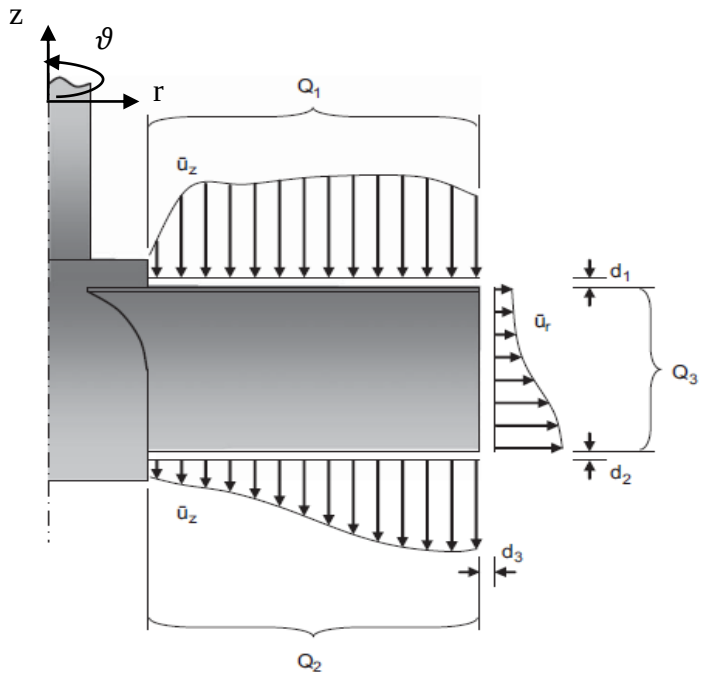

Figure 3.7. Schematic diagram of flow rates for PBTD impeller taken from (Guida et al., 2010).

For radial flow impellers (RTD), the flow number of the impeller (see **Figure 3.7**) can be calculated from the radial pumping rate Q_3.

$$Fl = \frac{Q_3}{ND^3} \quad (8)$$

For all the aforementioned impellers the flow number of the impeller used was determined by a distance $d_1 = d_2 = 1.80$ mm and $d_3 = 1.5$ mm away from the surface of the impeller blades. According to Khan (2005), the above distances are best for minimizing the process error from the PIV measurements. Khan (2005) investigated the effect of different distances from impeller on the flow number and showed that flow calculation are quite sensitive to the distance from the impeller. Specifically, the flow number calculated closer to the blade shows lower values than that calculated at bigger distances from the blades (Khan, 2005).

Finally, as seen in Guida (2010), the flow numbers Fl_1, Fl_2 and Fl_3 may be calculated from the flow rates Q_1, Q_2 and Q_3 for three different types of impellers (PBTD, PBTU, and RTD) (Guida, 2010).

$$Fl_1 = \frac{Q_1}{ND^3} \tag{9}$$

$$Fl_2 = \frac{Q_2}{ND^3} \tag{10}$$

$$Fl_3 = \frac{Q_3}{ND^3} \tag{11}$$

It should be noted that a negative value of flow rate means the flow leaves the plane of the impeller. The ratio of net axial flow rate to the net radial flow rate (*Qa /Qr*) passing the impeller blade was also used to quantify the capacity of impeller discharge.

Chapter 4

EFFECT OF THIXOROPY ON FLUID MIXING IN A STIRRED TANK

The aim of this work is to investigate the effects of time dependency on fluid mixing in a stirred vessel. To achieve this various rheological variable were fixed by choosing a time independent reference fluid that exhibited the similar rheological properties as the main fluid of this study.

The PIV technique is employed to characterize the flow fields of a transparent, colloidal dispersion of 2.2 *w%* Laponite thixotropic fluid in a stirred tank for three mixing regimes: $Re_{HB} = 7$, $Re_{HB} = 61$ and $Re_{HB} = 158$. A time independent transparent, aqueous 1*w*% Carbopol fluid that exhibited similar rheological properties behaviour is used as reference fluid to help to distinguish time effect from other rheological properties of the time-dependent 2.2*w%* Laponite fluid. The PLIF visualization technique is applied to further investigate the evolution of the cavern volume with time. The mixing efficiency of the impellers is analysed in terms of size and growth of a cavern over time and impeller pumping efficiency. Furthermore, the effect of impeller bottom clearance with three impellers (PBTU, PBTD, and RTD) in the mixing of a thixotropic fluid was investigated. Finally, an un-baffled stirred tank configuration was investigated to understand mixing performance in terms of cavern size and growth and flow fields.

4.1 Introduction

Thixotropy is one of the challenging rheological phenomena in non-Newtonian fluid science. Mixing of thixotropic fluids is widely used in food, polymer and pharmaceutical industries. Thixotropy is encountered in a vast group of materials such as pigment dispersions (paints, paper coating etc.), biological systems, dispersions of clay minerals (ceramic, cement, etc.), emulsions and rubber, etc. Most of them are noticeably colloidal dispersions, whereby fine particles are dispersed in the heterogeneous system (Mewis, 1979). Despite the extensive application of such fluids in industrial and natural systems, thixotropy is still poorly understood due to the complexity of the microstructure of thixotropic fluids.

As such a complete description of the rheological properties of these fluids is not given and understanding a rheological model for time-dependent fluids is still a challenging problem. In a recent review Mewis and Wagner (2009) categorized existing models for thixotropic rheology.

The word “Thixotropy” derives from the combination of two ancient Greek words, “thixis” (meaning to touch) and “trepo” (meaning turning or changing). In other words, thixotropy states a characteristic behaviour of fluids to changes due to stirring, however that is not the whole story (Barnes, 1997). Thixotropy is currently defined as a continuous reduction of viscosity of structured liquids over time for a constant applied shear stress. In addition the process is fully reversible, in that once the stress is discontinued there is a gradual recovery of viscosity with time.

Thixotropic fluids exhibit shear-thinning, time dependent and mostly yield stress rheological behavior. Mixing of non-Newtonian fluids with yield stress rheological

behavior results in the formation of a cavern region surrounded by a poorly mixed, relative immobile region.

In a stirred tank fluid is mobile in regions around the impeller, where shear stresses are high. These regions are defined as the cavern. Outside the cavern region, away from impeller where shear stresses are low, fluid is stagnant. Determination of cavern size and shape of yield stress fluids are key factors taken under consideration for a wide range of mixing process design and optimization.

Initially, Amanullah (1998) developed a mathematical model to predict cavern diameter. Recently, Xiao et al. (2014) developed a new torus model for the mixing of fluids with yield stress which provides significantly better prediction than the original model of Amanullah (1998). Hirata et al. (1994), Adams and Barigou (2007), and Arratia et al. (2006a) have used both CFD simulation and experimental methods to investigate formation and cavern size inside a stirred tank of shear-thinning fluids with yield stress. Despite the recent studies, mixing of non-Newtonian fluids with complex rheology such as thixotropic fluids with shear-thinning, yield stress, and time-dependent rheological behavior is still a challenge in research and industry. Specifically, there is a lack of complete studies to fully understand time effects on design, efficiency, and scale-up of stirred vessels. Couerbe et al. (2008) recently studied stirring of thixotropic liquids with a mixel TT impeller in a stirred tank using both experiment techniques and numerical simulations. Their results suggested that an unusual flow pattern, found at the lowest stirring speed setting ($N = 1\ s^{-1}$), was due to wall slip effects. Derksen (2010) subsequently applied a direct numerical simulation of transitional and turbulent flows of thixotropic liquids in a stirred tank. One of the main results of that study shows the profound impact

of the liquids' relaxation time - characterized by the dimensionless Deborah number on the flow patterns in the mixing tanks.

4.2 Material and Experimental Design

4.2.1 Rheology of Test Fluids

4.2.1.1 Time Dependent Fluids (Thixotropy)

The non-Newtonian fluid chosen for investigation was a 2.2*w%* Laponite (Laponite RD, conservation resources UK Ltd) dispersion in distilled water. Laponite, a synthetic layered silicate, is an additive which improves performance and properties of an extensive range of industrial and consumer products such as surface coatings, household cleaners and personal care products. This component allows a controlled rate of restructuring after applied shear and improves the stability of a product. Laponite is also used as a film former agent to produce electrically conductive, antistatic and barrier coatings.

Laponite fluids exhibit thixotropic, shear-thinning and yield stress properties. The detailed properties of this fluid are discussed in detail in the work of Coussot et al. (2002), Coussot et al. (1993) and Bonn et al. (2002).

The fluid is prepared according to the preparation method described in Couerbe et al. (2008). Laponite powder was added gradually in agitated distilled water and left to fully mix for one hour at $N = 7\ s^{-1}$. 6 ppm of NaCl was then added to the stirring liquid so as to increase the pH of the fluid to approximately pH = 10. When the process was completed a clear, colorless colloidal dispersion was produced. The prepared fluid was then left at rest for a few days to complete absorption of water molecules into the powder (solid matrix), a process needed in order to prevent irreversible aging during the experiments

(Couerbe et al., 2008). The thixotropic suspension was transferred into the experimental vessel from the preparation tank. Air bubbles trapped inside fluid were removed by stirring the fluid constantly for up to 10 min at $N = 5\ s^{-1}$.

4.2.1.2 Time Independent Fluids

To investigate the effects of the time dependency of the fluid on mixing, a time-independent fluid with the similar rheological properties was also analyzed. In this study the time-independent fluid was prepared from white powder Carbopol 940 (B. F. Goodrich Co) polymer used as a 0.1*wt*.% transparent, shear-thinning solution.

The desired quantity of Carbopol powder was added to distilled water under high stirring conditions ($N = 7\ s^{-1}$) to avoid the formation of clumps. The powder was fully dissolvable at room temperature.

An aqueous solution of Carbopol, by its very nature, is not transparent. The fluid is sensitive to pH which causes changes in rheological properties, i.e. higher pH causes the fluid to become thicker with a higher yield stress (Adams, 2009). Therefore, once the fluid was transferred to the experimental vessel a few drops of sodium hydroxide (NaOH) solution (0.8 *wt.%*) were gradually added on the impeller blade in the vessel, so as to make the fluid transparent and exhibit viscoplastic behavior. The pH of the prepared fluid was measured by a pH meter as being pH = 4.7.

4.2.2 Rheology Results

The rheological properties of the test fluids were measured using an AR1000 Advanced Rheometer (TA Instrument, USA) with a cone (diameter 60 mm, angle 2°) and plate geometry, at a constant temperature of 20° C. Due to the prolonged times needed to

measure the rheological properties of the selected liquids, a solvent trap was used throughout the experiments to reduce evaporation of the fluids. In order to acquire to a consistent shear history the above configuration was also used to take measurements of the viscometric properties of the fluids. Thixotropy samples were initially pre-sheared for 400 s at a shear rate of 100 s^{-1} and then left to rest, to reduce the effect of shear on the sample.

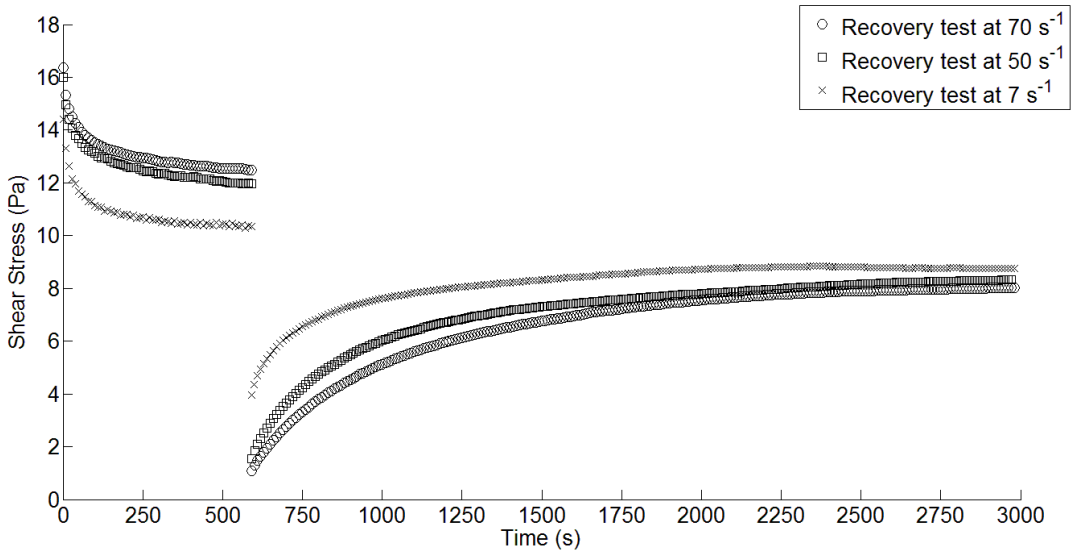

Figure 4.1. 2.2*w*% Laponite fluid under application of shearing followed by a recovery period for three different shear rates.

Shear stress for three different shear rates (70, 50, and 7 s^{-1}) was monitored within 600s, as depicted in **Figure 4.1**. As is shown in the image, the viscosity is mainly reducing in the first 300 s. This suggests that the entire PIV observation process should take place within the first 5 min of mixing.

Following shearing of the fluid at a constant shear rate for a length of time (600s), the samples were left at rest for 2500 s, in that the shear rate was reduced to $\dot{\gamma} = 0.01\ s^{-1}$on

the rheometer. This was done to monitor their shear stress recovery with time. **Figure 4.1** shows the recovery process lasted for around 1300s for all samples.

To ensure the data is repeatable, samples that were subjected to stress were subsequently left to rest in the rheometer for the 1300s, after which they were subjected to shear at a constant shear rate. This allowed for monitoring of shear stress and viscosity with time. **Figure 4.2** shows the viscosity curve of the sheared samples and proves that 1300 s is a reasonable time for fluid recovery (i.e. ensures the same rheological properties in each run of PIV experiments).

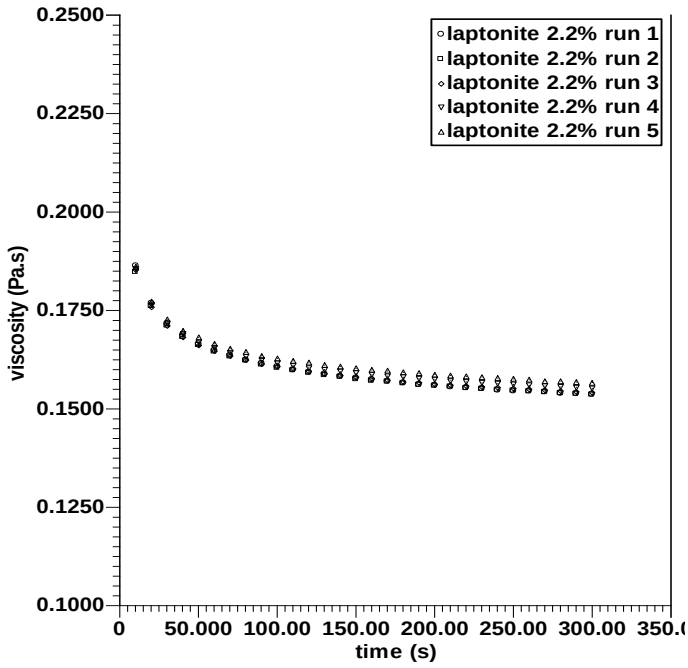

Figure 4.2. Viscosity curve overlap in test runs.

4.2.2.1 Hysteresis Loop Test

Thixotropic fluid samples were shear ramped up to six times, from 0.1 to 500 s^{-1} and then ramped down six times symmetrically over the same period.

This test was conducted to confirm the time dependency of the thixotropic fluid qualitatively. The results are shown in **Figure 4.3a,** whereby a hysteresis loop is observed. This phenomenon appears as a response to the simultaneous breakage and reforming of the samples' structure due to shearing, with the reforming process being slower than the breakdown process. The area enclosed by the hysteresis loop can be used as a measure of the time dependency of the fluid.

The microstructure of the time-dependent, 2.2*w*% Laponite fluid was broken under shear, and viscosity decreased with time. With continuing shear of the fluid the viscosity reached the steady point, and the later loops overlap each other as shown **Figure 4.3a**. In contrast and as was expected for the time-independent fluid, the Carbopol solution did not show a hysteresis loop (see **Figure 4.3b**).

4.2.2.2 Steady State Shear Viscosity

The viscosity of the various fluids changes over the period of shearing, therefore the conventional method of applying shear stress is not suitable to obtain the steady shear flow curve of these fluids. The samples were therefore sheared at a given number of constant shear stresses (i.e. $\tau 1$, $\tau 2$, $\tau 3$, $\tau 4$, $\tau 5$) for 600 s and the responses in shear rate (i.e. $\dot{\gamma}1, \dot{\gamma}2, \dot{\gamma}3, \dot{\gamma}4, \dot{\gamma}5$) were monitored, as shown in **Figure 4.4a**.

(a)

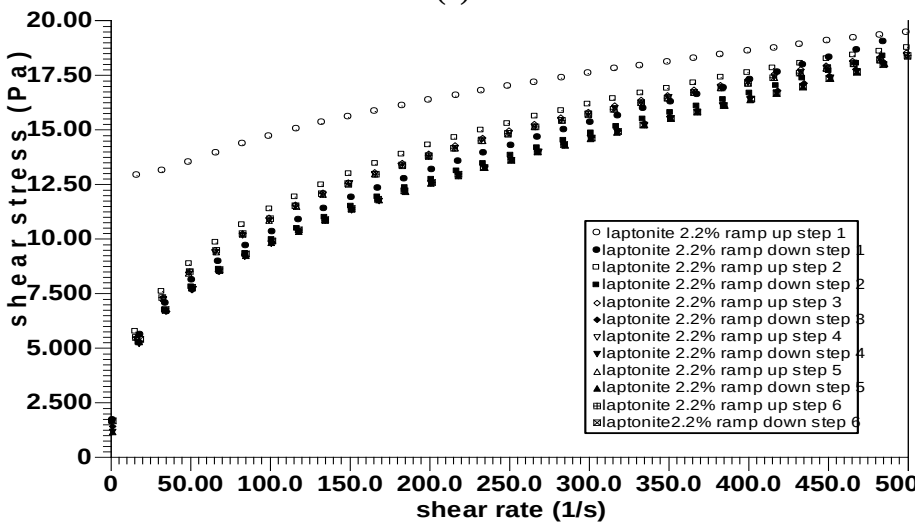

(b)

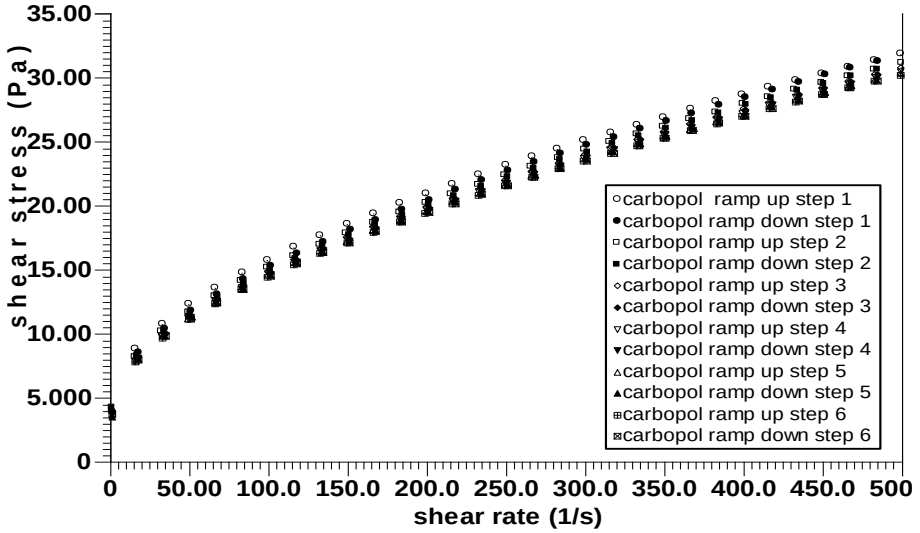

Figure 4.3. (a) Full shear ramp experiment of 2.2*w*% Laponite fluid (six ramps), (b) Full shear ramp experiment of 1*w*% Carbopol fluid (six ramps).

The shear rate values were subsequently extracted at various shearing times (i.e. t_1=1, t_2=2, t_3=3, t_4=4, t_5=5) and the fluid's shear flow curves corresponding to the different shearing time intervals were plotted. The instantaneous viscosity was then obtained (see **Figure 4.5b**). This methodology is based on the work of Lim (2005), where it was used to characterize thixotropic foams. The resulting data was fitted to the Herschel–Bulkley model for different time intervals of shearing (see **Figure 4.5**):

$$\tau = \tau_y + k\dot{\gamma}^n \quad (2)$$

These parameters are listed in Table 4.1 for various time intervals.

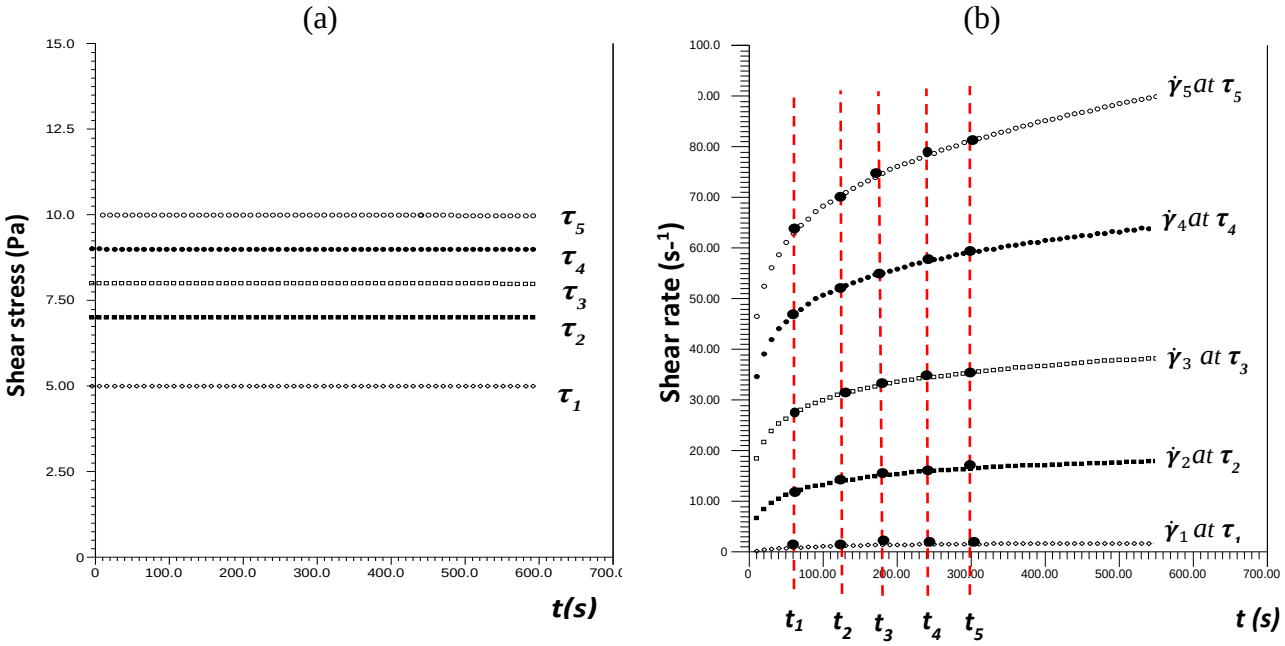

Figure 4.4. Schematic of steady shear flow tests; (a) few constant shear stress applied to the thixotropic fluid (b) response of shear rate at constant shear stress over a time of experiments.

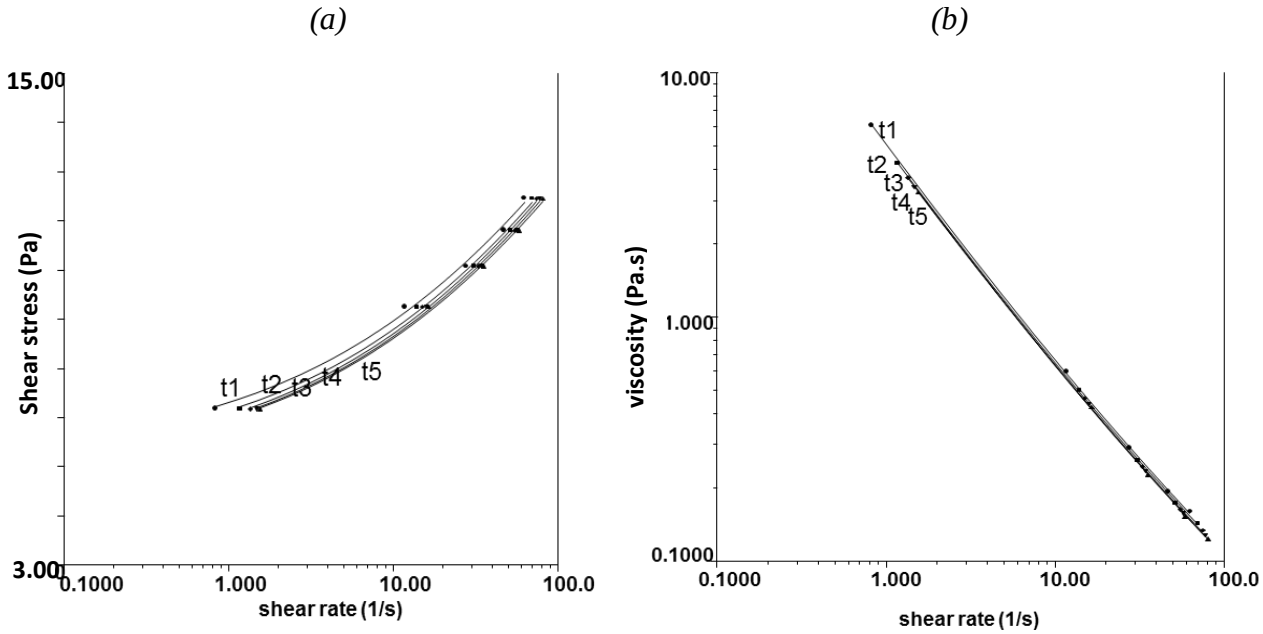

Figure 4.5. Flow curves corresponding to different shearing times of 2.2*w*% Laponite.

Table 4.1. Rheology parameters of Herschel–Bulkley model for different shearing times during experiment 2.2*w*% Laponite fluid

***t* (min)**	τ_y **(pa)**	***k* (Pa. s^n)**	***n***
1	4.26	0.84	0.45
2	4.16	0.80	0.45
3	4.11	0.798	0.45
4	4.07	0.795	0.45
5	4.05	0.795	0.45

To obtain the shear flow curves of 1*w*% Carbopol a shear rate 0-500 s^{-1} was applied to the fluid until a steady state viscosity was attained. Consequently the Herschel-Bulkley model was fitted to the measurements, which resulted in the values of τ_y= 3.72 Pa, k = 0.71 Pas^n and n = 0.55 as shown in **Figure 4.6**. The above show that 1*w*% Carbopol has about the same yield stress, *n* and *K* values as the thixotropic 2.2*w*% Laponite fluid, with the major difference being that the former is not time dependent.

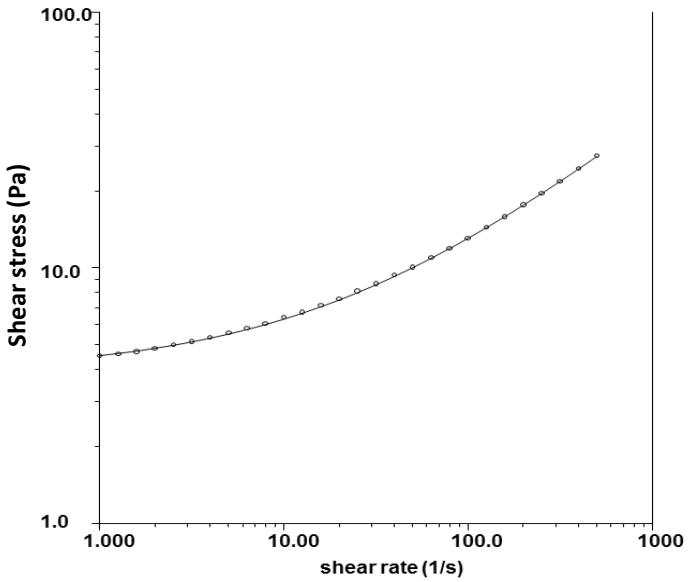

Figure 4.6. Flow curve of 1*w*% Carbopol fluid at different shearing times.

4.2.3 Experimental Design

The stirred vessel and impellers used in this work were discussed earlier in Chapter 3.1 for the different configurations used. Summarized results for all configurations tested are demonstrated in Table 4.2. The Reynolds numbers Re_{HB} used throughout this chapter are calculated based on the Herschel-Bulley model.

Table 4.2. Different configurations used in this study; B: baffled vessel, U: un-baffled vessel

Test Fluids	Flow Regime *Re*	Impellers used	Vessel configurations	Impeller off bottom clearance
2.2*w*% Laponite & 1*w*% Carbopol	7	PBTD	*B*	*C = T/3*
		PBTU	*B*	*C = T/3*
		RTD	*B*	*C = T/3*
	61	PBTD	*B*	*C = T/4, C = T/3, C = T/2, C=3T/4*
		PBTU	*B*	*C = T/4, C = T/3, C = T/2, C=3T/4*
		RTD	*B*	*C = T/3*
	158	PBTD	*B, U*	*C = T/4, C = T/3, C = T/2, C=3T/4*
		PBTU	*B, U*	*C = T/4, C = T/3, C = T/2, C=3T/4*
		RTD	*B, U*	*C = T/3*

4.2.4 Experimental Techniques

The set-up for both two-dimensional Particle Image Velocimetry (PIV) and Planar Laser Induced Fluorescence (PLIF) employed in all experiments presented in this work was discussed in chapter 3.2 and 3.3. The strategy used to investigate the flow field of a time-dependent fluid is to examine the flow during the initial shearing, e.g. within the first few minutes from a stagnant state, when fluid exhibits time dependency. A consistent procedure must be used throughout all experiments to ensure the fluid's rheological properties remain the same in each run of the experiment and are not altered due to shear

history. To prepare a fluid for PIV measurements, it must be first transferred into an experimental tank then stirred for 10 min at a high rotational speed (e.g. 300 rpm). The fluid is subsequently left to rest for a recovery time of around 20 min. At the end of the recovery time the laser, camera, and mixer motor should be turned on in the aforementioned order. During the PIV process, 500 image pairs were captured by the camera and at the end of the capturing process the fluid was left to rest for 20 min to prepare it for the following test. PIV measurements of a time-independent fluid were performed using the same process as described above, with the only difference being that extra time was not given to the Carbopol fluid to rest prior to PIV measurements. 2D PLIF was performed using a TSI PIV system. The details for the PLIF set up and measurement technique was discussed earlier in chapter 3.3.

4.3 Results and Discussion

The strategy to investigate how a thixotropic fluid develops in a stirred tank from an initial state (zero velocity) to a final state condition is through dividing PIV data into a series of time intervals. The interval length was chosen based on the shortest time necessary to calculate the time-averaged velocity data.

Accordingly, the flow pattern of the thixotropic fluid in the tank was analyzed every 15 s during mixing and compared to that of a non-thixotropic fluid. The analysis was performed during the mixing owing to the fact that efficient mixing mostly takes place inside the cavern and both fluids used showed the presence of a cavern in mixing due to yield stress. Parameters of interest as flow number such as area ratio of cavern to tank, radius and height of cavern, and ratio of axial to radial flow passing through impeller

were determined from the time-averaged velocity data during each shearing time. It should be noted that a negative value of flow numbers means the flow leaves the plane of the impeller.

The PLIF visualization technique was employed to help characterize the mixing efficiency in terms of cavern growth and size as well as measure the time required for the fluid inside cavern to become fully mixed.

2D normalized velocity contour plots for the three impeller configurations were determined under three different flow regimes (Re_{HB} = 7, Re_{HB} = 61, Re_{HB} = 158) and three time intervals (t_1 = 0-15 s, t_2 =125-139 s, t_3 = 261-277 s) during mixing. The PBT impeller in both UP and DP modes and the RTD impeller make it possible to investigate in more detail the efficiency of axial and radial flow discharge of the thixotropic fluid. Results are presented and discussed for each Re number.

4.3.1 Flow Fields

4.3.1.1 *Re* = 158

A primary anti-clockwise loop was observed in the PBTD impeller configuration in the first 15 s of stirring that appeared to extend both vertically and horizontally due to the reduction of viscosity taking place from time t_1 *to* t_3 (see **Figure 4.7**). The flow was induced vertically from above the impeller at t_1 and mostly to the left of the impeller, at an angle of 45° with respect to the downward direction. Hence the flow discharge is found to be mostly axially, with the ratio of axial to radial pumping being *Qa/Qr* = 3.10 (Table 4.3). Couerbe et al. (2008) observed a similar value for the same fluid mixed by a Mixel TT impeller at $N = 8\ s^{-1}$ whereby what was determined was the flow is in the transition

regime. The downward discharge from the impeller with time reaches the baffles and then moves upward to reach 0.7 *Z/H* at t_3 in a 2.2*w*% Laponite fluid (**Figure 4.8**).

A weak, second clockwise loop was observed below the primary loop, indicating good mixing in the lower part of the tank. Both loops were also present for the time independent 1*w*% Carbopol fluid (**Figure 4.9**), however in the later case the loop did not reach the baffles, resulting in a smaller loop being formed. In the case of 1*w*% Carbopol fluid, the calculated value of Fl was 0.462, which is in close agreement with the work of Ein-Mozaffari and Upreti (2009). This value of Fl was also similar to that of the thixotropic fluid at the beginning of stirring (i.e. at interval t_1). In contrast, as the mixing developed with time, the flow number for the 2.2*w*% Laponite fluid increased to Fl = 0.571 due to a reduction in viscosity, which is a response to the applied shearing. A comparison between the two cases is given in Table 4.3. Values of *Fl* and *Qa/Qr* for times t_2 and t_3 were very similar and as such, for brevity, only the values for t_1 and t_3 are presented in Table 4.3, Table 4.4 and Table 4.5. During agitation of thixotropic 2.2*w*% Laptonite, its apparent viscosity evolves in time. Higher values of flow number for 2.2*w*% Laponite relative to 1*w*% Carbopol may result from lower values of apparent viscosity of the former as shown in **Figure 4.3**.

Table 4.3. Characterized parameters of flow for the PBTD impeller.

Re	**7**			**61**			**158**		
Fluid	***2.2w%* Laponite**		***1w%* Carbopol**	***2.2w%* Laponite**		***1w%* Carbopol**	***2.2w%* Laponite**		***1w%* Carbopol**
Time	**t_1**	**t_3**	**-**	**t_1**	**t_3**	**-**	**t_1**	**t_3**	**-**
Fl	0.076	0.068	0.036	0.275	0.379	0.277	0.469	0.571	0.462
Qa/Qr	0.88	1.49	-	0.52	1.10	0.43	3.10	2.84	2.13
Fl_1	0.026	0.033	0.019	0.212	0.285	0.277	0.289	0.344	0.269
Fl_2	-0.032	-0.046	-0.036	-0.095	-0.199	0.195	-0.469	-0.571	-0.462
Fl_3	-0.036	-0.031	0.005	-0.18	-0.181	-0.083	0.151	0.201	0.217

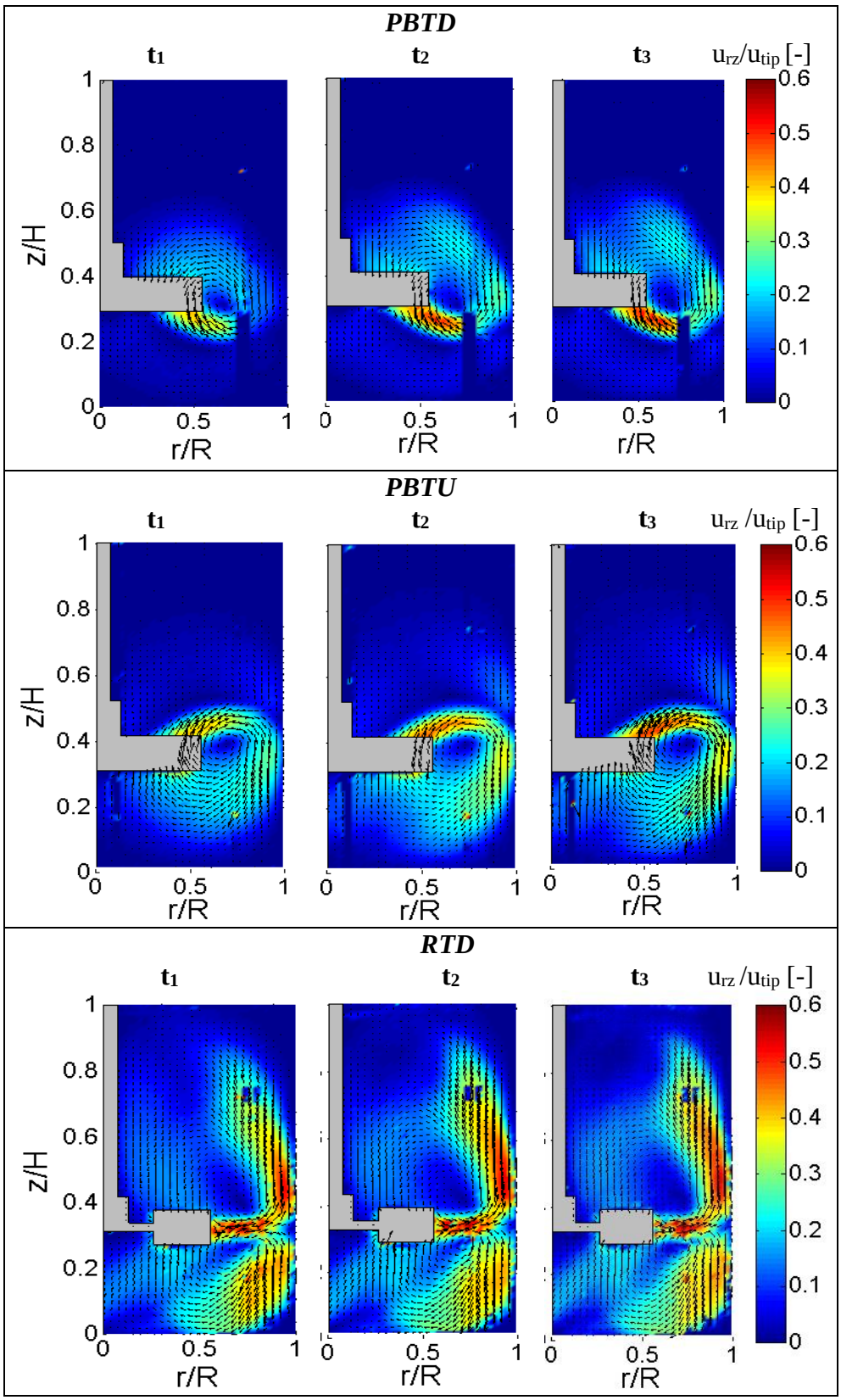

Figure 4.7. The contour of normalized velocity magnitude of three impellers for 2.2*w*% Laponite at Re_{HB} = 158.

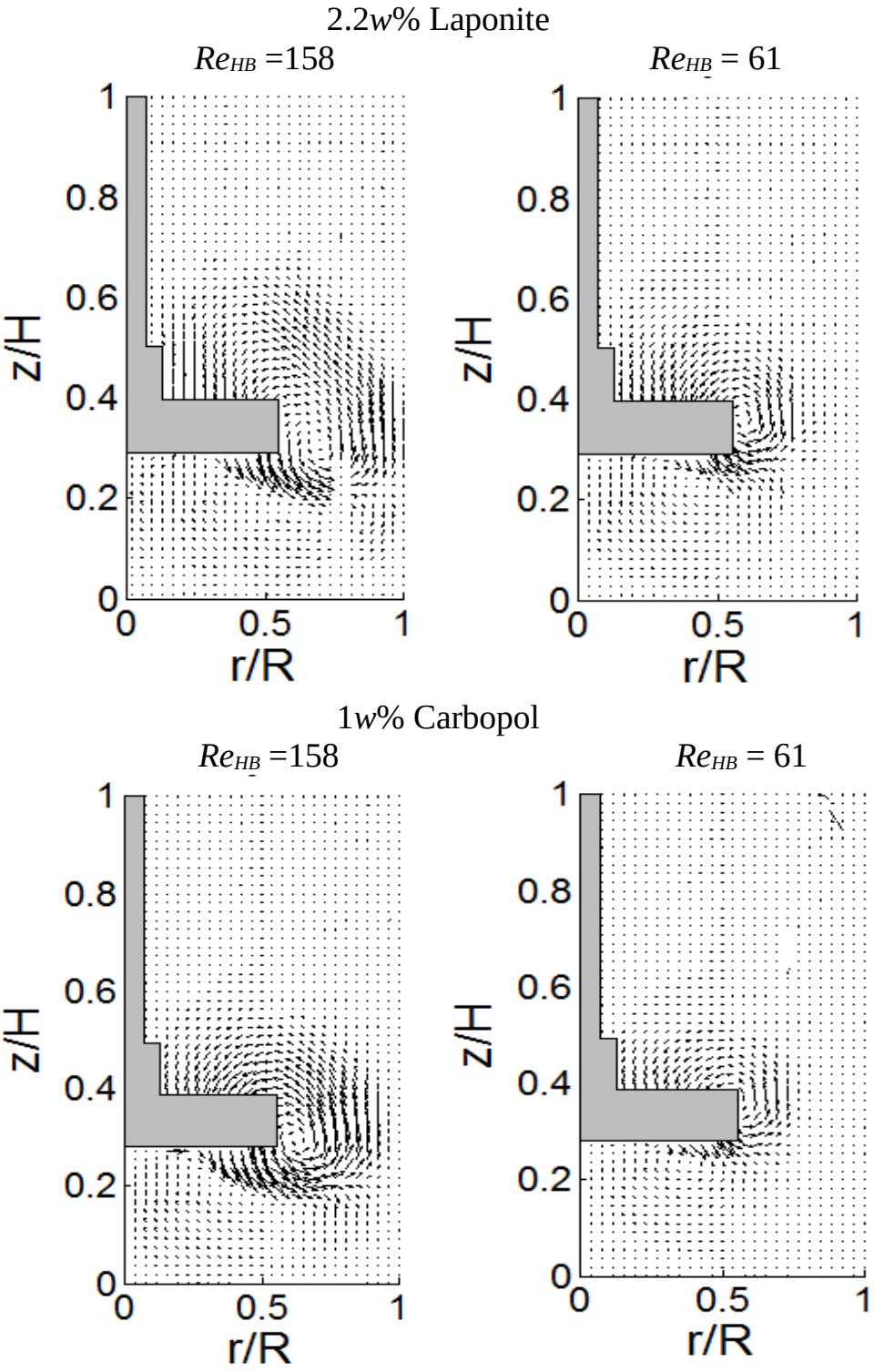

Figure 4.8. Velocity vector on an axial-radial plane for a two flow regime at Re_{HB} = 61 and Re_{HB}=158 for both fluids mixed by the PBTD impeller.

With the impeller type changed to the PBTU configuration, a primary clockwise and a secondary anti-clockwise loop, located above the primary, were observed. These loops developed with time and reached the tank walls, as demonstrated in (**Figure 4.7, Figure 4.10**). At the begging of stirring (interval t_1), the flow velocity and circulation were observed to be very small (**Figure 4.7)**. Nonetheless, they developed with time and reached a steady state condition at t_2. In this case, the impeller discharged the fluid mostly in the axial direction with the axial flow number Fl_1 = 0.431 being noticeably higher compared to the radially flow discharge flow number, Fl_3 = 0.082 (Table 4.4 and **Figure 4.10**).

Table 4.4. Characterized parameters of flow for PBTU impeller.

Re	**7**			**61**			**158**		
Fluid	***2.2w%* Laponite**		***1w%* Carbopol**	***2.2w%* Laponite**		***1w%* Carbopol**	***2.2w%* Laponite**		***1w%* Carbopol**
Time	**t_1**	**t_3**	**-**	**t_1**	**t_3**	**-**	**t_1**	**t_3**	**-**
Fl	0.027	0.03	0.012	0.203	0.304	0.12	0.412	0.435	0.241
Qa/Qr	-	0.70	1.56	0.05	0.189	0.04	2.83	3.64	-
Fl_1	-0.027	-0.03	-0.012	-0.01	-0.048	-0.005	-0.412	-0.431	-0.241
Fl_2	0.041	0.036	0.005	0.253	0.393	0.196	0.358	0.418	0.325
Fl_3	0.006	0.043	0.008	-0.193	-0.256	-0.115	0.145	0.082	0.003

Table 4.5.Characterized parameter of flow for RTD impeller.

Re	**7**			**61**			**158**		
Fluid	***2.2w%* Laponite**		***1w%* Carbopol**	***2.2w%* Laponite**		***1w%* Carbopol**	***2.2w%* Laponite**		***1w%* Carbopol**
Time	**t_1**	**t_3**	**-**	**t_1**	**t_3**	**-**	**t_1**	**t_3**	**-**
Fl	0.172	0.174	0.052	0.305	0.242	0.288	0.453	0.389	0.342
Qa/Qr	-	-	-	-	-	-	-	-	-
Fl_1	0.036	0.041	0.015	0.222	0.227	0.18	0.326	0.308	0.272
Fl_2	-0.097	-0.101	-0.051	0.028	0.007	0.066	0.015	0.046	0.071
Fl_3	-0.075	-0.073	-0.001	-0.305	-0.242	-0.288	-0.453	-0.389	-0.342

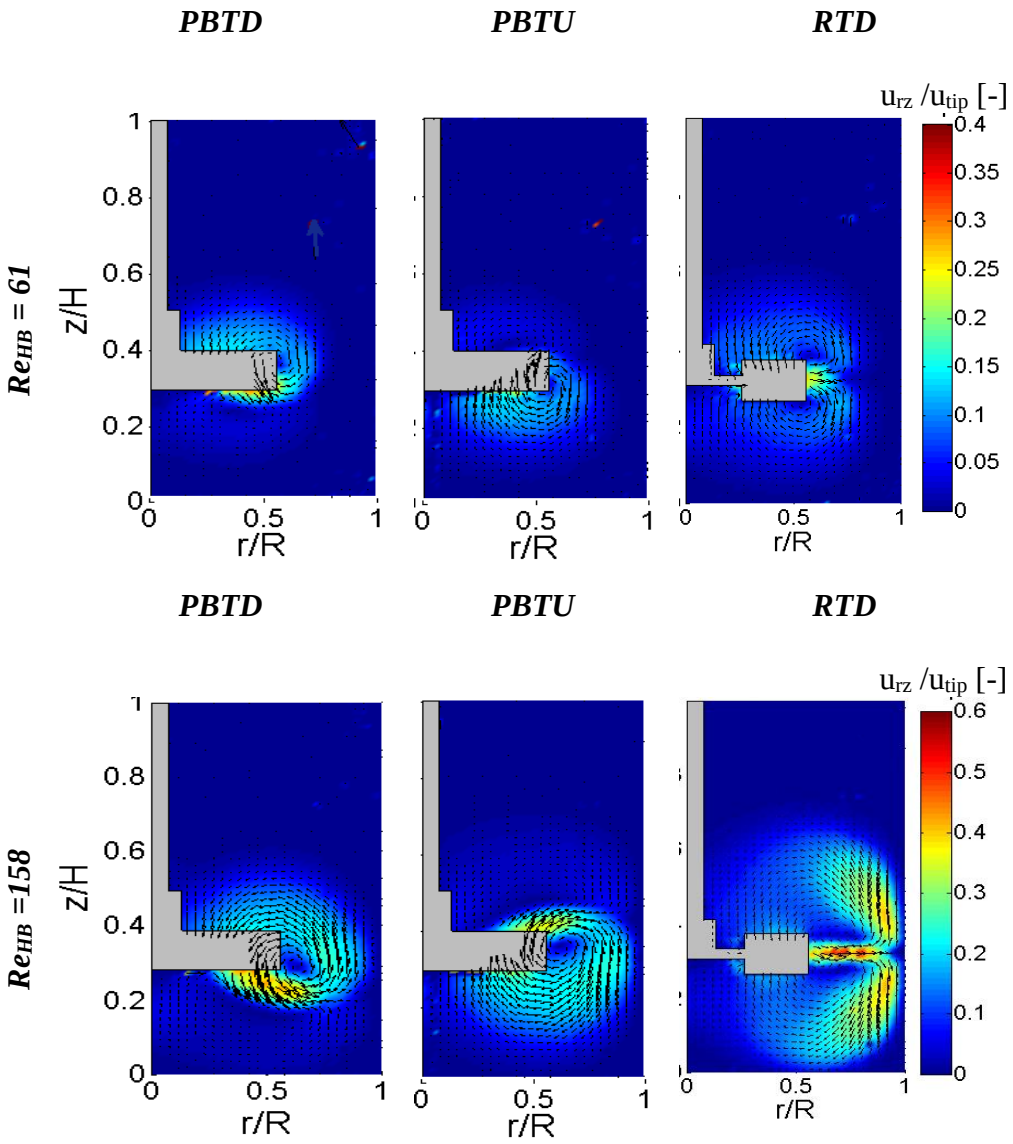

Figure 4.9. The contour of normalized magnitude velocity for the three impellers at Re_{HB} = 61 and Re_{HB}=158 for 1*w*% Carbopol.

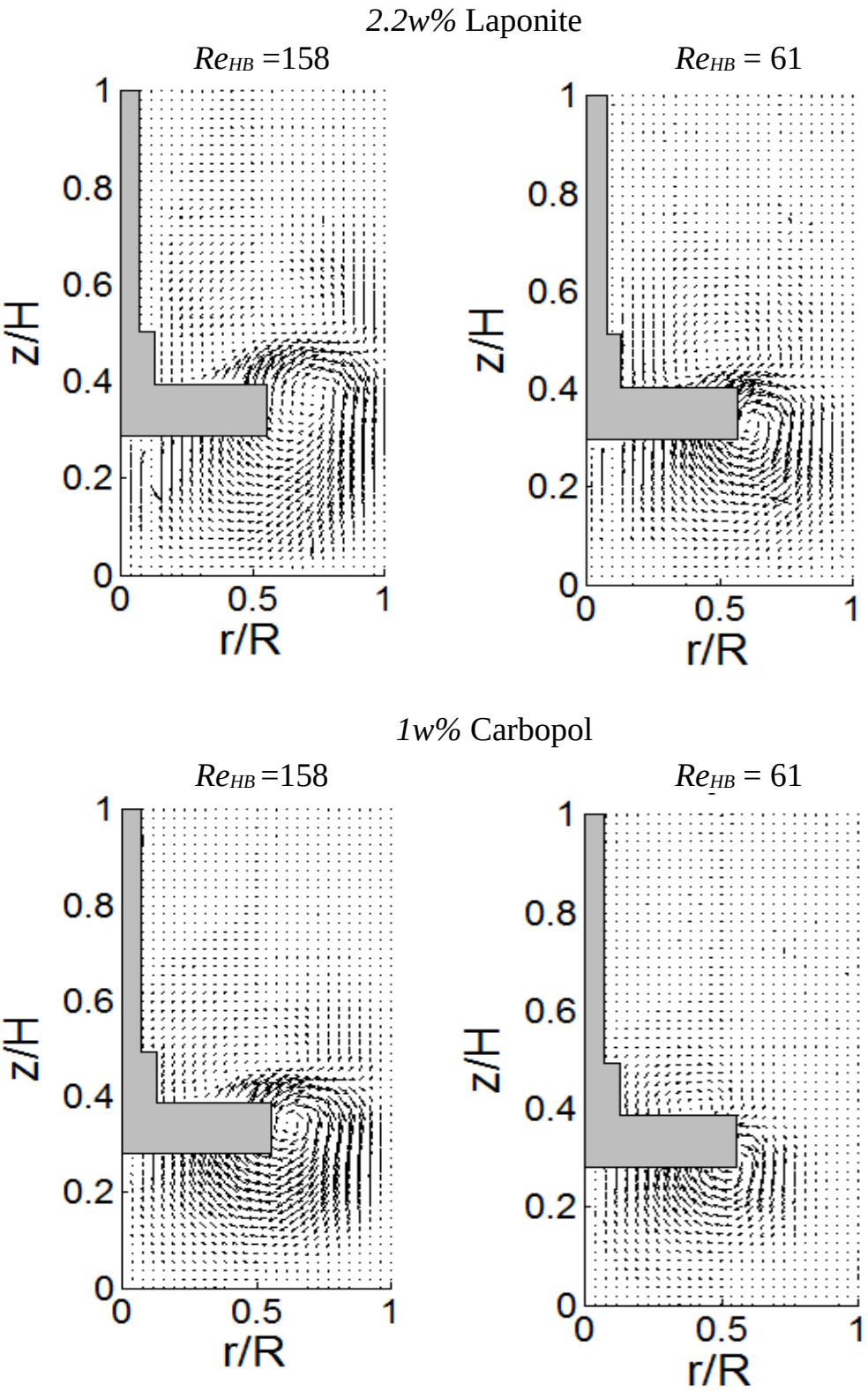

Figure 4.10. Velocity vector on an axial-radial plane for two flow regimes Re_{HB} = 61, Re_{HB} =158 for both fluids mixed with the PBTU impeller.

Moreover, flow circulations developed in regions close to the top of the tank at the height of Z = 0.8H. This suggests an overall improved flow circulation in the tank compared to the PBT DP case. For both PBTU and PBTD configurations the flow reached the steady state condition almost in the middle of mixing time, at interval t_2.

In comparison, the 1*w*% Carbopol fluid revealed a lower velocity, circulation and flow discharge (Fl = 0.241) to that of the thixotropic fluid (Fl = 0.435). A detailed summary is given in (Table 4.4).

The flow fields for the 2.2*w*% Laponite fluid under the RTD configuration showed no significant changes during mixing in terms of both velocity and circulation (**Figure 4.7**). The flow discharged radially reaching and then climbing the tank walls axially to cover almost the whole top surface of fluid, all before the time interval t_1. This shows that the shear stress applied to the fluid in the vicinity of the impeller was much higher than that of the thixotropic fluid. A high shear stress applied only in the radial direction resulted in causing the fluid's viscosity value to drop quickly. Consequently the fluid reached the steady state condition rapidly, as seen in **Figure 4.11**. In the case of RTD configuration, the shear strain rate induced by the impeller was significantly higher compared to that of the PBT (UP&DP) settings at the beginning of stirring.

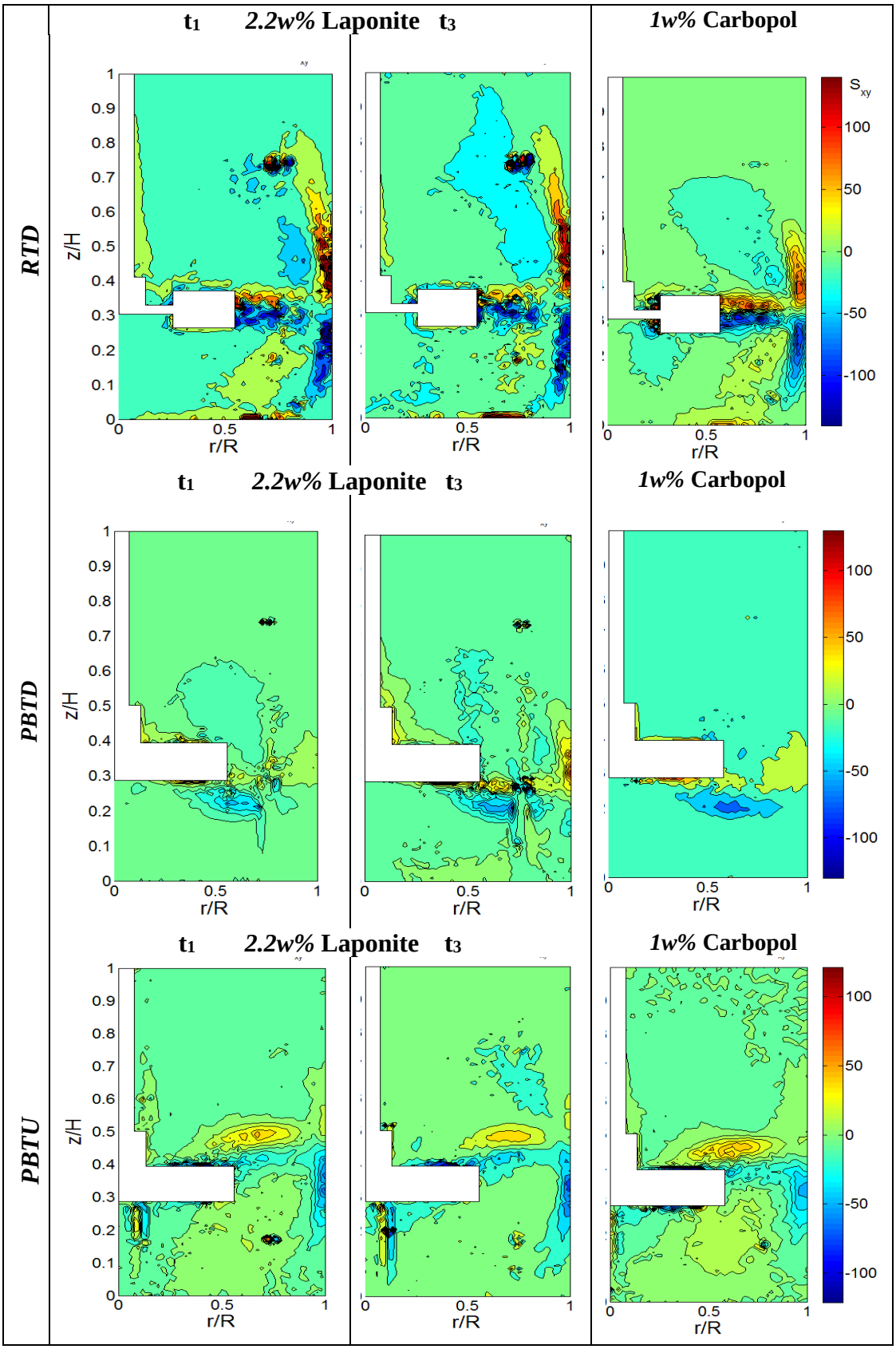

Figure 4.11. Contour of shear strain rate plot for 2.2*w*% Laponite (at t_1 and t_3) and 1*w*% Carbopol fluid.

4.3.1.2 *Re* = 61

shows the velocity fields for a reduced mixing speed at Re_{HB} = 61. The graph still shows presence of both the primary and secondary loops under the three different impeller configurations, however their velocity and circulation loop were reduced in terms of both value and size respectively, compared to the previous cases. The flow fields from the PIV data show the formation of a cavern that grows over the course of mixing, as shown in **Figure 4.12**. The flow was discharged more radially from the PBT impellers (UP&DP) than in the previous case (Re_{HB} = 158), causing a noticeable reduction in the ratio of axial to radial pumping *Qa/Qr* as seen in Table 4.3 and Table 4.4. This is in-line with the findings of Couerbe et al. (2008), Chung (2008) who observed a reduction of axial pumping in an axial impeller configuration for a thixotropic fluid and Newtonian fluid respectively at lower Reynold number. The *Fl* and *Qa/Qr* values exhibited the same increasing trend as seen before with time of stirring. Under the PBT configuration (DP&UP) both the 2.2 *w%* Laponite and the 1.5*w*%Carbopol fluids showed very low *Fl* and Qa*/Qr* values at the beginning of stirring t_1 (see Table 4.3, Table 4.4 and Table 4.5). The pumping capacity (*Fl)* of the thixtropic fluid increased with time and the impeller started to pump in the axial direction more than 50% (*Qa/Qr*) than the beginning of mixing (Table 4.3, Table 4.4, and **Figure 4.12**).

4.3.1.3 *Re* = 7

Further reduction of mixing speed brings the flow condition to the laminar regime at Re_{HB} = 7. As can be seen in **Figure 4.13** and Tables 4.3 to 4.5, the flow pumping capacity for the 2.2 *w%* Laponite fluid remained compariteveley the same from t_1 to t_3, being

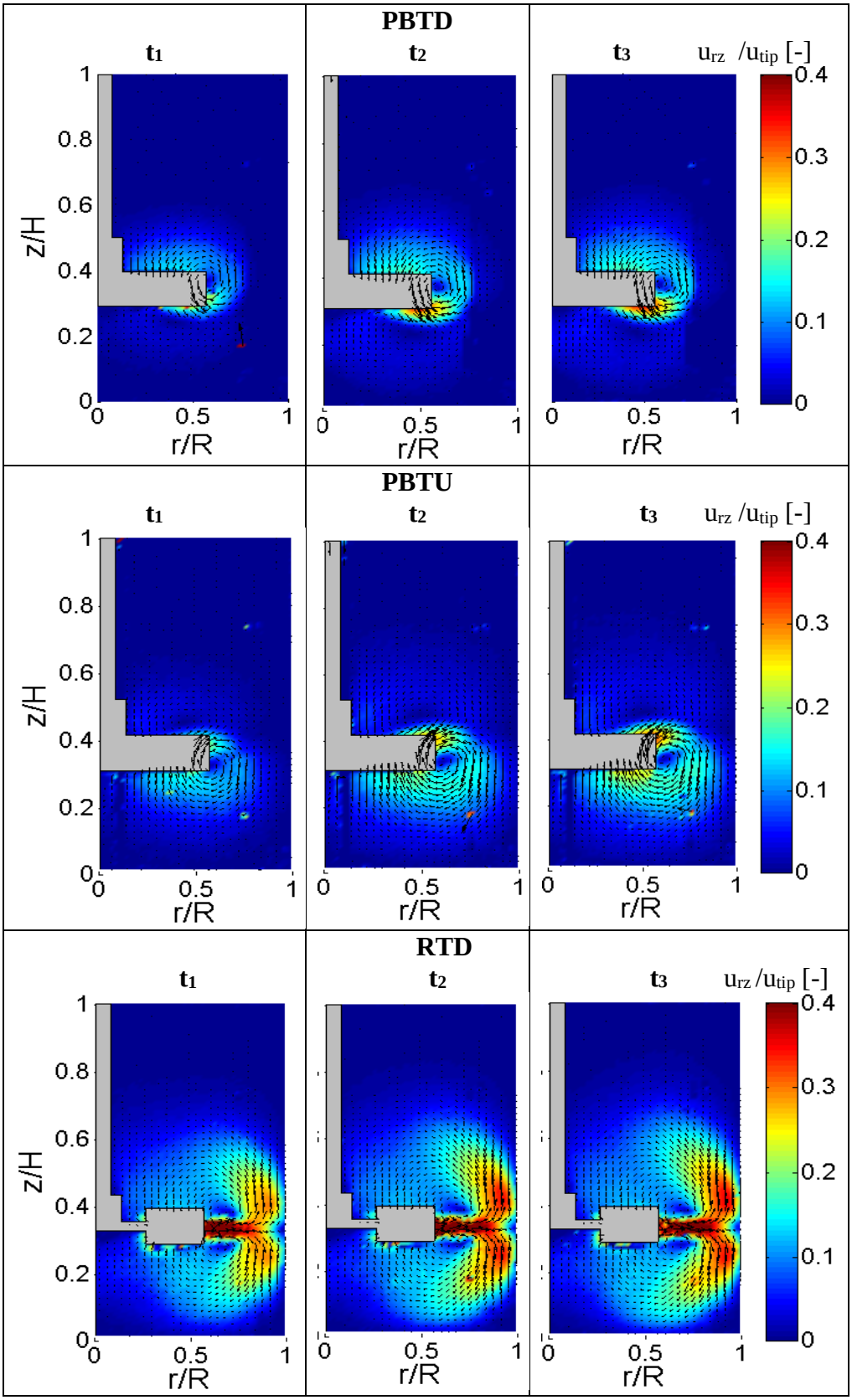

Figure 4.12. The contour of normalized magnitude velocity for three impellers for 2.2*w*% Laponite at Re_{HB} = 61.

significantly reduced at t_3 compared to the previous mixing speeds under the three impeller configurations (PBTU: Fl = 0.03, PBTD: Fl = 0.068, RTD: Fl = 0.174). Similar results were reported by Hall (2005) and Couerbe et al. (2008). The pumping capacity Fl = 0.02 in an axial impeller configuration at $N = 1\ s^{-1}$ was calculated by Couerbe et al. (2008) in both experiment and simulation. In comparision to the thixtropic fluid, the 1.5*w*% Carbopol fluid shows lower flow numbers Fl for all three impeller configurations (PBTU: Fl = 0.012, PBTD: Fl = 0.036, RTD: Fl = 0.052).

Using a radial RTD impeller showed that the flow pattern of the thixotropic fluid at a high Re changed significantly compared to a lower Re value. In the latter case, despite a fully radially discharged impeller being used, the flow was observed to leave the impeller blades at an angle to the radial direction and formed two familiar loops in the tank. This diverse flow pattern made by the RTD impeller was also observed for Newtonian and shear-thinning fluids (Rice et al., 2006, Arratia et al., 2006). Rice et al. (2006) observed a reduction in pumping capacity and change of flow pattern for an RTD impeller at Re = 1 compared to that observed at higher Reynolds number, which accounted for the flow diverging from the radial direction. In the case of a very low value of Re_{HB} = 7, the flow is mainly under a balance between viscous and pressure forces (that are generated by the rotation of the impeller) while inertial forces can be largely neglected. This results in an increased axial flow discharge (e.g. for the 2.2*w*% Laponite fluid PBTD: Qa/Qr = 1.49, PBTU: Qa/Qr = 0.7) compared to what is seen for Re_{HB} = 61 for all three impellers used, for both the time-dependent and time-independent fluids studied in this work (Table 4.3, Table 4.4 and Table 4.5). Nouri and Whitelaw (1990) reported that the flow angle

leaving a PBT impeller is dependent on Reynold number rather than fluid rheology for shear-thinning and Newtonian fluids.

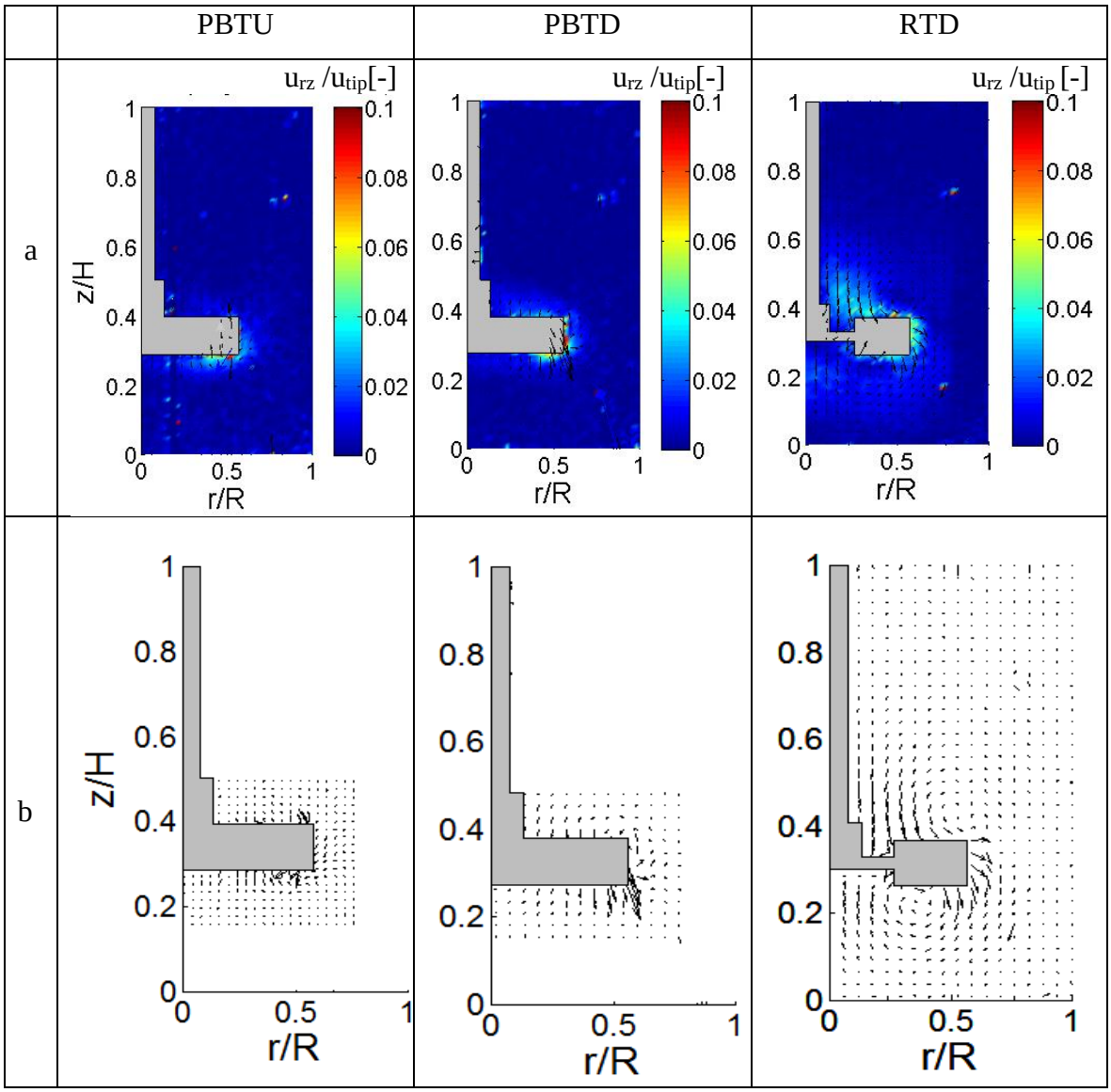

Figure 4.13. (a) Normalized magnitude velocity for three impellers at Re_{HB}= 7 for 2.2*w*% Laponite fluid at t_3, (b) velocity field for three impellers at Re_{HB} = 7 for 2.2*w*% Laponite fluid at t_3.

4.3.2 Cavern Growth

Due to the thixotropic fluids having a yield stress, a cavern is formed inside the tank at low velocities (i.e. low mixing speeds). Since all of the mixings takes place inside the cavern area, measurements of cavern size would provide valuable information about the extent of mixing of the fluid. A velocity threshold of $u_{uv} = 0.01u_{tip}$, as proposed by Adams and Barigou (2007), was used in this work to define the cavern boundary and subsequently obtain the cavern size. Cavern diameter (*Dc*), cavern height (H_c) and the ratio of cavern area to tank area (A_C/A_T) are the parameters that were used to characterize the cavern in these fluids.

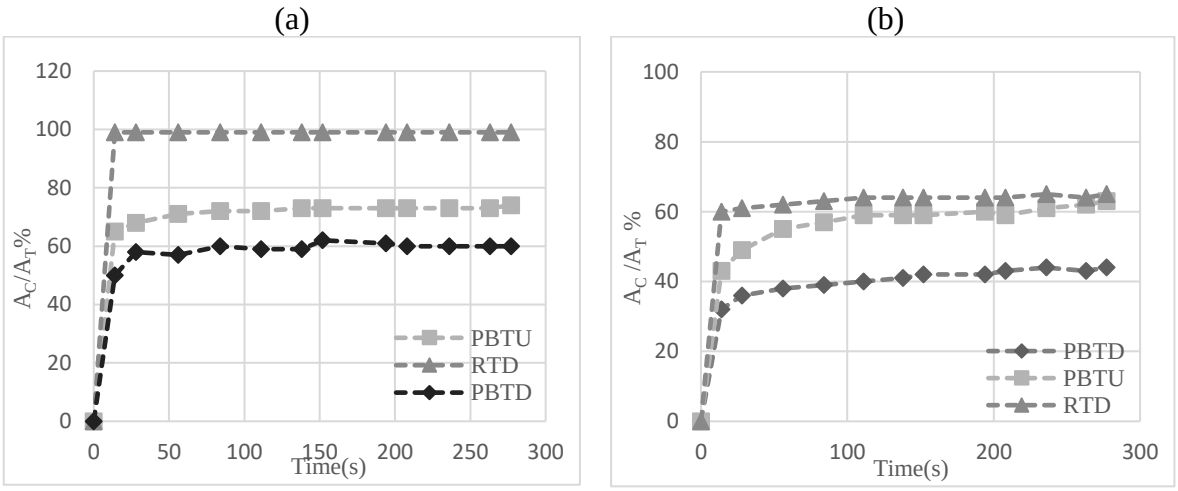

Figure 4.14. The changes of normalized cavern area % for the thixotropic fluid as a function of time for (a) Re_{HB}= 158 and (b) Re_{HB} = 61.

Variations of cavern size A_C/A_T with time for Re_{HB} = 61 and Re_{HB} = 158 are presented in **Figure 4.14**. The data shows that the cavern grows radially (*Dc*) at Re_{HB} =158 under the PBT (UP & DP) impeller configuration and reached the tank walls within t = 50 s (**Figure 4.15a**). The cavern then expanded axially (H_c) and reached a height of $Z = 0.86$

H in the case of an up pumping impeller, and *Z = 0.70 H* in a down pumping case, with its size (A_C/A_T) becoming steady at *t* = 150 s (**Figure 4.14a**). In contrast, under the RTD impeller configuration the cavern suddenly expanded and its radius (D_c) and height (H_c) reached the tank walls and the top surface of the fluid before *t* = 14 s

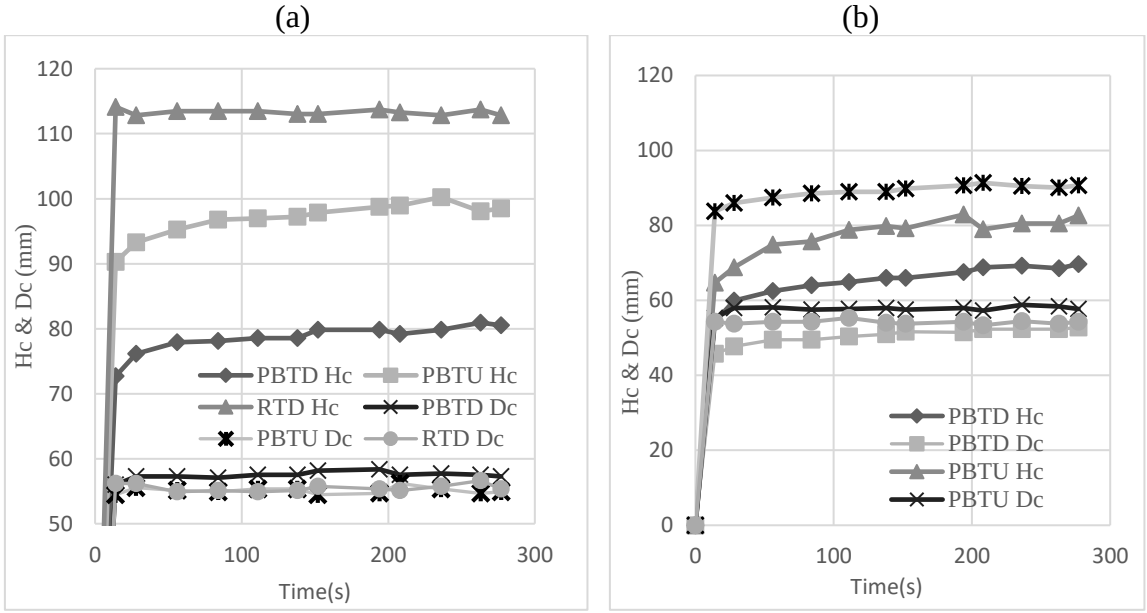

Figure 4.15. The cavern height and radius growth as a function of time for the thixotropic fluid at (a) Re_{HB} =158, (b) Re_{HB} = 61.

When the mixing speed was reduced to obtain Re_{HB} = 61, an elliptical-shaped cavern was formed around the impeller under the PBT impeller configurations, as demonstrated in **Figure 4.16**. In this case, the cavern radially grew (*Dc*) until *t* = 100 s then expanded axially to reach the height of vessel at *Z = 0.7 H* (PBTU) and *Z = 0.6 H* (PTBD) until *t* = 200 s (see **Figure 4.15b**). However, under an RTD impeller configuration, the cavern continued to develop until *t* = 100 s and reached its steady state size at Z = 0.78H (see **Figure 4.15b**).

The difference between cavern boundary of the Laponite fluid compare to the Carbopol fluid is illustrated in **Figure 4.16**. The evaluation of cavern over time under the PBT impeller configurations shows that both fluids have almost the same cavern shape and size at t_1, although with time the 2.2*w*% Laponite cavern develops to reach its final form at t_3. In constrast, the cavern in the Carbopol developed instantly and did not grow further as a function of time (Adams and Barigou, 2007). Finally, under the RTD impeller configuration the cavern boundary of the 2.2*w*% Laponite at t_1 had been almost entirely developed.

PLIF measurements at Re_{HB} = 7 (see **Figure 4.17)** show the cavern growth in the 1 *w*% Carbopol to be instant. As the fluorescent dye mixes inside the cavern it begins to slowly expand into the fluid cavern, thus giving an indication of the rate of fluid mixing while reaching the actual cavern boundary.

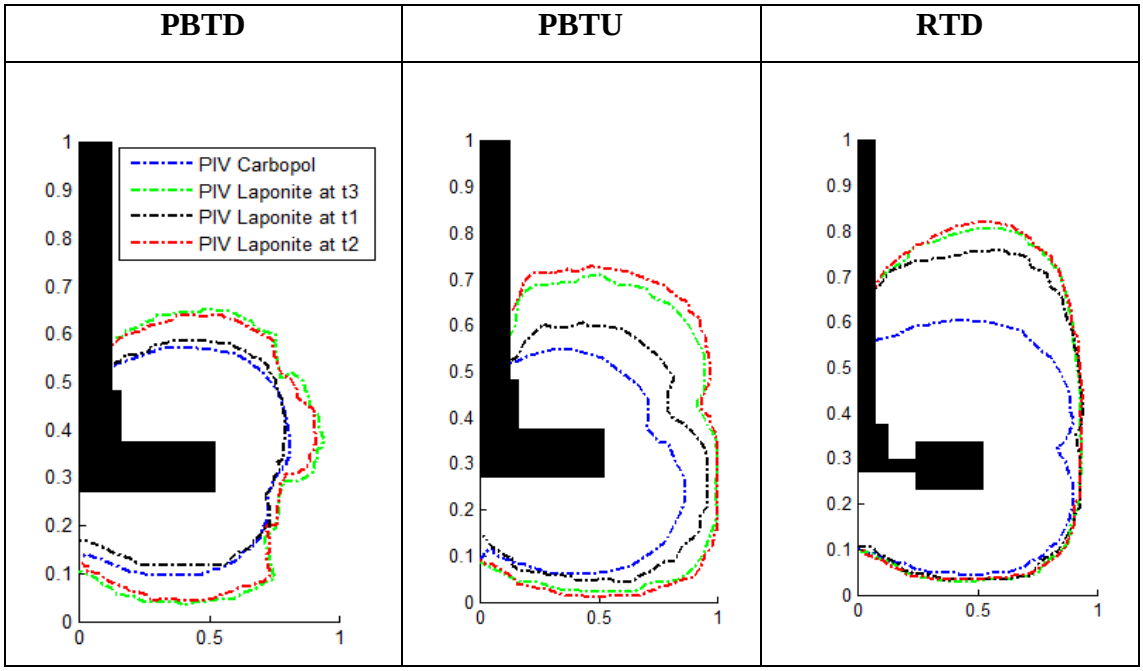

Figure 4.16. Schematic diagram of cavern growth while mixing for 2.2*w*% Laponite and 1*w*% Carbopol at Re_{HB} = 61.

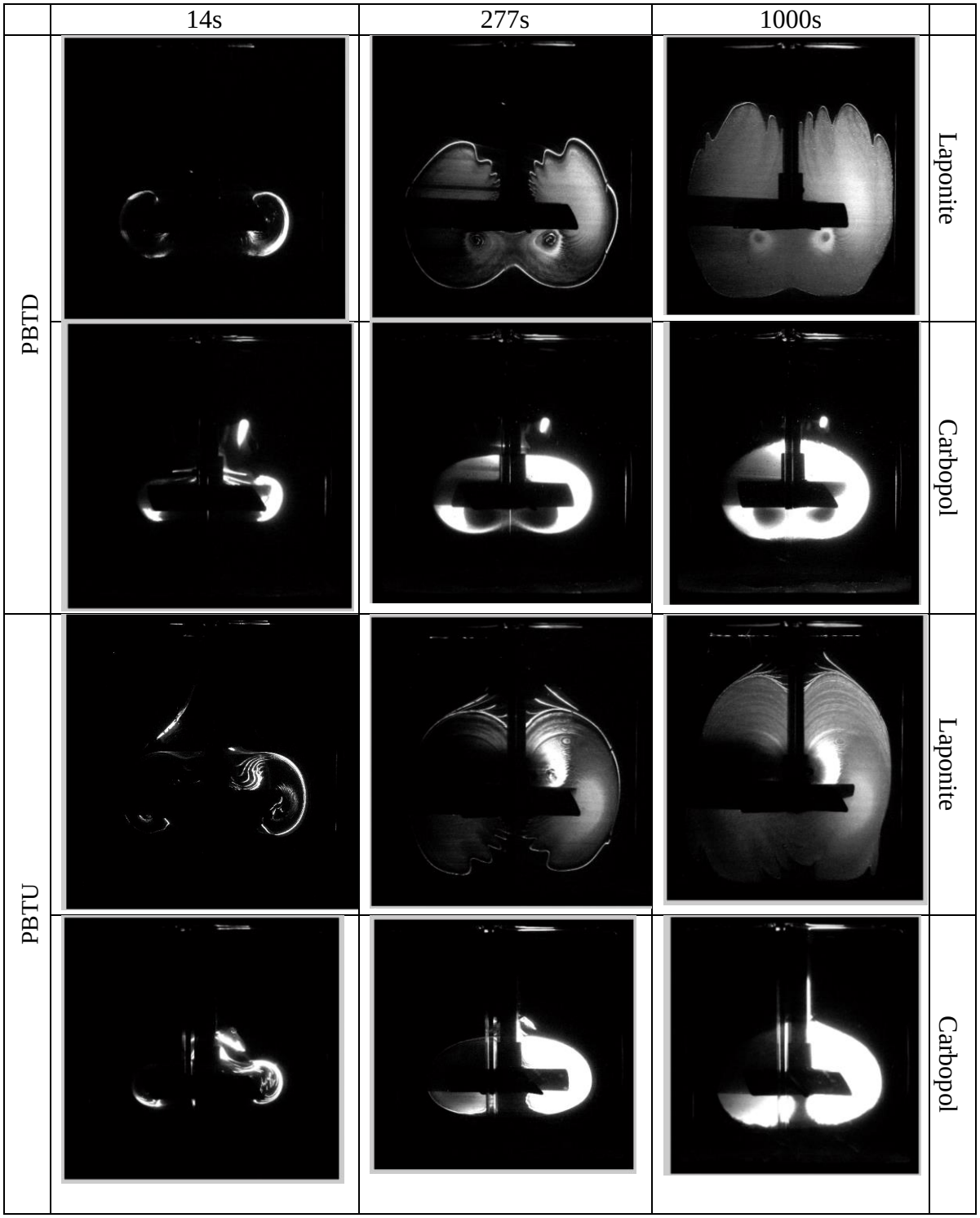

Figure 4.17. The cavern growth from PLIF experiments for both 1w% Carbopol and 2.2w% Laponite fluid at Re_{HB} = 7.

The cavern boundary in the Laponite fluid started to develop very gradually until it stopped growing at t = 1000 s, with the fluorescent dye being found to still be inhomogeneously mixed inside the cavern as shown in **Figure 4.17**. The difference in cavern shape and development pattern for the thixotropic and viscoplastic fluids indicate that for the former a significant axial growth was also followed by a radial growth, resulting in an irregular cavern boundary.

4.3.3 Effect of Non-standard Configurations

4.3.3.1 Un-baffled Vessel

Conventionally, baffles are used to prevent solid body rotation of fluid in a tank, so as to enhance mixing performance. In Newtonian fluids, especially in a turbulent regime, it is desirable to use baffles in order to improve axial circulation and prevent the formation of the free vortex at the surface of fluid as well as reducing mixing time (Armenante et al., 1997, Chung, 2008). However, this does not necessary apply for Non-Newtonian fluids; Hirata and Aoshima (1996) observed that baffles have a negative effect on the cavern size growth in the case of viscoplastic fluids.

Figure 4.18 shows a variation of Power number as a function of Reynolds number in the cases of baffled and un-baffled configurations with RTD impeller for both a viscoplastic fluid and a Newtonian fluid.

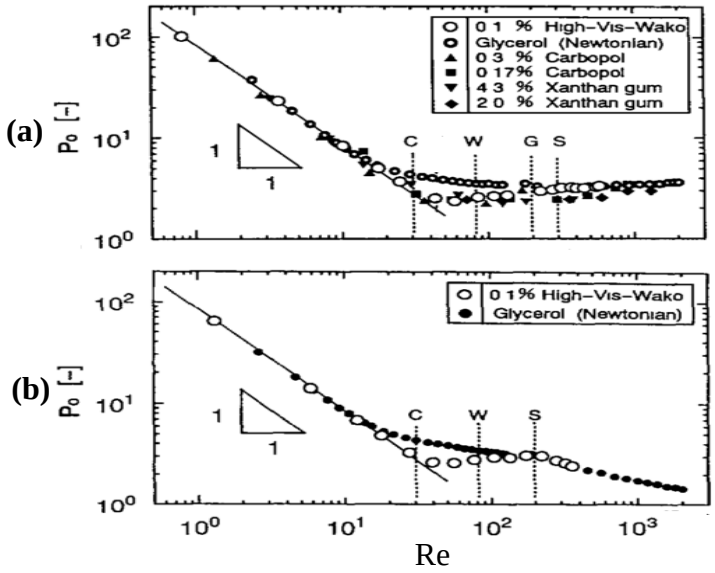

Figure 4.18. Variation of Power number as a function of Reynold number for viscoplastic fluid in the (a) baffled vessel and (b) un-baffled vessel. Image adopted from Hirata and Aoshima (1996).

The graph shows that the cavern began to grow at a Reynold number where the viscoplastic power number deviates from that of the Newtonian fluid (marked as point C in the graph). In this case, the cavern continued to develop until it reached the walls of the tank (marked as point *W* in the graph). The cavern growth is almost the same for both the un-baffled and baffled tank.

From this point onward for the baffled tank the cavern did not grow with increasing Reynold number. The cavern did, however, begin to redevelop vertically (marked as point *G* in the graph) until it reached the surface of the tank (marked as point S in the graph). In the *W-S* region the viscoplastic fluid in the un-baffled tank revealed a larger cavern size compared to that seen in the baffled tank (Hirata and Aoshima, 1996), indicating that the baffles prevented axial expansion of the cavern.

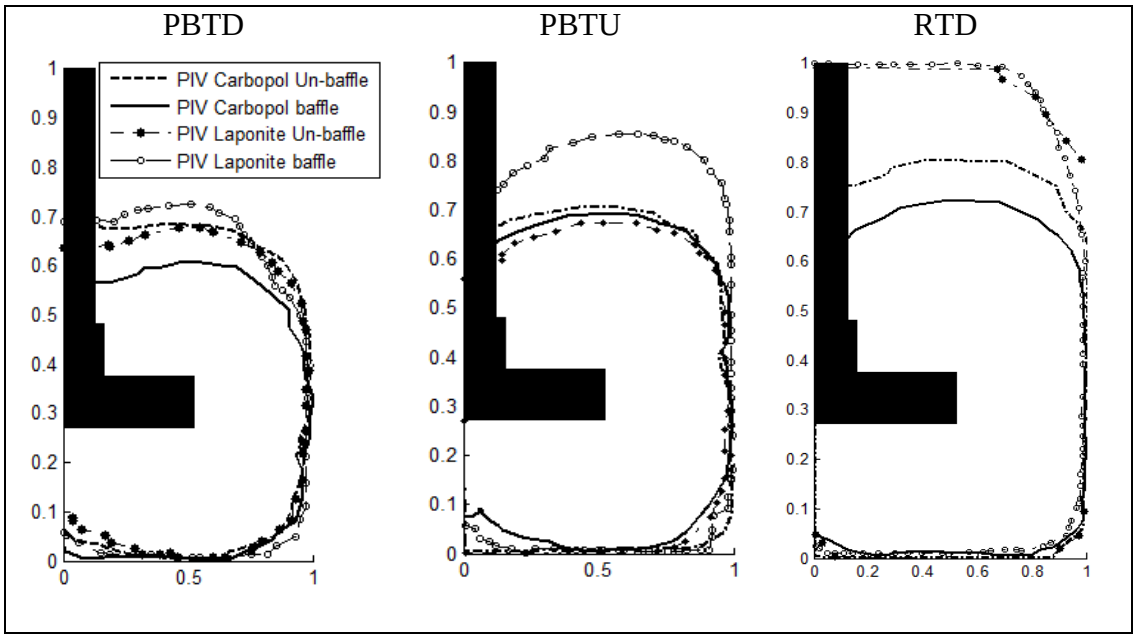

Figure 4.19. The cavern shape and size for the thixotropic and viscoplastic fluids in the baffled and un-baffled vessel at Re_{HB} = 158.

This unusual behavior of the viscoplastic fluid motivated a study on the thixotropic fluid, in order to investigate whether it exhibited similar behavior under the same condition. To this end a flow regime at Re_{HB} = 158 was chosen. A series of PIV measurements were performed on a viscoplastic fluid (1*w*% Carbopol). The results confirmed Hirata and Aoshima (1996) works that the cavern size was smaller in a baffled tank compared to the un-baffled case for all three impeller configurations, **Figure 4.19**.

Table 4.6. Characterized parameters of flow for thixotropic fluid in the un-baffled vessel.

Re	**PBTD**			**PBTU**			**RTD**		
Fluid	***2.2w%* Laponite**		***1w%* Carbopol**	***2.2w%* Laponite**		***1w%* Carbopol**	***2.2w%* Laponite**		***1w%* Carbopol**
Time	**t_1**	**t_3**	**-**	**t_1**	**t_3**	**-**	**t_1**	**t_3**	**-**
Fl	0.421	0.590	0.504	0.323	0.414	0.350	0.300	0.425	0.367
Qa/Qr	1.71	0.42	1.32	1.96	0.58	1.76	-	-	-
Fl_1	0.369	0.536	0.435	-0.214	-0.152	-0.223	0.425	0.478	0.315
Fl_2	-0.266	-0.176	-0.286	0.359	0.482	0.425	0.264	0.290	0.034
Fl_3	-0.155	-0.414	-0.218	-0.109	-0.262	-0.127	-0.300	-0.425	-0.367

This can be explained by the inability of the fluid to overcome its yield stress due to momentum losses taking place near the baffles. However, the PIV measurements showed almost the same flow pattern (qualitatively) under the PBT impellers (UP & DP) in both of baffled and un-baffled tank (see **Figure 4.20**). For the un-baffled tank the flow number has a higher value of Fl = 0.504 (PBTU) and Fl = 0.35 (PBTD) than for the baffled tank. A comparison is given in Table 4.6. Moreover, the radial velocity component along the axial direction at $r = 0.85R$ in $z = 0.3H$ (**Figure 4.21**) shows a higher value in the un-baffled tank under the PBT impeller configurations compared to the baffled case. However, along the radial direction noticeable difference were not observed in axial and radial velocities between the baffled and un-baffled tanks (**Figure 4.22**). Under the RTD configuration the impeller induced a radial flow, which developed to the side walls of the tank. Two circulation loops were formed which were observed to be larger in the un-baffled tank, despite a lower velocity magnitude being observed (**Figure 4.20**). This, however, is due to the limitation of the PIV procedure in capturing the tangential velocity component (the third component normal to the plane of view), which is dominant in the un-baffled case.

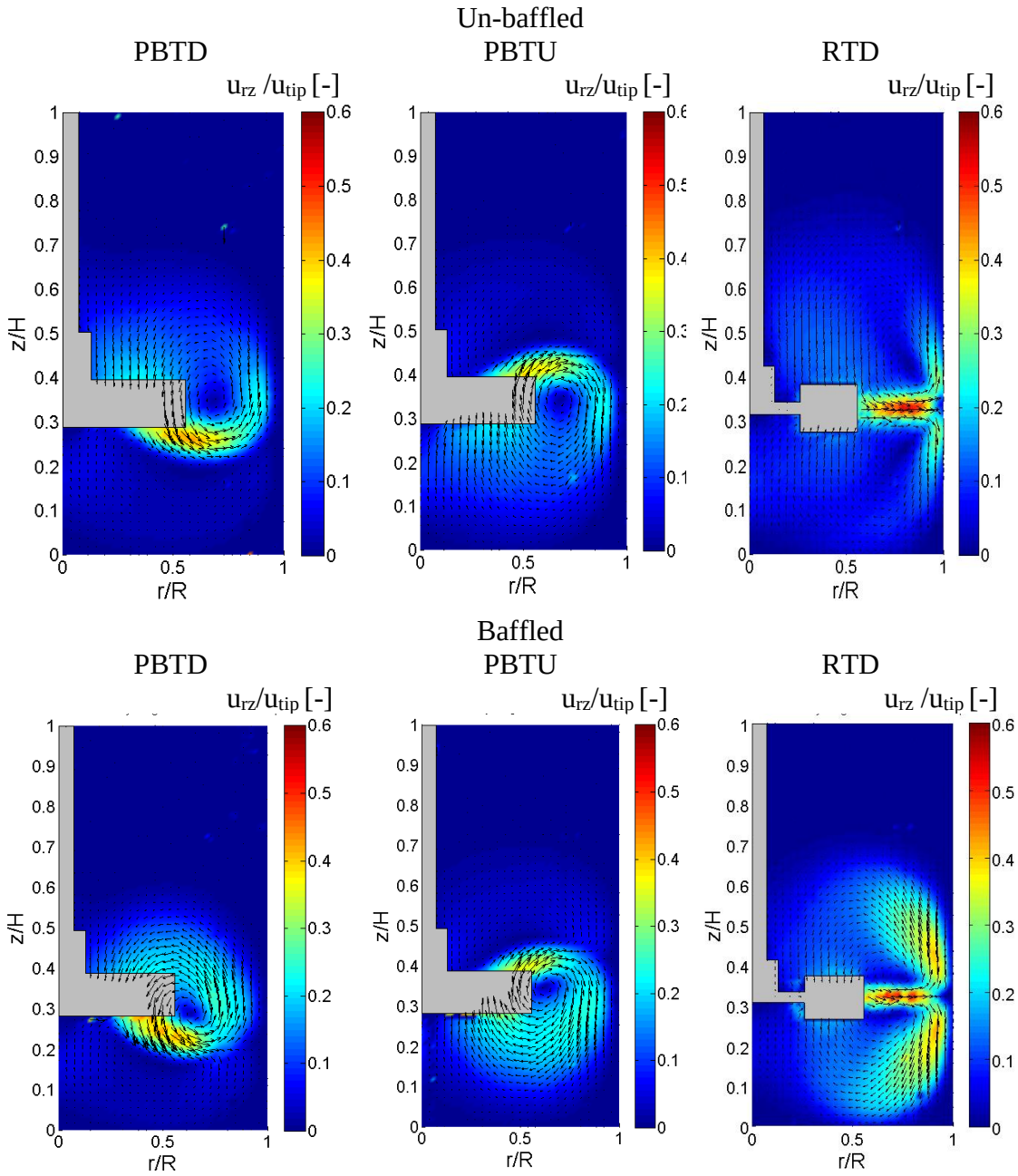

Figure 4.20. The contour of normalized magnitude velocity of three impellers at Re_{HB} = 61 for 1 *w*% Carbopol.

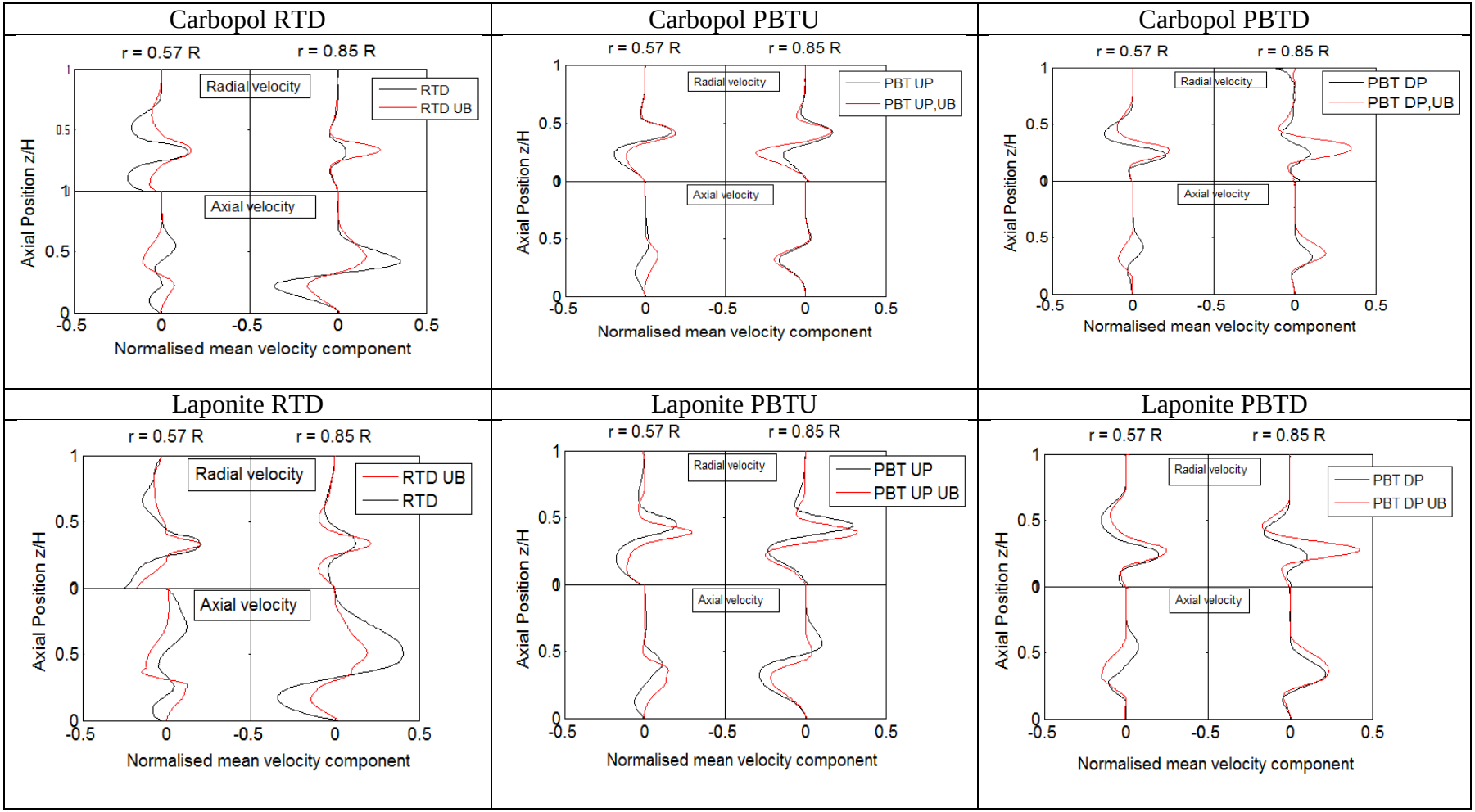

Figure 4.21. The Normalized mean velocity component (radial and axial) at two axial positions for 1*w*% Carbopol and 2.2*w*% Laponite at Re_{HB} =158 in a baffled and un-baffled tank.

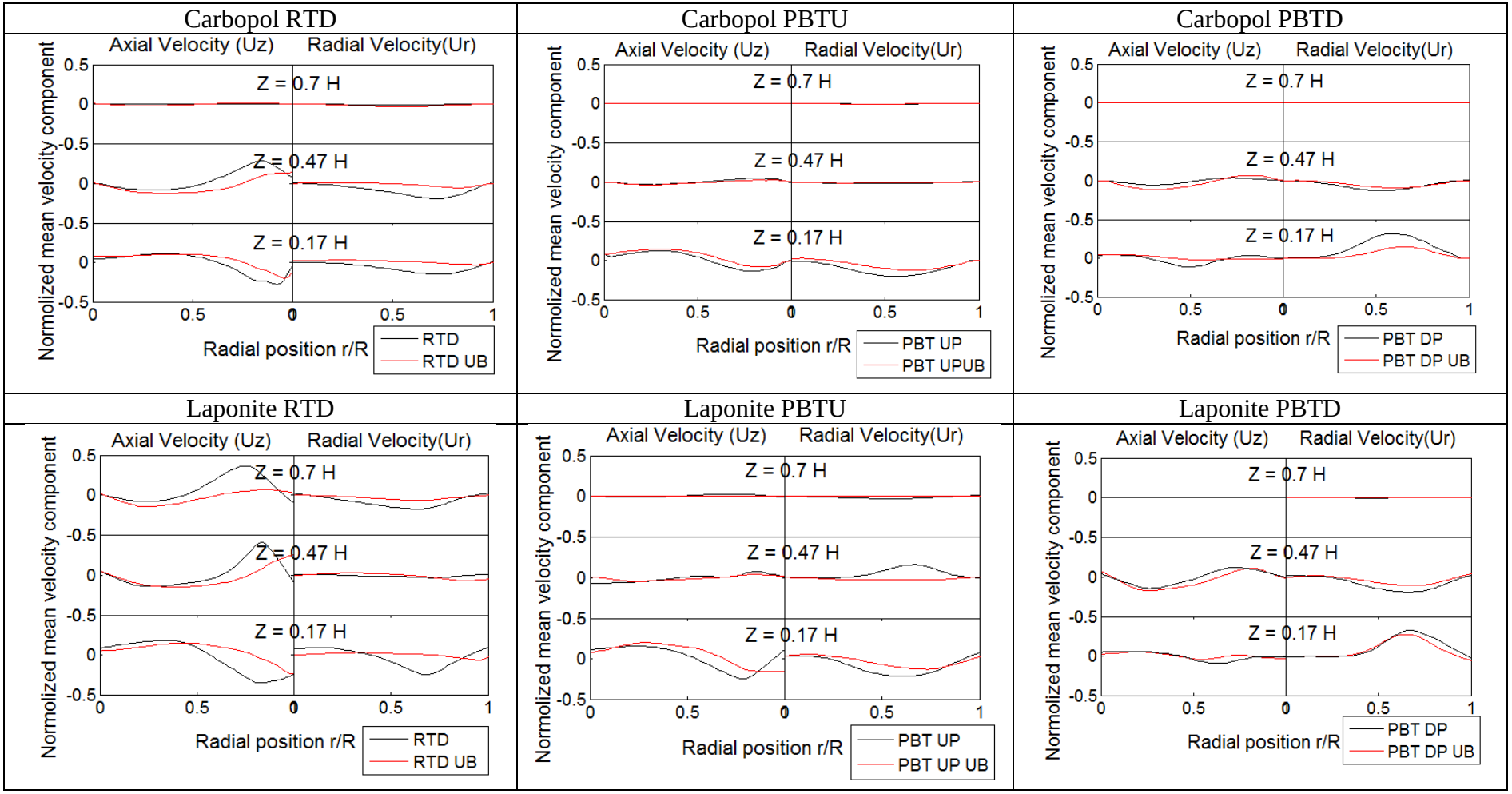

Figure 4.22. The normalized mean velocity component (radial and axial) at three horizontal positions for 1*w*% Carbopol and 2.2*w*% Laponite at Re_{HB} = 158 in a baffled and un-baffled tank.

Regarding cavern size for the thixotropic fluid, an unexpectedly opposite response to the baffle presence was observed. The larger cavern was formed in the baffle tank compared to the un-baffled tank (**Figure 4.19**, **Figure 4.23**). In this case, the fluid's yield stress and apparent viscosity were reduced during the mixing; therefore, the energy supplied to the fluid was mostly consumed to divert the flow from a tangential direction to an axial one, as the fluid's momentum increased with time.

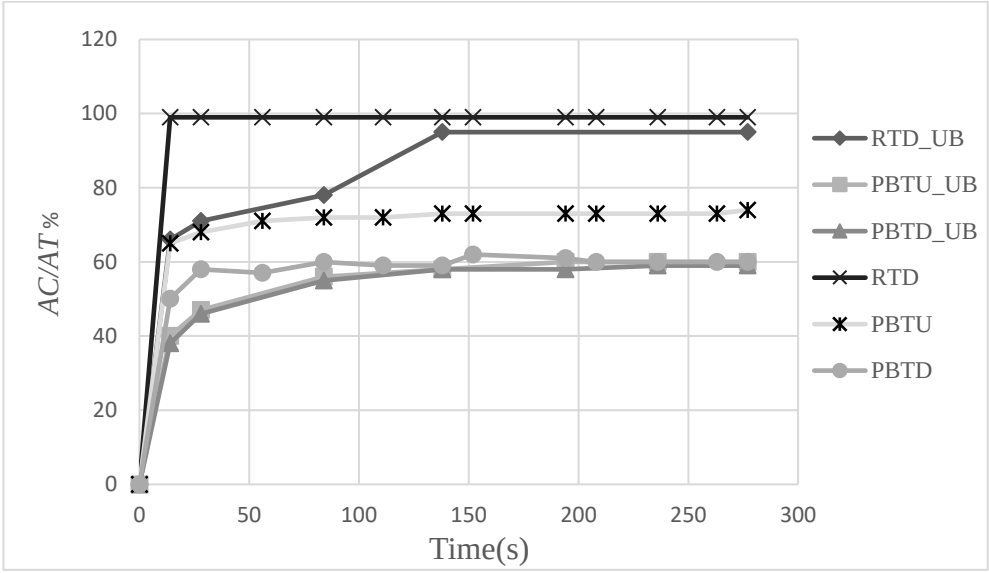

Figure 4.23. The cavern size growth ratio for the thixotropic fluid during mixing in the baffled and un-baffled vessel at Re_{HB} =158.

Furthermore, under the RTD impeller configuration, the cavern was observed to reach the top surface of the fluid in both cases of the baffled and un-baffled tank, although in the former case the cavern took longer to reach the same condition (**Figure 4.23**, **Figure 4.24**). Overall, under all impeller configurations, the flow number was found to be lower in the case of the un-baffled tank (Table 4.6). The axial discharge ratio *Qa/Qr* for the PBT impellers was higher at the initial time interval t_1 (PBTD: *Qa/Qr =1.71,* PBTU*: Qa/Qr = 1.96)* compared to the final time interval t_3 (PBTD: *Qa/Qr = 0.42, PBTU: Qa/Qr = 0.58)*

(Table 4.6). This indicates that the radial flow became more dominate during the mixing, and the axial discharge was reduced with time. In the baffled tank, the axial velocity component was found to be higher along the axial direction at $r = 0.47R$ and 0.85 R (see **Figure 4.21**) and also along the radial direction at $Z = 0.17H$, $0.47H$ and $0.70H$ (see **Figure 4.22**).

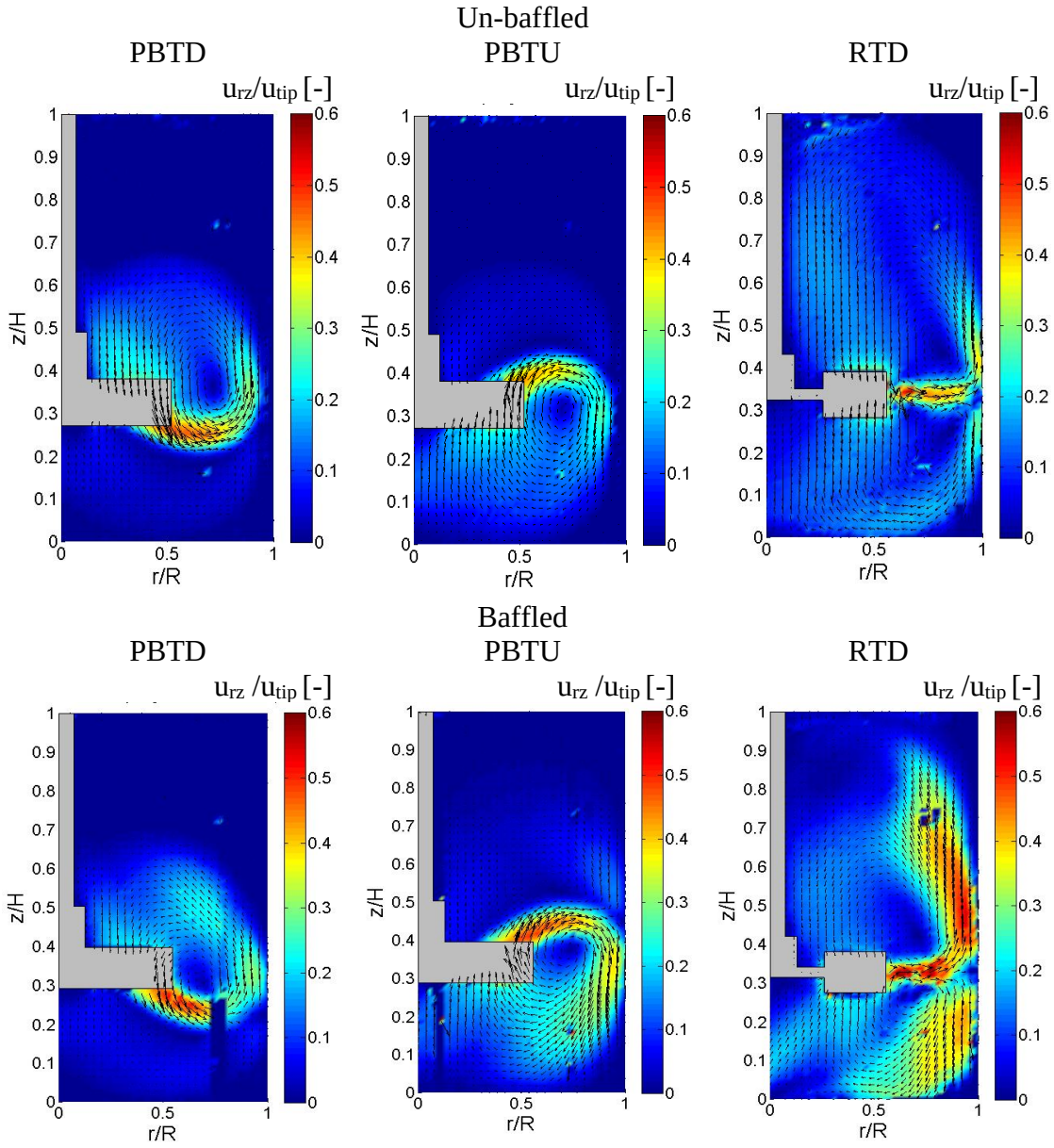

Figure 4.24. The contour of normalized magnitude velocity for three impellers at Re_{HB} = 158 for 2.2*w*% Laponite.

4.3.3.2 Off-bottom Clearance Effects

In order to investigate the effect of the impeller bottom clearance on the mixing of a thixotropic fluid agitated by PBT impellers (DP & UP), the impeller was moved from the standard position (*T/3*) to the higher (*T/2, 3T/4*) and lower (*T/4*) positions for two Re number: Re_{HB} = 61 and Re_{HB}=158. For the RTD impeller, the fluid cavern reaches almost to the top surface and bottom of the tank in both flow regimes and as such the effect of off bottom clearance of impeller on the cavern size and growth was not considered in this study.

Figure 4.25 and **Figure 4.26** show the velocity flow fields from PIV measurements at Re_{HB} = 158 for both the viscoplastic and thixotropic fluids mixed by PBT impellers. The PBT impellers created the familiar flow pattern at different off bottom clearances. Impeller position had less of an effect on flow pattern for the viscoplastic fluid (1*w*% Carbopol), owing to the fact that the flow velocity and circulation loop size remained almost constant for different off bottom clearances. The same effect was observed by LIU (2013).

For the thixotropic fluid at impeller position (*T/3*) and (*T/2*), for both impellers modes, higher flow velocity was observed compared to other impeller positions at Re_{HB} = 158, as seen in **Figure 4.26**. Moving the impeller position from *C = 0.25T* to *C = 0.33T,* then further to *C = 0.5T* resulted in the formation of an increasingly larger secondary flow circulation loop above the primary circulation loop for the PBTU impeller close to the top free surface of the fluid. Further increase of the impeller position to *C = 0.75T* led to a reduction in flow velocity, with the upper circulation loop no longer being present.

Whereas, from the above it is clear to see that the secondary circulation at higher flow regimes is affected significantly by off bottom clearance, impeller bottom clearance appeared to have no effect on the discharge angle of flow in a thixotropic fluid. Specifically, as was discussed previously in this chapter, the discharge angle of PBT impeller was mainly affected by impeller speed (Reynold numbers).

The effect of the impeller bottom position on the cavern size and growth during mixing of thixotropic fluid was studied by variation of the normalized cavern area (*Ac/Tc* %) as calculated via results from PIV experiments (**Figure 4.27**). Cavern size (*Ac/ Tc*) is noticeably low for an impeller bottom clearance of *C = 0.25T* for both PBT impellers and flow regions (Re_{HB} = 61, Re_{HB} = 158). Increasing the impeller position to *C = 0.33T* significantly enhanced the cavern growth for both PBT impeller configurations. Further increase of impeller position to *C = 0.5T* generated a larger cavern in the PBTU configuration at Re_{HB} =158, whereas no change in cavern size was observed for the PBTD configuration. Ein-Mozaffari and Upreti (2009) observed better mixing efficiency and lower mixing time at higher impeller positions than the standard position T/3 in the viscoplastic fluid. Furthermore, moving the impeller to the top of tank at C=*3T/4* caused the cavern size reduced in both up and down pumping impellers.

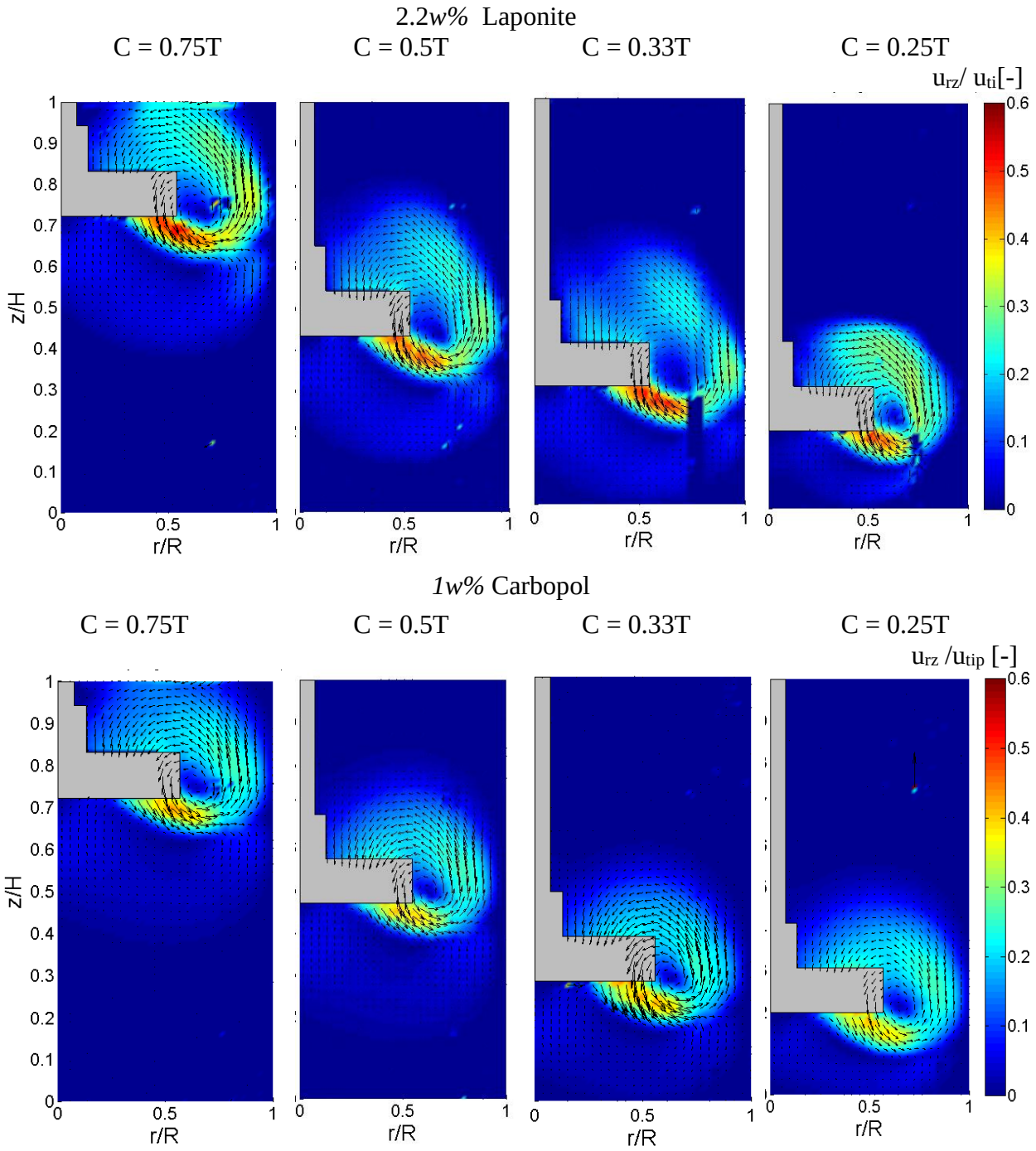

Figure 4.25. The contour of normalized velocity magnitude plot of 2.2*w*% Laponite at t_3 and 1*w*% Carbopol for the PBTD impeller at Re_{HB} = 158 and for four off bottom impeller clearances.

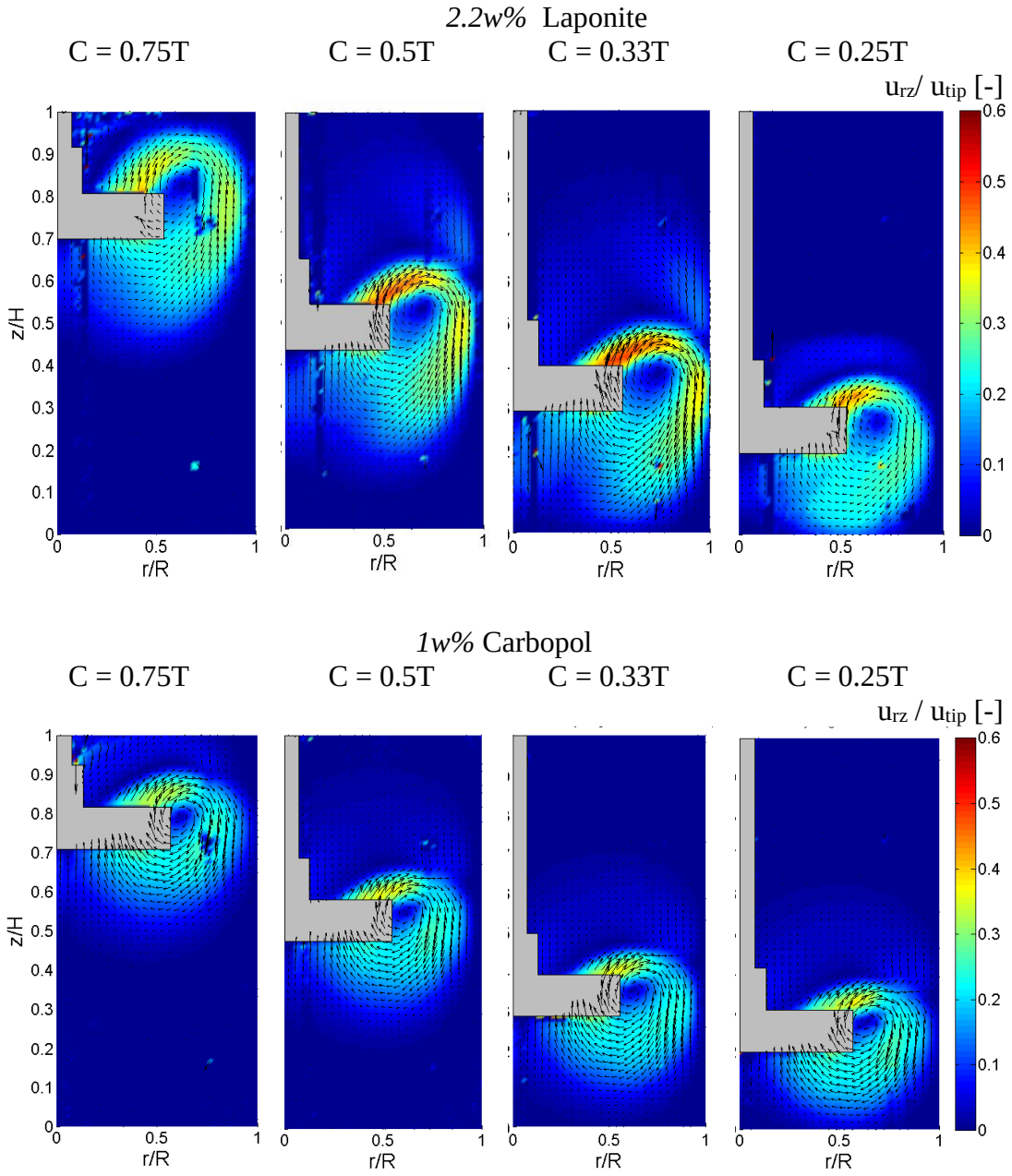

Figure 4.26. The contour of normalized magnitude velocity plot of 2.2*w*% Laponite at t_3 and 1*w*% Carbopol for the PBTU impeller at Re_{HB}=158 and for four off bottom impeller clearances.

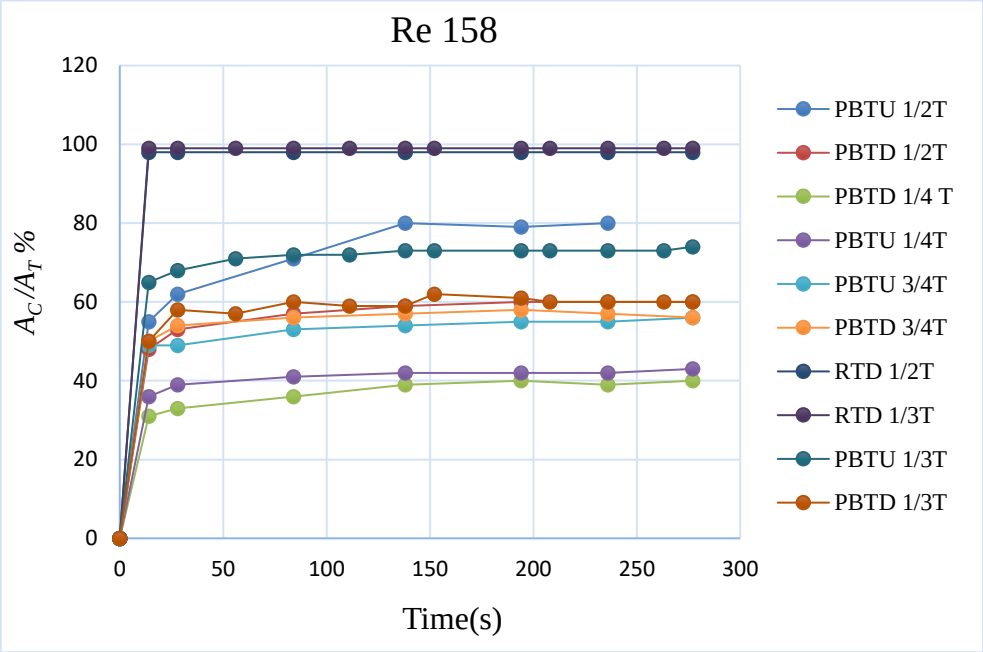

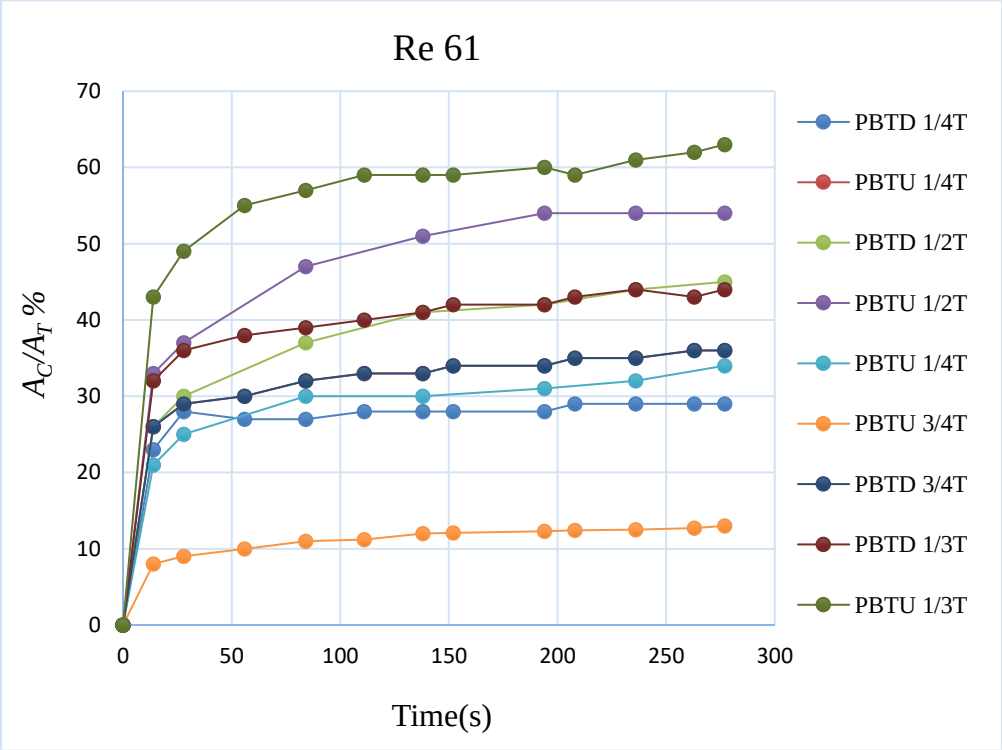

Figure 4.27. The cavern size growth ratio for 2.2*w*% Laponite as a function of time for four impeller clearance positions.

4.4 Conclusions

In this chapter, a time-dependent thixotropic fluid (2.2*w*% Laponite) with yield stress behavior was investigated within a stirred tank by means of two non-intrusive flow visualization techniques, PIV and PLIF. To achieve this, a time-independent fluid (1*w*% Carbopol) with a yield stress and shear-thinning properties was also analyzed as a reference fluid, to help better observe the time effects on the thixotropic fluid mixing.

In this regard, flow pattern, normalized mean velocity and cavern growth in the tank was characterized during the mixing for the thixotropic fluid, and the results were compared to the reference fluid under three different flow regimes (Re_{HB} = 7, Re_{HB} = 61, Re_{HB} = 158).

The results suggest that under the PBT (UP & DP) impeller configuration, flow developed with time and two flow patterns, as primary and secondary loops, were formed. The flow reached a steady state condition at approximately t =138s for R_{HB} =158. For the RTD impeller, the flow fields of the thixotropic fluid showed an unexpectedly higher magnitude velocity specifically in the vicinity of the impeller compared to the PBT impellers and reached the steady state condition prematurely. The above can be seen in the following:

a) The shear strain plot **Figure 4.11** shows that the shear applied to the fluid in the vicinity of the impeller was found to be much higher in the RTD impeller compared to the PBT impellers.

b) A high shear was applied by RTD impeller mostly in a radial direction, causing the viscosity of the fluid to reduce more quickly.

Lowering the Reynold number to Re_{HB} = 7 saw a further significant reduction in magnitude velocity and pumping capacity under the three impeller configurations, with the flow pattern of the radial RTD impeller changing most noticeably. In this case, the flow was observed to leave the impeller blades at an angle to the radial direction in spite of a fully radially discharged impeller being used.

While both fluids showed the presence of cavern in mixing, due to yield stress, reduction of apparent viscosity with time helped the cavern to develop in the case of the thixotropic fluid. Therefore, the cavern sizes in **Figure 4.16** and **Figure 4.19** are larger for 2.2*w*% Laponite relative to 1*w*%Carbopl. Under the RTD impeller configuration and at Re_{HB} = 158, the cavern for the thixotropic fluid reached to the top surface of the tank. A PBTU impeller developed a bigger cavern at Re_{HB} =158 and Re_{HB} = 61 compared to the PBTD impeller. Furthermore, it was found that impeller design did not contribute to cavern evolution at a low Reynold number regime as the trend and size of the caverns under the three impeller configurations remained almost the same for the thixotropic fluid. In addition the thixotropic fluids in an un-baffled vessel configuration, show noticeably different behavior when compared to a viscoplastic fluid. In the case of the baffled vessel, the cavern size become larger, and improved flow fields are obtained compared to an un-baffled case. In viscoplastic fluids, however, the conventional baffled vessel reduces the mixing efficiency by reducing cavern size and flow velocity.

The yield stress and apparent viscosity of the studied thixotropic fluid declined with time during stirring, meaning the energy supplied to the fluid is mostly consumed to divert the flow from a tangential direction to an axial one. In viscoplastic fluids a yield stress acts as a barrier to the fluid momentum.

Increasing the impeller bottom clearance from $C = 0.25T$ to a higher position of $C = 0.33T$ significantly enhanced the cavern size and flow field for all impeller configurations. With further increase of clearance to $C = 0.5T$, the cavern size becomes larger for the PBTU impeller, whereas no significant effect was found in the other impeller configurations. Moving the impeller to a higher position of $C = 0.75T$ resulted in the inverse effect on cavern growth and flow field for all the three impeller types.

Overall, compared to the reference fluid, the thixotropic fluid with yield stress generates improved flow fields and larger cavern size and demand less energy during mixing.

Chapter 5

THE EFFECT OF VISCOELASTICITY IN A STIRRED TANK

This chapter aims to study the effects of elasticity and shear-thinning behavior of fluids on their flow and mixing by using model fluids that exhibit only one of these behaviors at a time. Thus, the effects of each rheological behavior can be separately studied and identified. Viscoelastic Boger fluids with constant viscosity were used to investigate the elasticity effect on mixing. An inelastic shear-thinning fluid assisited in the understanding of the shear-thinning effect on mixing in the absence of elasticity. In addition the behaviour of viscous Newtonian fluids was studied whilst using them as reference fluids. Particle Image Velocimetry (PIV) was applied to visualize the flow behavior of the viscoelastic, the shear-thinning and the Newtonian fluids. Flow pattern and velocity were investigated in the stirred tank using three impeller configurations: Pitch Blade Turbine in both up and down pumping mode (PBTD, PBTU) and Ruston Disk Turbine (RTD).

5.1 Introduction

Mixing of viscoelastic fluids is common to many chemical and biochemical process industries and yet there is very little known about the effects of fluid elasticity on mixing performance. Elasticity impacts mixing in two ways: it can affect the power required for agitation and it can change flow patterns, as such it can influence the time needed for homogenization (Collias and Prud'homme, 1985).

Most viscoelastic fluids show a combination of rheologically complex behaviors and therefore it is difficult to separate the effect of viscoelasticity from these other behaviors. In 1977, Boger introduced a liquid that exhibited a constant high viscosity but was elastic at room temperature. Therefore, by using this liquid the effect of elasticity can be studied in the absence of shear-thinning effects. Another property of this fluid is that it is optically clear, which is important to flow visualization measurements (Mackay and Boger, 1987).

The first Boger fluid was introduced as a solution of polyacrylamide in a concentrated sugar solution (corn syrup) and had high elasticity with a constant, high viscosity close to 22 Pa·s, (Boger and Nguyen, 1978). Later Prilutski et al. (1983) introduced a new formulation of the Boger fluid which was a mixture of polyisobutylene (PIB) in Polybutene (PB) and a small amount of kerosene oil. The disadvantage of using this fluid is that the PB solutions requires large amounts of an organic solvent for cleaning, making it hard to work with and expensive. More detail of rheological characteristics of other formulations of the Boger fluid can be found in a recent review of James (2009). The difficulties encountered using the first Boger fluid (polyacrylamide-corn syrup mix) in a rheometer were reported by Choplin and Carreau (1986) and the two major ones are as follow: i) formation of corn syrup crystals when exposed to air ii) rheological properties are not reproducible from one batch to another. Choplin and Carreau (1986) therefore proposed a new solution of polyacrylamide in a mixture of glycerin and water, which exhibited lower viscosity and elasticity. This formulation was also used in the work presented in this thesis.

There are a few select studies investigating hydrodynamics of viscoelastic fluids, with most of the research being focused on studying mixing effects such as mixing times or

power draw. However, mixing effects may vary from on study to another and are dependent on the flow regimes and the type of viscoelastic fluids used (e.g. shear-thinning and elastic fluids will give different results to Boger fluids). Elastic forces in viscoelastic fluids are opposed to the centrifugal forces, reducing the formation of a vortex and often causing the viscoelastic fluid to climb a rotating shaft (Collias and Prud'homme, 1985). The effect of elasticity on power consumption is studied by measuring the torque on the mixing vessel. Özcan-Taskin and Nienow (1995) investigated the power consumption in the mixing of Boger fluids. A much more recent work conducted by Seyssiecq and Tolofoudy (2003) used a Boger fluid to monitor power consumption in a stirred tank. It was observed that in the laminar region the power consumption of the specific Boger fluid showed a 300% increase compared to that of a Newtonian fluid, whereas in the low transitional region a 15% increase in power consumption was observed for the Boger fluid with respect to the Newtonian fluid (Seyssiecq and Tolofoudy, 2003).

The study of flow patterns is of upmost importance, as flow patterns show how the system is mixed. The formation, shape and velocities of these flow patterns are critical to designing and optimization of mixing systems. Nonetheless, little research has been performed in this area. Stokes (1998) examined the confined swirling flow of Boger fluids with different viscosities for situations where inertia or elasticity dominated the flow field. The Elasticity number, *El*, which characterizes the elasticity of fluids, is the parameter that defines the flow field (Stokes, 1998, Stokes et al., 2001).

The present work is focused on the effects of viscoelasticity and shear-thinning on mixing in a stirred vessel with three type of impellers (PBTD, PBTU, RTD), as observed by using the powerful, non-intrusive, flow visualization technique of PIV. Flow dynamics of

viscoelastic fluid and shear-thinning fluid have been determined from PIV measurements and compared to respective results for the Newtonian fluid.

5.2 Rheology and Material Characterization

5.2.1 Test fluids

Five fluids were used in this study: two viscous Newtonian fluids (N93, N95), two viscoelastic Boger fluids (100PAA and 300PAA), and a shear-thinning inelastic fluid (1.5*w*% CMC). The complete composition of the fluids used can be found in Table 5.1.

5.2.1.1 Viscoelastic Fluid (Boger Fluid)

The Boger fluids exhibited a constant viscosity but were elastic at room temperature. In addition, their optical transparency was imperative in obtaining results from the PIV flow visualization technique (Mackay and Boger, 1987). The Boger fluids (100PAA, 300PAA) used in this work were prepared by first dissolving a small amount of polyacrylamide (PAA) Separan AP30 (supplied by SNF Ltd, UK) into deionized water to make a stock solution. According to the manufacturer's specifications, AP30 has a molecular weight (Mw) of approximately 5×10^6. The water was heated to about 30-40°C, and the polymer was added little by little to the water that was being constantly mixed by a magnetic stirrer in order to facilitate the dispersion of the polymer and to avoid agglomeration. To reduce bacteriological degradation of the solution biocide Kathon LXE, (produced by Rohm and Haas, UK) was added to the fluid. NaCl was also added to the stock solution to reduce the shear-thinning effect in the Boger fluids. Details on the effects of salt concentration on the rheology of viscoelastic fluids can be seen in Stokes (1998). The stock solution was placed on an overhead stirrer at very a low rotation rate of 80 rpm, until the polymer was completely dissolved. The experimental solutions

were made by adding the polymer stock solution to the appropriate amount of glycerol (Palm –OLEO SDN.BHD, UK). The solutions were subsequently mixed using an impeller at low rotation rates for 12-48 h (Stokes et al., 2001). The fluid densities were measured at 20 °C using a density bottle. Fluids composition and density are listed in Table 5.1.

Table 5.1. Composition and density of test fluids used

Fluid	**PAA** ***(ppm)***	**Glycerin** **(*w%*)**	**Water** ***(w%)***	**NaCl** ***(w%)***	**Kathon** ***(ppm)***	**CMC** **(*w%)***	**ρ** ***(kg/m³)***
N93	–	93	5.5	1.50	25	–	1253
N95	–	95	3.5	1.50	25	–	1255
100PAA	100	90.99	7.50	1.50	25	–	1247
300PAA	300	90.97	7.50	1.50	25	–	1248
1.5*w%* CMC	–	–	98.5	–	–	1.5	1005

5.2.1.2 Newtonian Fluid

Two glycerin based Newtonian fluids (N93, N95) were used in this work as reference fluids for comparison with the viscoelastic fluids. The viscosities of the Newtonian fluids (N93, N95) were adjusted close to that of the respective Boger fluids (100PAA, 300PAA) for accurate comparisons. N93 and N95 were prepared by adding the appropriate amount of distilled water to glycerin stock (Palm –OLEO SDN.BHD, UK) (see Table 5.1).

5.2.1.3 Shear-thinning Inelastic Fluid

The effect of shear-thinning behaviour on mixing of the fluids is investigated by using a shear-thinning inelastic fluid, 1.5*w*% CMC. In order to prepare this fluid, powdered Carboxymethyl Cellulose (CMC) with a medium viscosity (Sigma-Aldrich, UK) was added gradually to water stirred at a high rotation of 400 rpm, in order to avoid the

formation of clumps. The mixture was stirred for 4-5 hours until the CMC was completely dissolved, and then left to rest for a few hours before use. The fluid densities were measured at 20 °C using a density bottle. The composition and density are presented in Table 5.1.

5.2.2 Rheology of Test Fluids

The rheological properties of the test fluids were examined using an AR2000 Advanced Rheometer (TA Instrument, USA) with a 60 mm cone and a 2° cone angle, at a constant temperature of 20° C. Due to the long timeframes needed to measure the rheological properties of the selected liquids, a solvent trap was used throughout the experiments to reduce evaporation of the solvent.

In order to obtain the shear flow curves of a specific fluid, a shear rate was applied to the fluid to attain its viscosity. The shear properties of the various fluids used are presented in **Figure 5.1**. The two polyacrylamide solutions have a constant viscosity, and the slopes are all near unity for the shear stress vs. shear rate curves. A slight shear-thinning effect of the Boger fluids was taken under consideration in the measurements. The rheological properties are summarized in Table 5.2, with the power-law model (Equation 1) being used to correlate the shear stress to shear rate and to explain the degree of shear-thinning behaviour for each fluid:

$$\tau = k\dot{\gamma}^{n} \tag{1}$$

The flow behavior index *n* for viscoelastic fluids was close to unity. Hence, the effects of the elasticity could be studied in the absence of shear-thinning behaviour.

Consequently, the power low model was fitted to the experimental measurements from the shear-thinning fluid 1.5*w*% CMC, which resulted in the values of k = 0.49 and n = 0.77, whereas the apparent viscosity of the fluid remained similar to that of the other fluids, as listed in Table 5.2. The viscosities for the two Newtonian fluids N93 and N95 were found to be similar to those of 100PAA and 300PAA respectively, as shown in **Figure 5.1.**

The primary normal stress difference (N_1) against the shear rate for the two Boger fluids that have different degrees of elasticity is presented in **Figure 5.2.** In addtion the first normal stress difference (N_1) was correlated to the shear rate using the power law (Özcan-Taskin, 1993):

$$N_1 = A\dot{\gamma}^b \tag{2}$$

where A and b are arbitrary constants. The value of A and b are shown in Table 5.2 for the two Boger fluids. The second normal stress difference (N_2) is generally much smaller than N_1 and is difficult to measure with normal a rheometer, subsequently being usually neglected in measurements. More details of the measurement for the second normal stress difference for a highly elastic Boger fluid can be found in the work of Magda et al. (1991).

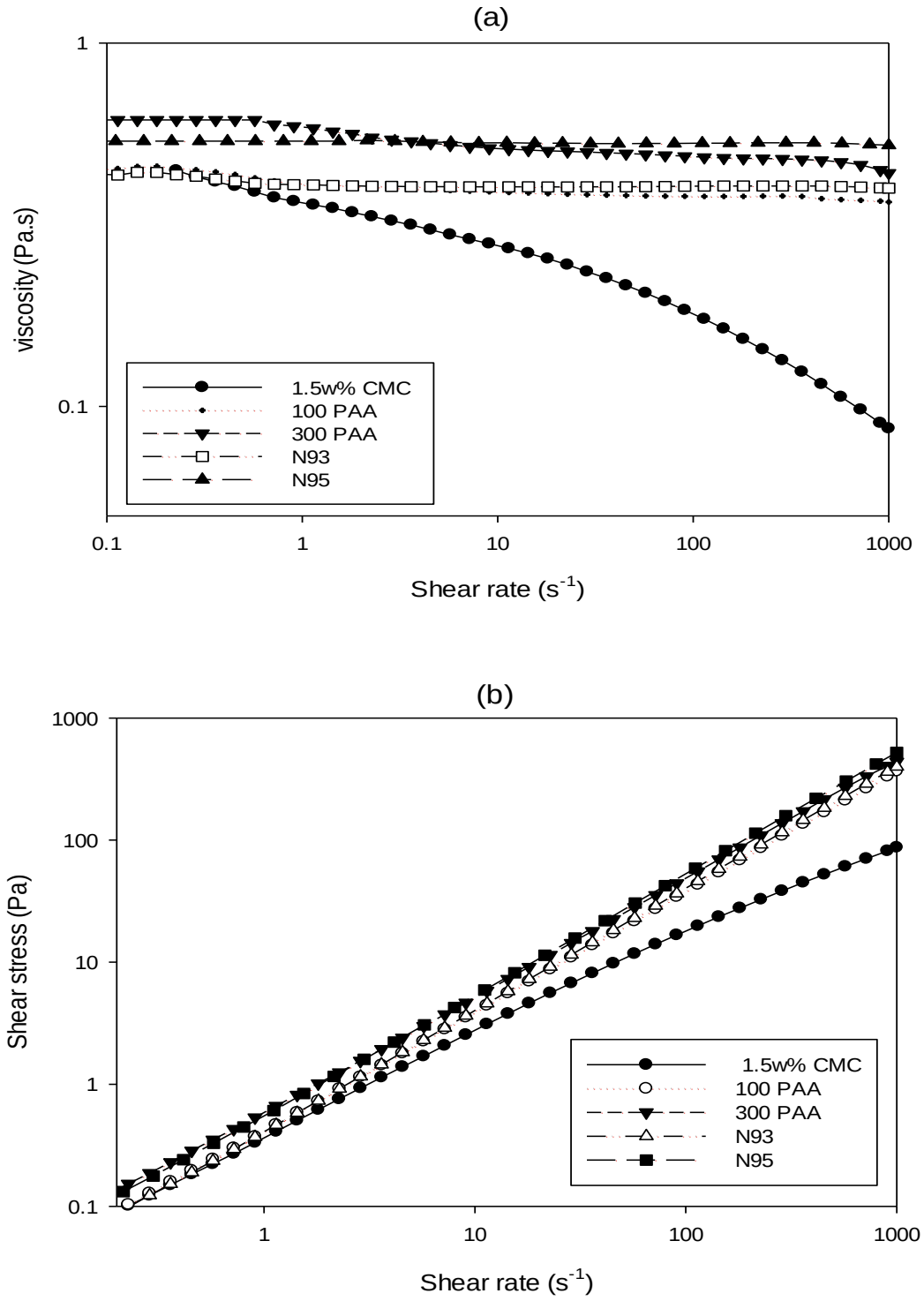

Figure 5.1. Steady shear properties for all tests fluids a), viscosity versus shear rate and b) shear stress versus shear rate.

Table 5.2: Rheological properties of fluids used in the experiments.

Fluid	***μ (Pa s)***	***k (Pa s^n)***	***n***	***A***	***b***
100PPA	-	0.41	0.99	0.07	1.68
300PPA	-	0.54	0.97	0.12	1.78
1.5*w*% CMC	-	0.49	0.77	-	-
N93	0.40	-	-	-	-
N95	0.51	-	-	-	-

The average shear rate in the vessel is assumed to be specified by the Metzner and Otto correlation as follows:

$$\dot{\gamma}_{av} = k_s N \tag{3}$$

where k_s is the mixer shear rate constant, which is slightly dependent on impeller type and size. It has a value in the range of 10-13, but for most practical purposes the value of 11 is used for the PBT impeller (Adams and Barigou, 2007) and for the RTD impeller 11.5 has been suggested (Özcan-Taskin and Nienow, 1995) and was used here. The Reynolds number, *Re*, for a non-Newtonian fluid in a stirred tank may be defined as follows:

$$Re = \frac{\rho N D^2}{\mu_a} \tag{4}$$

where μ_a is the effective viscosity of the non-Newtonian fluid.

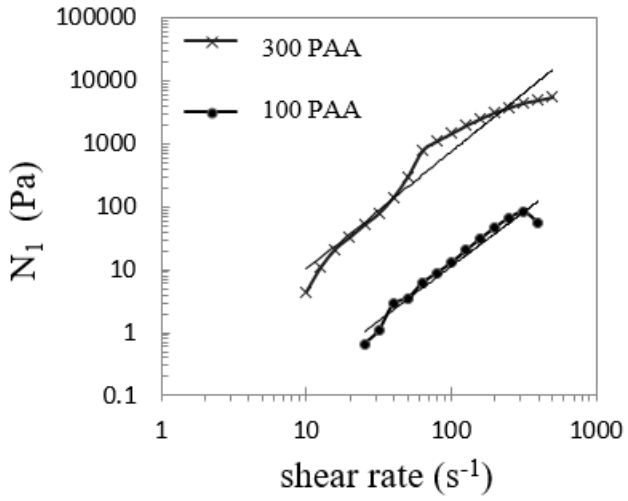

Figure 5.2. First normal stress difference N_1 (Pa) of viscoelastic fluids as a function of shear rate (s^{-1})

The Reynolds numbers investigated were within the range of 7-80, covering laminar to low transitional flow regimes. A dimensionless number that characterizes viscoelasticity is the Weissenberg number, W_i, which is evaluated as the ratio of normal stress (N_1) to shear stress of the fluid in this study, although other definitions have also been used in the literature (Özcan-Taskin and Nienow, 1995).

$$W_i = \frac{Elastic\ forces}{vicous\ forces} = \frac{N1}{\tau} = \frac{A(k_s N)^{b-n}}{k} \quad (5)$$

The balance between inertia and elastic forces gives rise to an elasticity number, *El*, which is the ratio of the Weissenberg number to the Reynolds number (Özcan-Taskin and Nienow, 1995):

$$El = \frac{Fluid\ elasticity}{Fluid\ inertia} = \frac{W_i}{Re} = \frac{A(k_s N)^{b-1}}{ND^2\rho} \quad (6)$$

where ρ is the fluid density and D the impeller diameter. The properties given in Table 5.2 were used for defining the dimensionless numbers governing the flow of elastic liquids in the stirred tank, as listed in Table 5.3.

Table 5.3: Dimensionless numbers over the range of impeller speed for the viscoelastic fluids used in the experiments.

Fluid	**Impeller Speed (rps)**	***Re***	***El***	$\boldsymbol{W_i}$
100PAA	0.51	7	0.038	0.272
300PAA	0.71		0.169	1.183
100PAA	3.30	45	0.023	1.036
300PAA	4.41		0.114	5.162
100PAA	5.83	80	0.019	1.561
300PAA	7.73		0.105	8.126

From **Figure 5.2** and by relating the first normal stress difference to the shear rate (Equation 2) as measured for the two Boger fluids 100PAA and 300PAA, the values that were derived for the power law parameter b are 1.64 and 1.78 respectivly. The elasticity number did not greatly depend on the impeller speed or, subsequently, on the Reynolds number because the values of b were relatively close to 2.0. Increasing the polymer concentration from 100PAA to 300PAA resulted in an increase of fluid elasticity. Daily sampling of the Boger fluids from inside the tank showed that the shear stress data was reproducible over a large period time for the experiments. However the elasticity did slighltly decreased with time, probably due to shear degradation of the polymer. This, nevertheless, did not effect measurements as the experimental time is noticeably lower than the time needed for polymer degradation.

5.3 Experimental Setup

The stirred vessel and impellers used in this work were discussed earlier in Chapter 3.1. All test fluids were measured in the laminar and transitional flow regimes, at Re_{PL} = 7, Re_{PL} = 45, and Re_{PL} = 80 and with different impeller configurations. This narrow range of flow regimes was necessary due the experimental limitations (fluids having high viscosity and elasticity), making it so higher Reynolds numbers could not be achieved Table 5.4 presents a summary of the all the test configurations used in this study. The Reynolds numbers symbol Re_{PL} used throughout this chapter are calculated based on the Power low model. The details of the PIV set up, data processing and measurments were also peresented in Chapter 3.2.

Table 5.4: All experimental configurations and setup used in this study.

Test Fluids	*Re*	Impeller	Vessel configuration
100PAA	7	PBT DP	Baffled, *C = T/3*
		PBT UP	Baffled, *C = T/3*
300PAA		RTD	Baffled, *C = T/3*
	45	PBT DP	Baffled, *C = T/3*
N93		PBT UP	Baffled, *C = T/3*
		RTD	Baffled, *C = T/3*
N95	80	PBT DP	Baffled, *C = T/3*
		PBT UP	Baffled, *C = T/3*
1.5*w*% CMC		RTD	Baffled, *C = T/3*

5.4 Results and Discussion

The presentation and discussion of the experimental results was divided into four sections. The first section examines the Newtonian fluids (N95, N93) in order to evaluate the flow structure in viscous Newtonian fluids and to serve as a reference for comparison against the results for the elastic Boger fluids. The second section examines viscoelastic behavior using the 100PAA Boger fluid that has low elasticity. The third section discusses

the Boger fluid 300PAA that exhibits a high elasticity number, such that elasticy and viscous forces become increasingly more dominant over the inertia force. Lastly, mixing of the shear-thinning inelastic fluid 1.5*w*% CMC was studied to assess the effect of shear-thinning behavior in the absence of other rheological effects, in a stirred tank. The elasticity effect on the axial and radial impeller's efficiency was studied throughout the experiments.

5.4.1 Newtonian Fluid (N93, N95)

The flow pattern obtained for each Newtonian fluid with three impeller configurations at Re_{PL} = 80, Re_{PL} = 45 and Re_{PL} = 7 by the time-averaged velocity data from the 500 PIV images obtained is illustrated in **Figure 5.3** and **Figure 5.4**. The contour of normalized mean velocity magnitude plots are useful in that they shows the considerably different flow patterns produced by each impeller and each fluid. The velocities were normalized by the impeller tip speed $u_{tip} = \pi ND$. The flow properties of the fluid passing through the impeller were measured by using flow numbers (see Table 5.5 and Table 5.6).

5.4.1.1 *Re* = 80

At the highest Reynolds number of Re_{PL} = 80 that was investigated in this study, a primary anti-clockwise loop was observed in the PBTD impeller configuration for the N93 fluid, as shown in **Figure 5.3.** A second, clockwise flow loop was found below the main loop. The flow was induced vertically above and mostly to the left of the impeller, radially, with a slight deviation to the downward direction. As such the discharged flow from the impeller was noticeably higher in the radial direction Fl_3 = 0.578 compared to that of the axial direction Fl_2 = 0.043, as seen in Table 5.5. The Newtonian fluid N95, which has a higher viscosity comapred to N93, showed the second circulation loop below the impeller

becoming slower and the flow discharge from the impeller became more radial, reaching towards the wall of the tank and then moving upward to reach a height of 0.8 *Z/H* in the vessel. The PBT impeller would tend to discharge more radially for the viscous Newtonian fluid rather than showing the true mixed flow behavior. This behavior also was observed by Hall (2005). Moreover, as seen in Table 5.5 and Table 5.6, the flow number for the N95 fluid was reduced (*Fl* = 0.541) compared to that of the N93 fluid (*Fl* = 0.621).

With the impeller type changed to the PBTU configuration, a primary clockwise and a secondary anti-clockwise loop located above the primary were observed. Moreover, flow circulations developed in the regions close to the top of the tank, at a height of 0.8 *Z/H*. In this case the flow pattern and flow number for the two Newtonian fluids was observed to be almost the same and subsequently no significant change of flow behavior was observed under the PBTU configuration between the two different viscous Newtonian fluids.

Table 5.5. Characteristic parameters of flow for the Newtonian fluid N93.

Impeller	PBTD			PBTU			RTD		
Re	7	45	80	7	45	80	7	45	80
Fl	0.124	0.516	0.621	-	0.208	0.314	0.075	0.472	0.595
Fl_1	0.153	0.394	0.501	-	-0.089	-0.058	-	-	-
Fl_2	-0.101	-0.002	-0.043	-	0.345	0.367	-	-	-
Fl_3	-0.023	-0.516	-0.578	-	-0.208	-0.314	-0.026	-0.472	-0.595

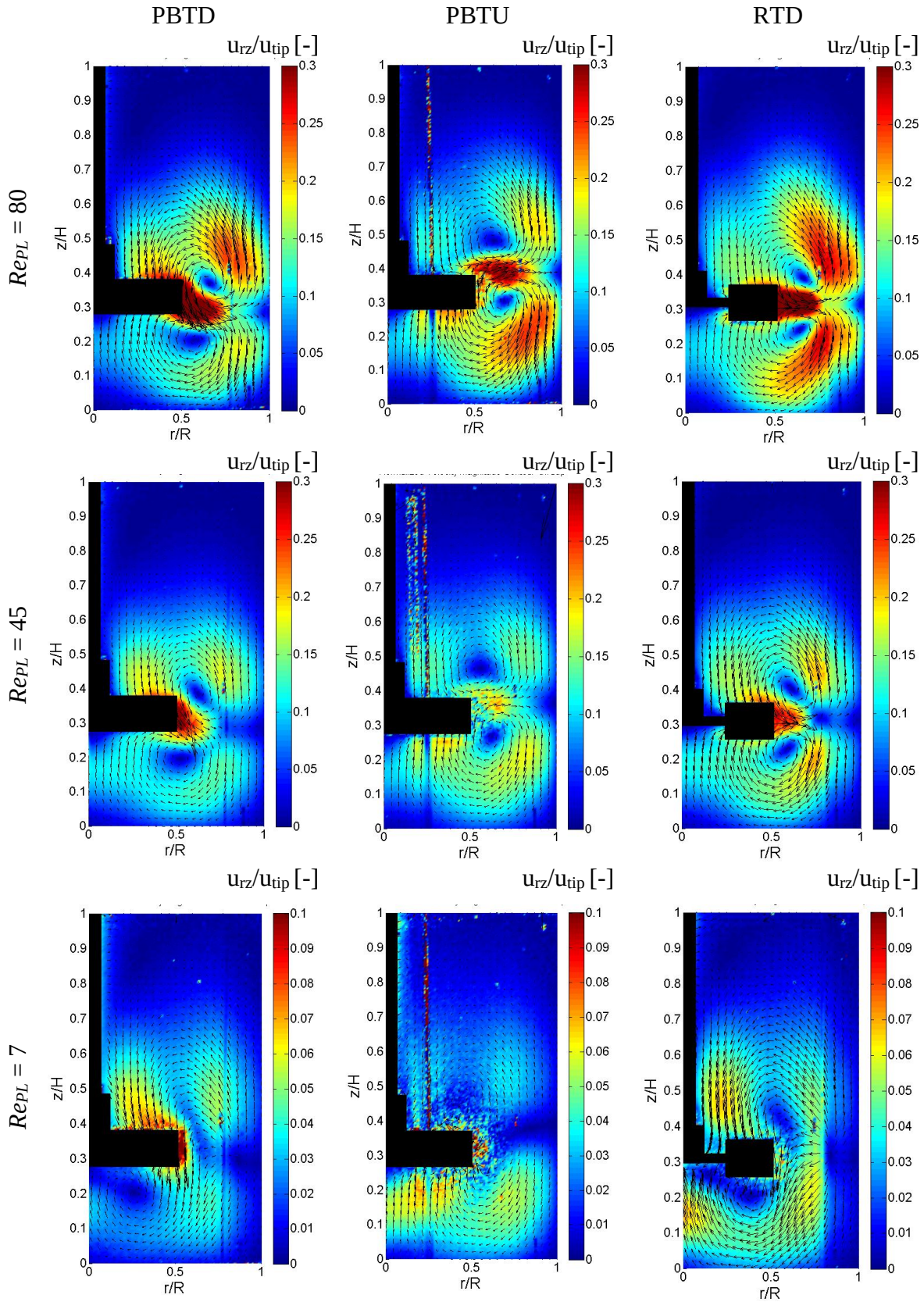

Figure 5.3. The contour of normalized velocity magnitude of three impellers for the Newtonian fluid N93, at three flow regimes: Re_{PL} = 80, Re_{PL} = 45, Re_{PL} = 7

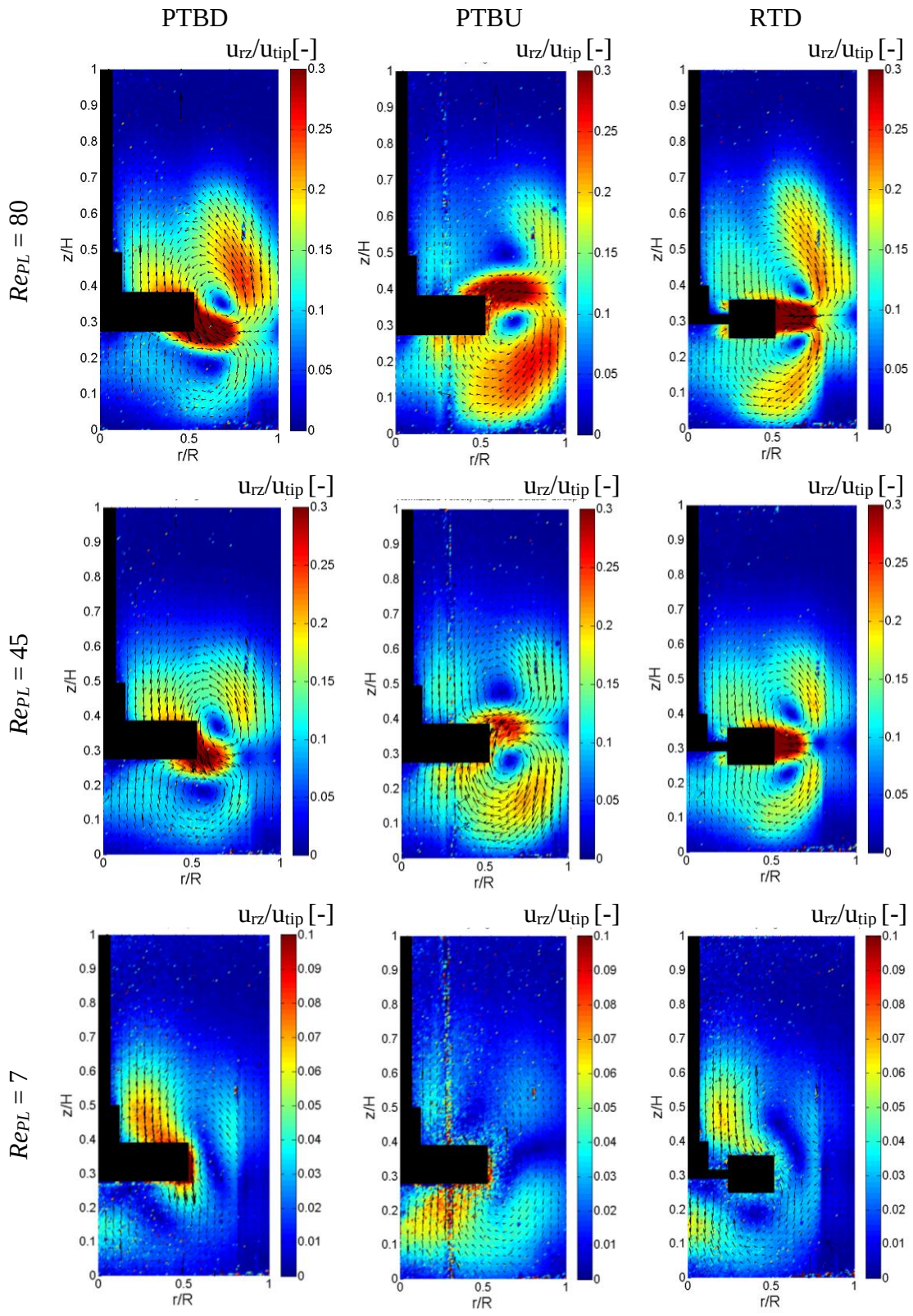

Figure 5.4. The contour of normalized velocity magnitude of three impellers for the Newtonian fluid N95, at three flow regimes: Re_{PL} = 80, Re_{PL} = 45, Re_{PL} = 7.

The flow fields of the Newtonian fluids under the RTD configuration showed that the flow discharged radially, and the radial discharge formed two circulation loops above and below the plane of the disc of the RTD impeller (see **Figure 5.3**, **Figure 5.4**). The flow for N93, with a flow number of $Fl = 0.595$, appeared to be pumped out radially from the impeller reaching the wall of the vessel and then climbing it axially to almost the top of the surface of the liquid, at $Z = 0.9\,H$. The time-averaged mean velocity ($u_{rz} > 0.3U_{tip}$) in N95 was found to be 33.3% higher compared to N93, and a slightly stronger circulation was found in the flow field of the Newtonian fluid N95. The flow number in N93 was found to be slightly smaller than that of the N95 flow number, most likely due to the movement of flow being more in a tangential direction around the impeller vicinity for the N95 fluid compared to the flow movement of the less viscous N93 fluid.

Table 5.6. Characteristic parameters of flow for the Newtonian fluid N95.

Impeller	PBTD			PBTU			RTD		
Re	7	45	80	7	45	80	7	45	80
Fl	0.136	0.503	0.541	-	0.234	0.341	0.132	0.617	0.621
Fl_1	0.154	0.464	0.455	-	-0.101	-0.052	-	-	-
Fl_2	-0.097	-0.065	-0.122	-	0.472	0.464	-	-	-
Fl_3	-0.039	-0.437	-0.420	-	-0.234	-0.341	-0.036	-0.617	-0.621

5.4.1.2 *Re* = 45

At this lower Reynolds number of $Re_{PL} = 45$, the graph still shows the presence of both the primary and secondary loops under the PBTD impeller configuration (see **Figure 5.3** and **Figure 5.4**). The flow discharge was reduced to $Fl = 0.516$ (Table 5.5) and $Fl = 0.503$ (Table 5.6), for the N93 and N95 fluids respectively. In addition the flow was discharged more radially compared to what was observed at the higher Reynolds number of $Re_{PL} = 80$. As such the flow discharge from the radial direction was found to be

significantly higher $Fl_3 = 0.516$ and $Fl_3 = 0.437$ for N93 and N95 respectively - compared to the flow discharge from the axial direction, Fl_2 (see Table 5.5 and Table 5.6). Under the PBTU configuration the pumping capacity Fl was reduced ($Fl = 0.208$ and $Fl = 0.231$ for N93 and N95 respectively) compared to that seen at the higher Reynolds number (see Table 5.5, Table 5.6). This reduction trend in pumping capacity of the impeller with decreasing Reynolds number was also observed by (Rice et al., 2006).

5.4.1.3 $Re = 7$

At the lowest studied Reynolds number, $Re_{PL} = 7$, under the PBTD configuration the fluid flow showed a reduction in terms of velocity and circulation. The flow was induced vertically to the impeller and left it in mostly an axial direction, hence the Fl_2 is significantly higher compared to the Fl_3 for both Newtonian fluids (see Table 5.5, Table 5.6). From Table 5.5 and Table 5.6 it is obvious that the flow pumping capacity was also reduced significantly ($Fl = 0.124$ and $Fl = 0.136$ for N93 and N95 respectively) for both Newtonian fluids under the PBTD configuration. For the RTD impeller the flow number was measured ($Fl = 0.075$ and $Fl = 0.132$ for N93 and N95 respectively) and found to be slightly lower than that reported by Rice et al. (2006), who measured $Fl = 0.21$. This difference is due to the fact that a fluid with higher viscosity was used in the present work. The flow pattern also changed significantly under a radial RTD impeller. In this case, the flow that was induced from the impeller blades was at an angle to the radial direction and formed two circulation loops in the tank. This diverse flow pattern made by the RTD impeller was observed for Newtonian and shear-thinning fluids by both Rice et al. (2006) and Arratia et al. (2006).

5.4.1.4 Shear-thinning Inelastic Fluid

Figure 5.5 shows the contour of the normalized velocity magnitude of three impellers for the shear-thinning fluid 1.5*w*% CMC at three flow regimes (Re_{PL} = 80, Re_{PL} = 45, Re_{PL} = 7). A primary, anti-clockwise loop was observed in the PBTD impeller configuration. The flow was induced vertically above and mostly to the left of the impeller, at an angle of 45° to the downward direction. The flow velocity and flow number were slightly smaller compared to the Newtonian fluid for all flow regimes: Re_{PL} = 80, Fl = 0.439; Re_{PL} = 45, Fl = 0.426; Re_{PL} =7, Fl = 0.185 (see Table 5.7). No significant change was observed regarding the flow pattern, velocity and flow number of the shear-thinning fluid under the PBTU and RTD configurations compared to the Newtonian fluids. Shear rates were highest in the region around the impeller and tapered off towards the wall of the vessel. Due to the shear-thinning effect of the fluid the apparent viscosity around the impeller reduced rapidly compared to what was observed for the Newtonian fluids. A comparison of pseudo-cavern formation for a shear-thinning fluid to cavern formation of other fluids has been discussed in section 5.4.4.

Table 5.7. Characterized parameter of flow for shear-thinning fluid 1.5*w*% CMC.

Impeller	PBTD			PBTU			RTD		
Re	7	45	80	7	45	80	7	45	80
Fl	0.185	0.426	0.439	-	0.134	0.364	0.127	0.519	0.658
Fl_1	0.130	0.351	0.349	-	-0.010	-0.120	-	-	-
Fl_2	-0.096	-0.035	-0.093	-	0.174	0.382	-	-	-
Fl_3	-0.090	-0.391	-0.346	-	-0.134	-0.244	-0.113	-0.519	-0.658

5.4.2 Low viscoelastic Boger Fluids (100PAA)

The flow patterns of a viscoelastic fluid depend highly on the viscoelasticity of the fluid (*Wi*) (elasticity force/viscous force) and the range of operation (*Re*) (inertial force/viscous force). The contour of normalized velocity magnitude and streamline of the Boger fluid 100PAA for the three impellers types and different flow regimes are presented in **Figure 5.6**, **Figure 5.9** and **Figure 5.11**.The flow number was not accurate in Boger fluid due to the fact that flow moved in a highly tangential direction for this viscoelastic fluid, as seen by the 2D PIV velocity measurements.

5.4.2.1 RTD Configuration

Figure 5.7a is the well-known standard flow field of the RTD configuration for a Newtonian fluid, whereby 2 primary loops above and 2 primary loops below the impeller are observed. Under the RTD impeller configuration and at the highest Reynolds number of Re_{PL} = 80, the flow pattern of the Boger fluid 100PAA, with an elasticity number of *El* = 0.019 (see Table 5.3), breaks into two regions. The flow close to the impeller region was discharged from the impeller and two circulation loops were observed above and below the impeller, as shown in **Figure 5.6.** The second, reversed circulation moving away from impeller can be observed in **Figure 5.7b** and is an undesirable result, leading to reduction in the mixing efficiency and loss of energy. In the lower flow region of Re_{PL} = 45 the flow pattern for 100PAA, with an elasticity number of *El* = 0.023, appeared to be like that observed for the Newtonian fluids, as shown in **Figure 5.7a** and **Figure 5.9**.

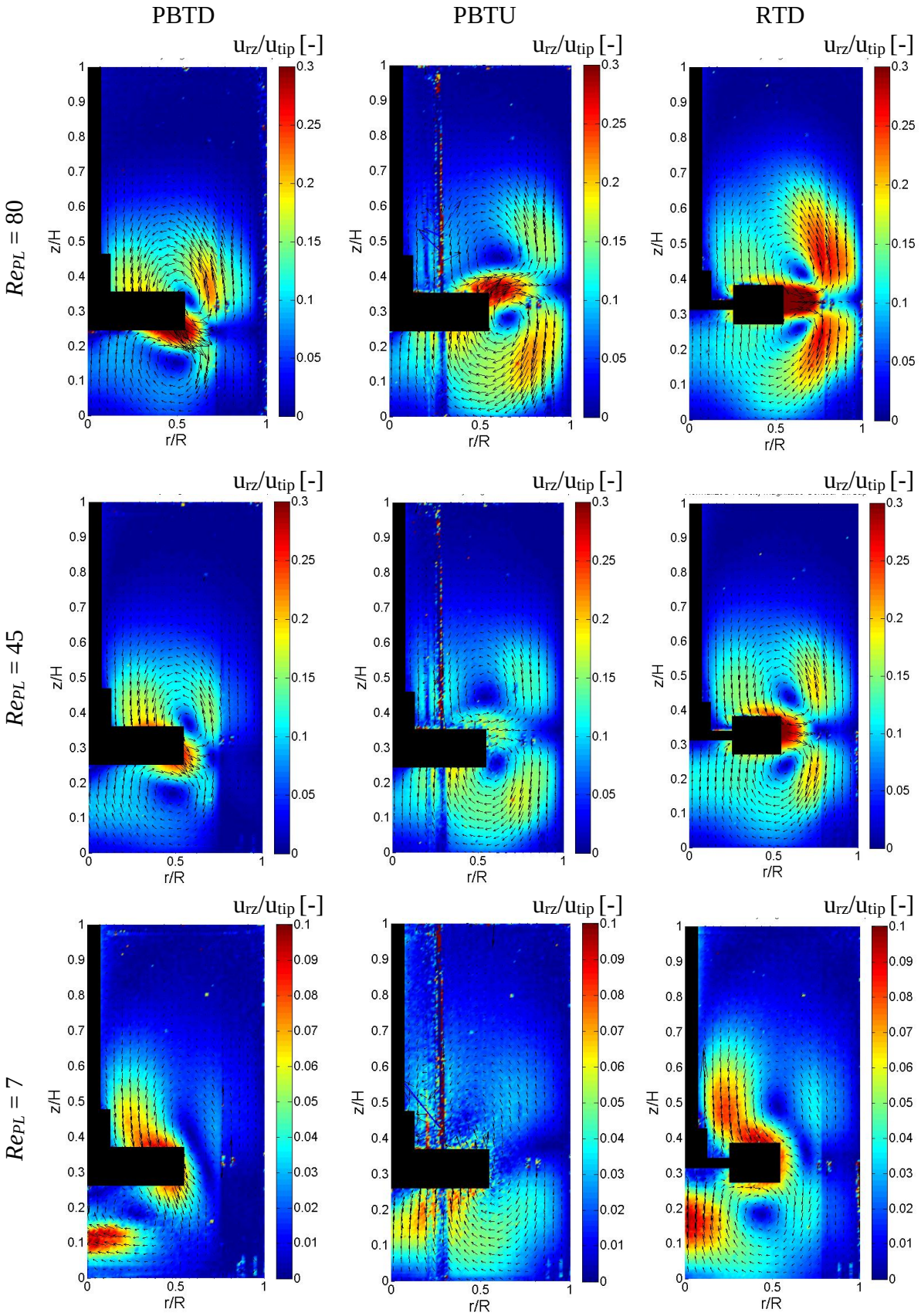

Figure 5.5. The contour of normalized velocity magnitude of three impellers for the shear-thinning fluid 1.5*w*% CMC, at three flow regimes: Re_{PL} = 80, Re_{PL} = 45, Re_{PL} = 7.

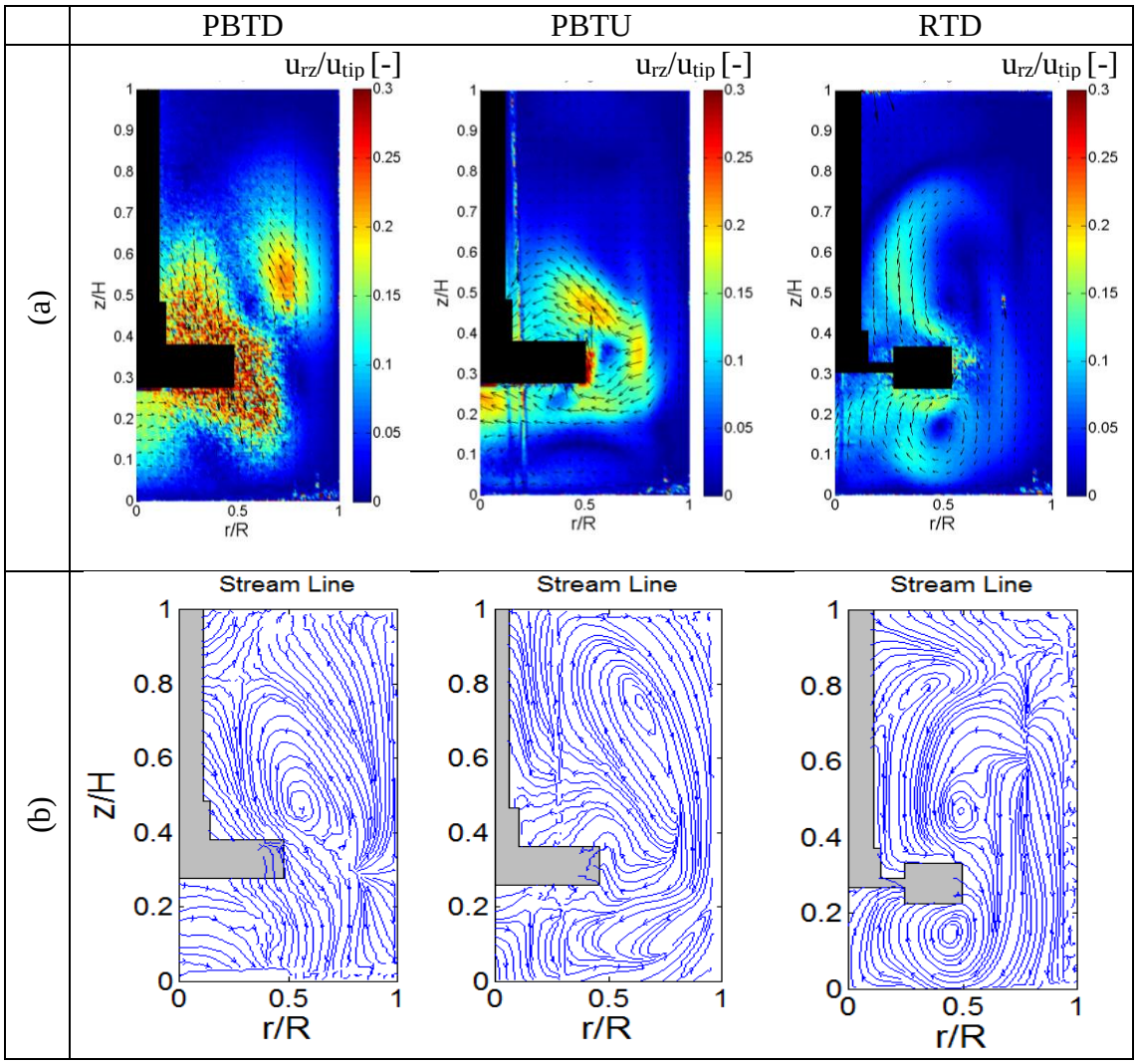

Figure 5.6. a)The contour of normalized velocity magnitude and b) the streamline plots of the viscoelastic Boger fluid 100PAA for three impeller types at Re_{PL} = 80.

The flow reversal was not observed since the elasticity force is weak compared to the inertial force. In this case, the flow field for Re_{PL} = 45 had a velocity of $u_{rz} = 0.3U_{tip}$ (see **Figure 5.9**) which is higher than $u_{rz} = 0.15\ U_{tip}$ (see **Figure 5.6**) as observed for Re_{PL} = 80. At the lowest Reynolds number, Re_{PL} = 7, flow reversal was observed. Two reverese circulation loops formed around the impeller region, as shown **Figure 5.11**. At this very low Reynolds number elasticity is more dominat over the inertia force, resulting in flow

reversal (**Figure 5.7c)**. This reverse flow circulation was observed by Stokes et al. (2001) in using a bottom rotating disc in a fully enclosed cylinder.

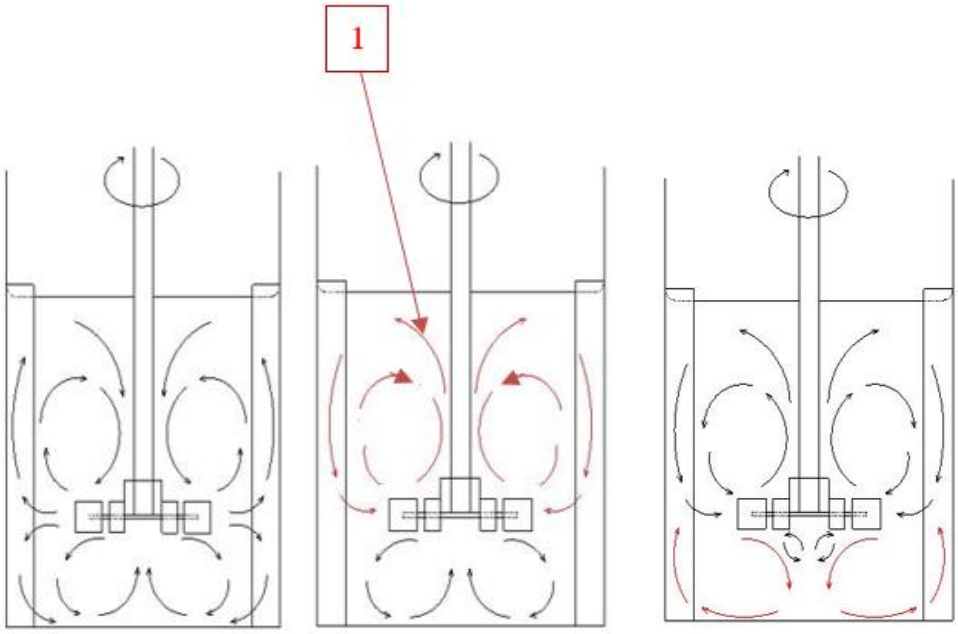

(a) (b) (c)

Figure 5.7. Flow pattern observation for the RDT impeller in a baffled vessel: (a) low (*El*), (b) intermediate (*El*) and appearance of secondary reverse flow (1), (c) high *(El*).

5.4.2.2 PBTU Configuration

Figure 5.8a is the well-known standard flow field of the PBTU configuration of a Newtonian fluid, having 2 primary loops above and 2 primary loops below the impeller. **Figure 5.8b** shows a reverse flow field on the primary loops above the impeller for the viscoelastic Boger fluid. Also, a secondary counter-rotating ring vortex began to form at the side of the vessel and grew, becoming the primary dominate circulation at high *El*. At the high Reynolds number of Re_{PL} = 80, the elasticity was high enough to have flow reversal, as seen in **Figure 5.8b**. Hence a primary reversed circulation above the impeller

was formed. The secondry counter-rotating ring flow under the impeller also grew and became the main circulation below the impller, as seen in **Figure 5.6**. In this figure a primary, small clockwise circulation underneath of the impeller in the center and bottom of the vessel can also be observed.

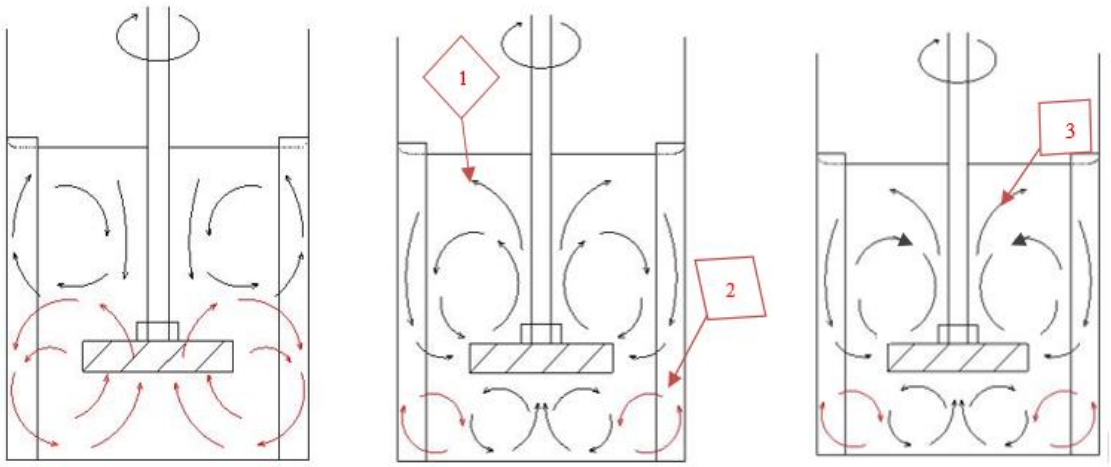

(a) (b) (c)

Figure 5.8. Flow pattern observation for the PBTU impeller in a baffled vessel a) Newtonian fluid b) viscoelastic fluid with high (*El*), c) viscoelastic fluid with intermediate (*El*) : Note the reverse flow field in (1), the appearance of secondary counter-rotating ring vortex in (2), and the secondary reverse flow in (3).

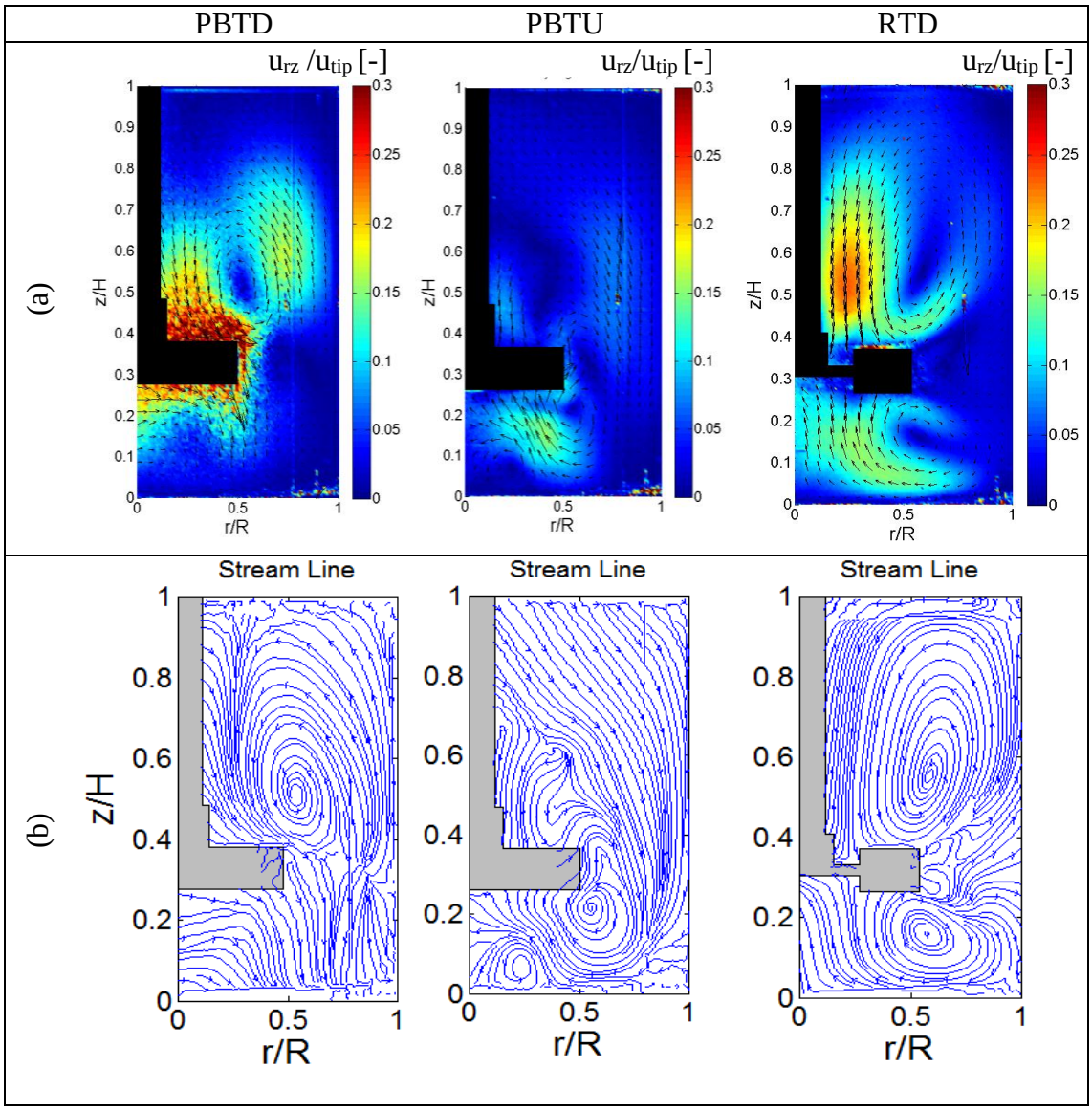

Figure 5.9. a) The contour of normalized velocity magnitude and b) the streamline plot of three impellers for the viscoelastic Boger fluid 100PAA at Re_{PL} = 45.

At the lower Reynolds number, Re_{PL} = 45, the elasticity was not sufficiently high enough to result in complete flow reversal. Hence, the flow pattern above the impeller broke into two regions as seen in **Figure 5.8b**. The flow close to the impeller area was discharged from the impeller; a primary circulation loop was observed above the impeller and a second, reversed circulation loop, away from impeller, was also observed as shown in **Figure 5.8b** and **Figure 5.9.** The secondary, counter-rotating circulation formed below

the impeller **Figure 5.8b**. In addition a small primary, clockwise circulation loop was found underneath the impeller, close to the bottom and center of the tank (see **Figure 5.9**)

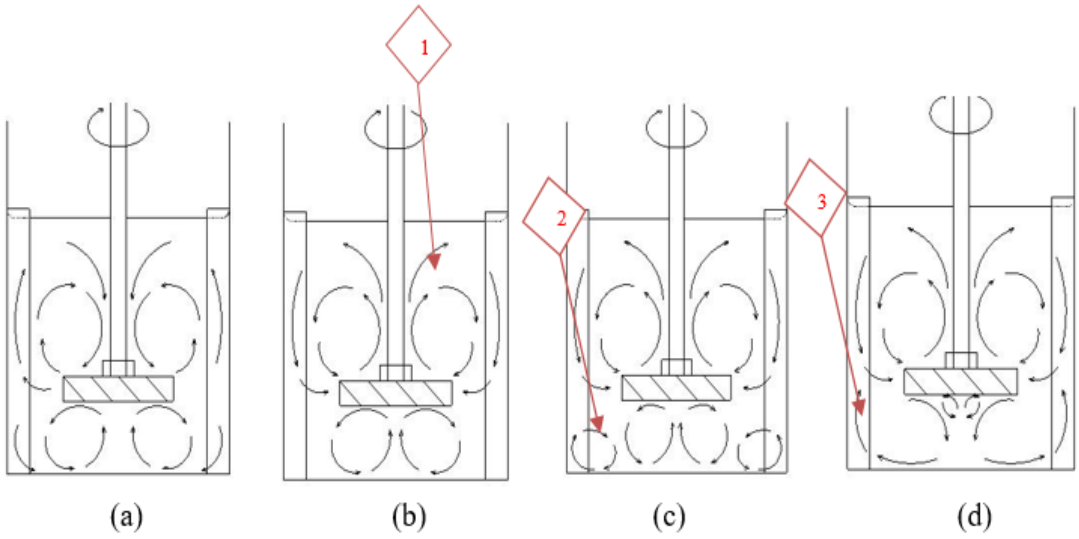

Figure 5.10. Flow pattern observation for the PBTD impeller in a baffled vessel: a) Newtonian fluid, b) viscoelastic fluid with low (El), c) viscoelastic fluid with intermediate (El), d) viscoelastic fluid with high (El); Note the reverse flow field in (1), the appearance of a secondary counter-rotating ring vortex in (2) and the growth of a secondary ring vortex in (3)

5.4.2.3 PBTD Configuration

Figure 5.10a shows the standard flow field of the PBTD impeller configuration for a Newtonian fluid, having 2 primary loops above and 2 primary loops below the impeller. **b** shows a reverse flow field on the primary loops above the impeller for a viscoelastic Boger fluid with low *El*. For the same fluid at an intermediate *El* a secondary counter-rotating ring vortex began to form at the side of the vessel (see **Figure 5.10c**) and grew to become the primary dominate circulation once a high *El* value was reached (see **Figure 5.10d**).

Under this same PBTD configuration, the flow pattern of the 100PAA Boger fluid is significantly different from that observed for the PBTU configuration. At the high

Reynolds number of Re_{PL} = 80 the elasticity was high enough to allow for flow reversal (see **Figure 5.10b** and **Figure 5.6)**. The flow induced by the impeller mostly left it at an angle of 45^{o}. The primary clockwise circulation below the impeller was observed for the 100PAA Boger fluid in the PBTD configuration. The flow pattern for this fluid remained relatively the same for the three studied flow regions when using the PBTD impeller configuration.

5.4.3 High viscoelastic Boger Fluid (300PAA)

Figure 5.12 shows the contour of normalized velocity magnitude of the 300PAA Boger fluid for the three flow regimes of interest: Re_{PL} = 80, Re_{PL} = 45 and Re_{PL} = 7. The flow field of this highly viscoelastic fluid - having El = 0.105 at Re_{PL} = 80, El = 0.114 at Re_{PL} = 45 and El = 0.169 at Re_{PL} = 7 (Table 5.3) - shows flow reversal under all three impeller configurations. Here the elasticity force (normal force) produced by the shearing flow is higher than the force due to fluid inertia. Therefore the flow direction was reversed (**Figure 5.12)** compared to what was seen for the Newtonian and shear-thinning fluids. Under all impeller configurations the reverse circulations formed above and below the tank. In addition a small, primary circulation, just below the impeller and in the center of the tank, was observed in both PBT impeller configurations at Re_{PL} = 80 and Re_{PL} = 45. Moreover, a climbing eddy motion around the shaft was formed due to the presence of normal forces in the viscoelastic fluid. Comparisons between flow patterns of all test fluids used in this study under all three impeller configurations at Re_{PL} = 80 and Re_{PL} = 45 are presented by streamline plots, as shown in **Figure 5.13** and **Figure 5.14**.

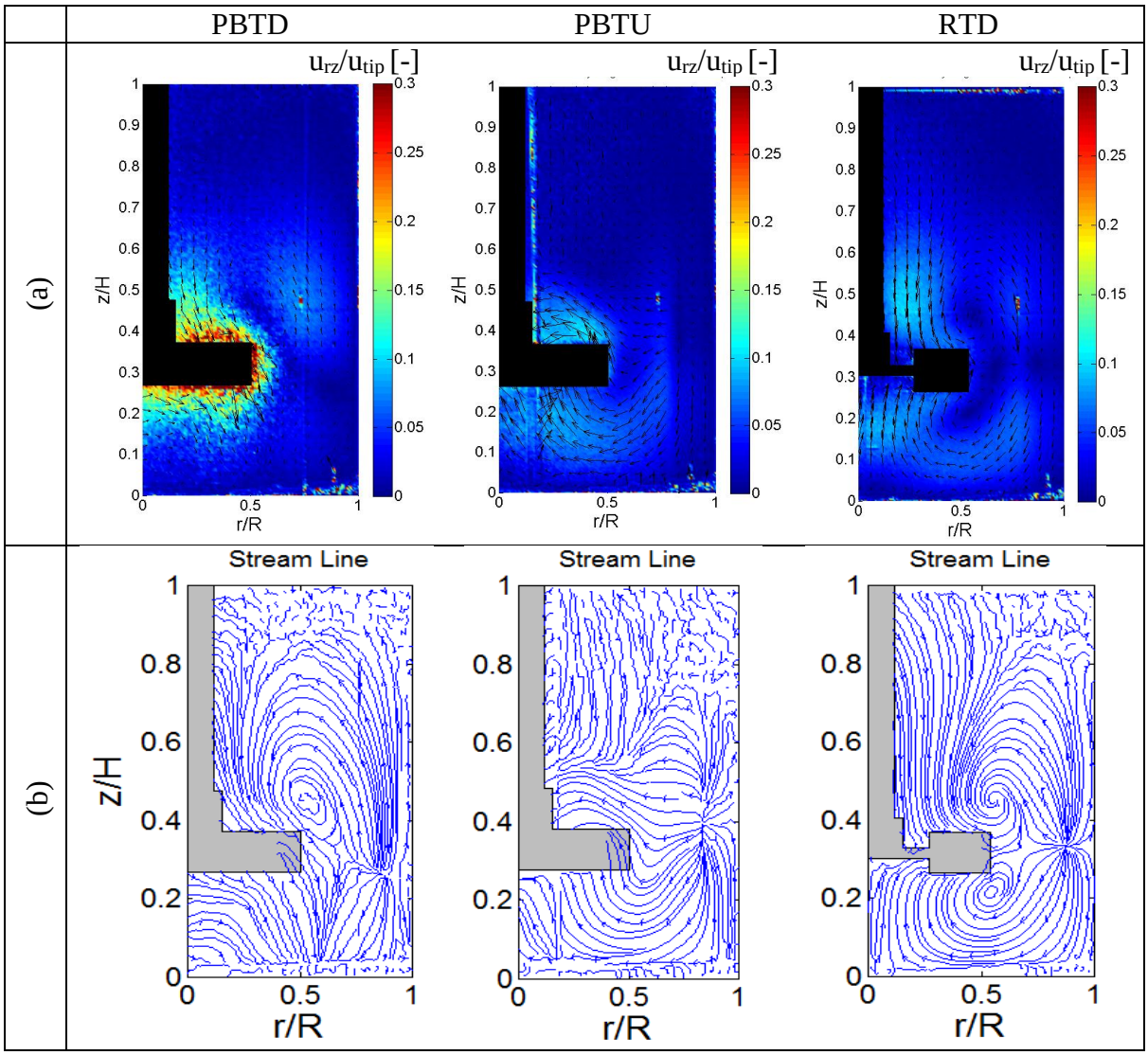

Figure 5.11. a)The contour of normalized velocity magnitude and b) the streamline plot of the three impellers for the viscoelastic Boger fluid 100PAA at Re_{PL} = 7

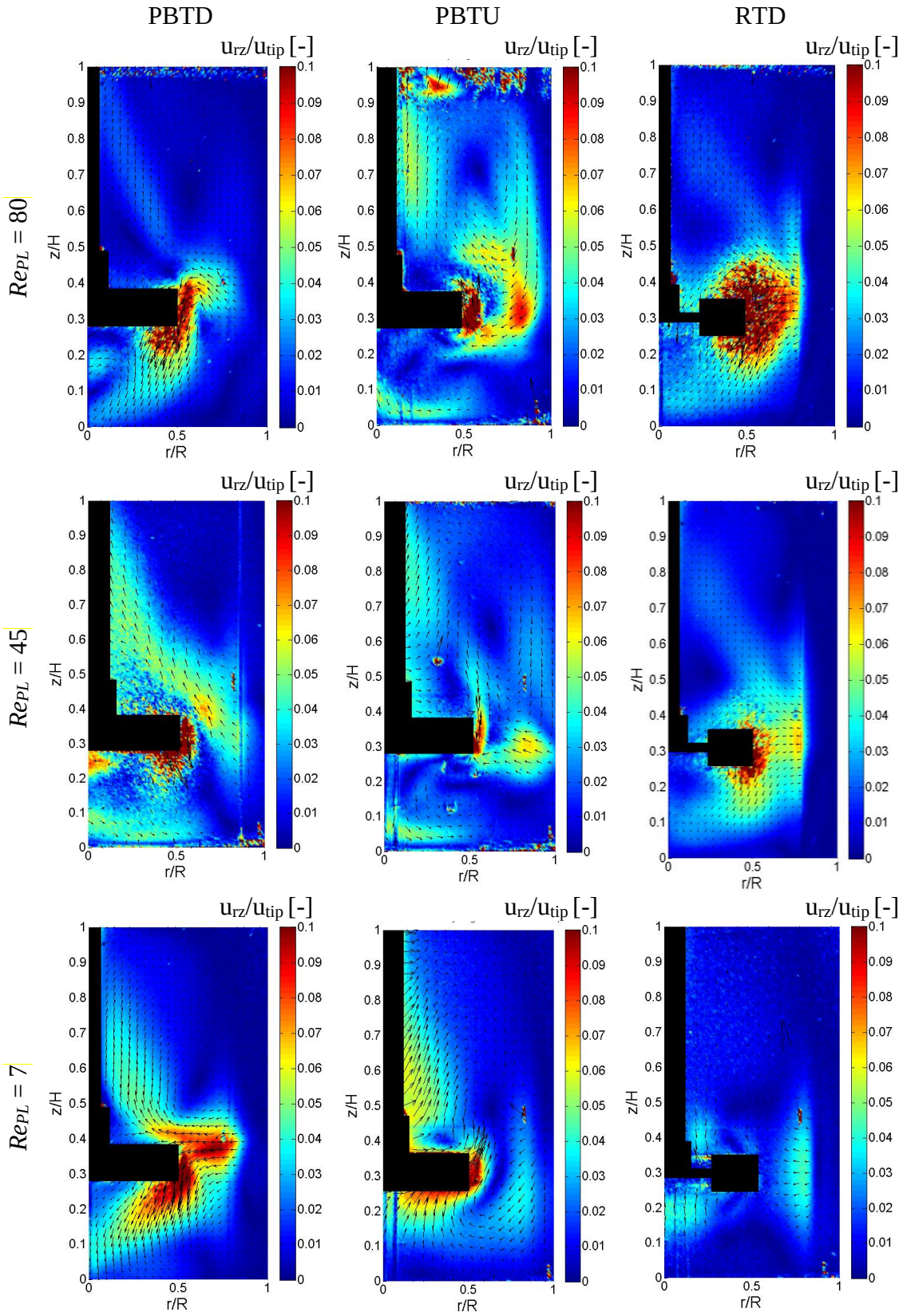

Figure 5.12. The Contour of normalized velocity magnitude of three impellers for the 300PAA Boger fluid, at three flow regimes: Re_{PL} = 80, Re_{PL} = 45, Re_{PL} = 7.

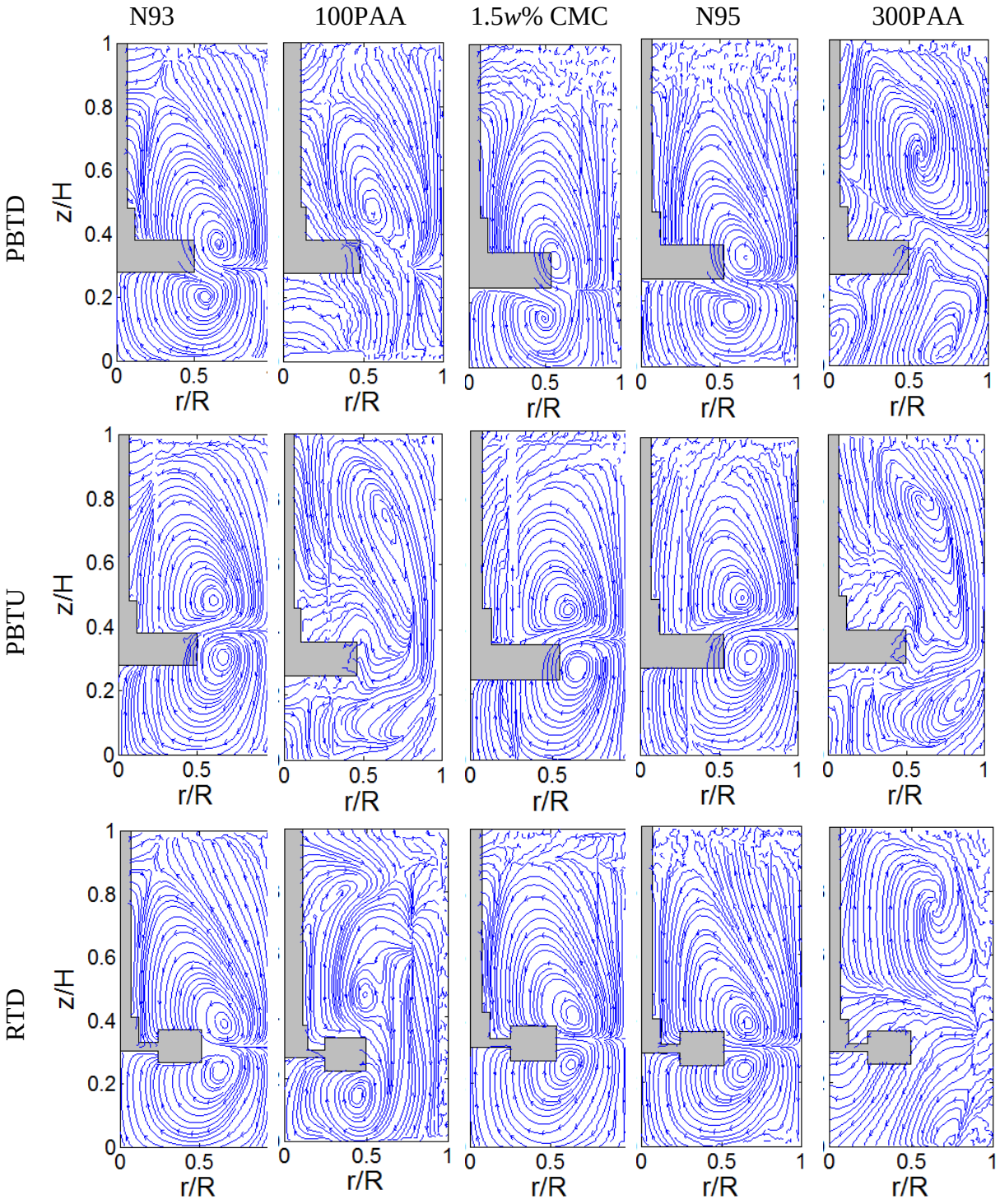

Figure 5.13. The streamline plots for all test fluids used in this study at Re_{PL} = 80 under three impeller configurations.

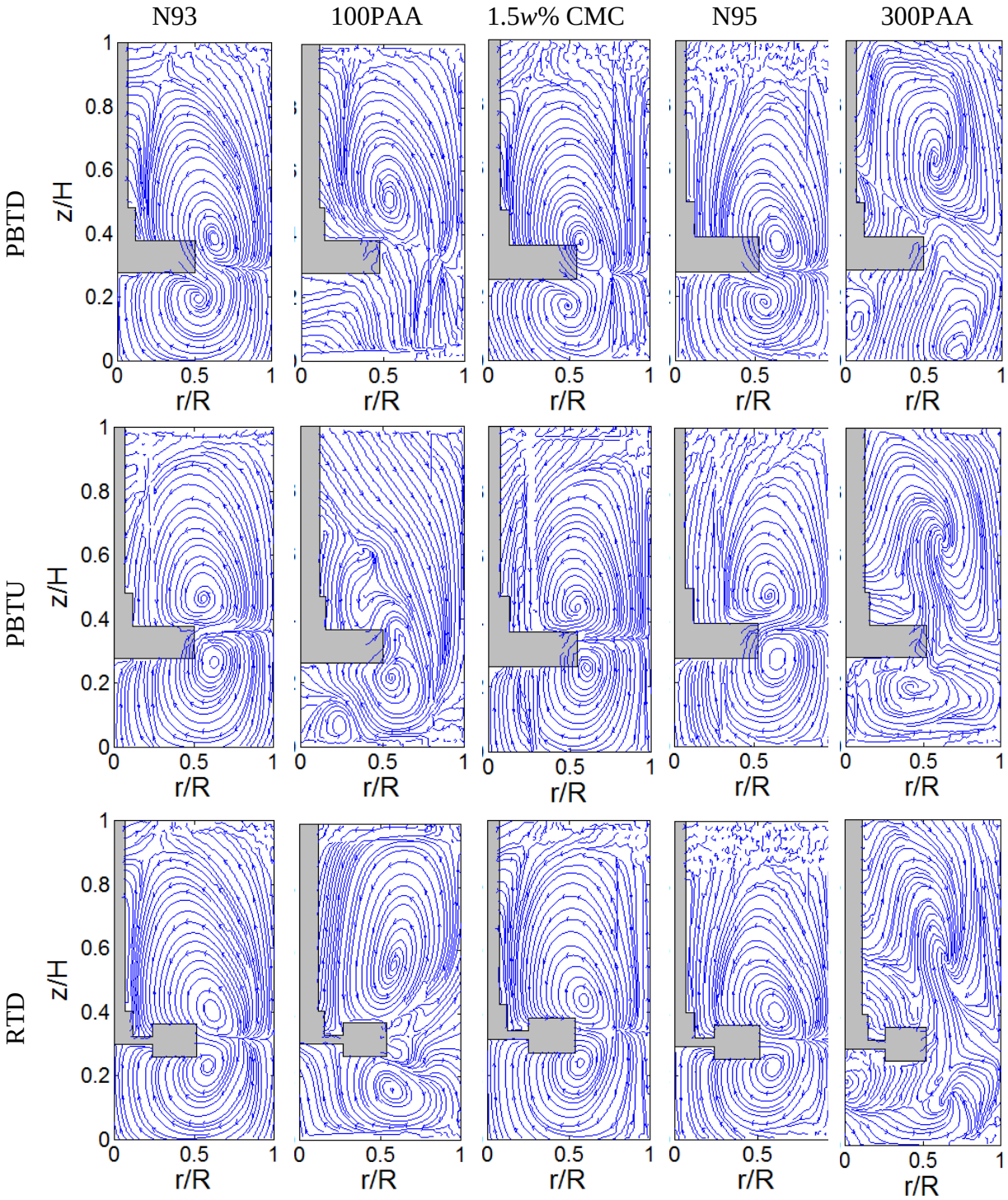

Figure 5.14. The streamline plots for all test fluids used in this study at Re_{PL} = 45 under three impeller configurations.

5.4.4 Pseudo-Caverns

In shear-thinning fluids the impeller induces a high shear on the fluid close to the impeller area, causing the viscosity of the fluid in this area to be significantly reduced compared to that of the fluid further away from the impeller. This phenomenon causes the formation of a pseudo-cavern in the fluid. The fluid outside of the pseudo-cavern is in very slow motion compared to the fluid inside the pseudo-cavern. Such pseudo-cavern formations can also be present in highly viscous Newtonian fluids (Chung, 2008). A velocity threshold of $u_{rz} = 0.01u_{tip}$, as proposed by (Hall et al., 2005), is used in this thesis to define the boundary of the pseudo-cavern for all fluids under investigation in this work.

The results from the PIV data show that pseudo-caverns can also occur in viscoelastic fluids such as Boger fluids (**Figure 5.15)**. Variations of cavern size for varying *Re* are presented in Table 5.8. Increasing the Reynolds number from Re_{PL} = 7 to Re_{PL} = 45 showed an increse of the ratio of pseudo-cavern area to tank area, A_C/A_T *%*. Increasing *Re* from 45 to 80 did not seem to have a major impact on the pseudo-cavern size. The exception to the aforementioned trends was the Boger fluid, whereby the area of the pseudo-cavern for this fluid in the PBTD impeller configuration remained constant at all three *Re* values.

Table 5.8. Ratio of pseudo-cavern area to tank area (A_C/A_T) *%* for the test fluids N93 and 100PAA

A_C/A_T *%*	N95			1.5*w*% CMC			300 Boger		
	PBTD	PBTU	RTD	PBTD	PBTU	RTD	PBTD	PBTU	RTD
Re = 7	72%	76%	59%	61%	73%	72%	60%	62%	53%
Re = 45	78%	82%	76%	70%	86%	79%	60%	67%	66%
Re = 80	79%	84%	81%	70%	87%	80%	60%	68%	67%

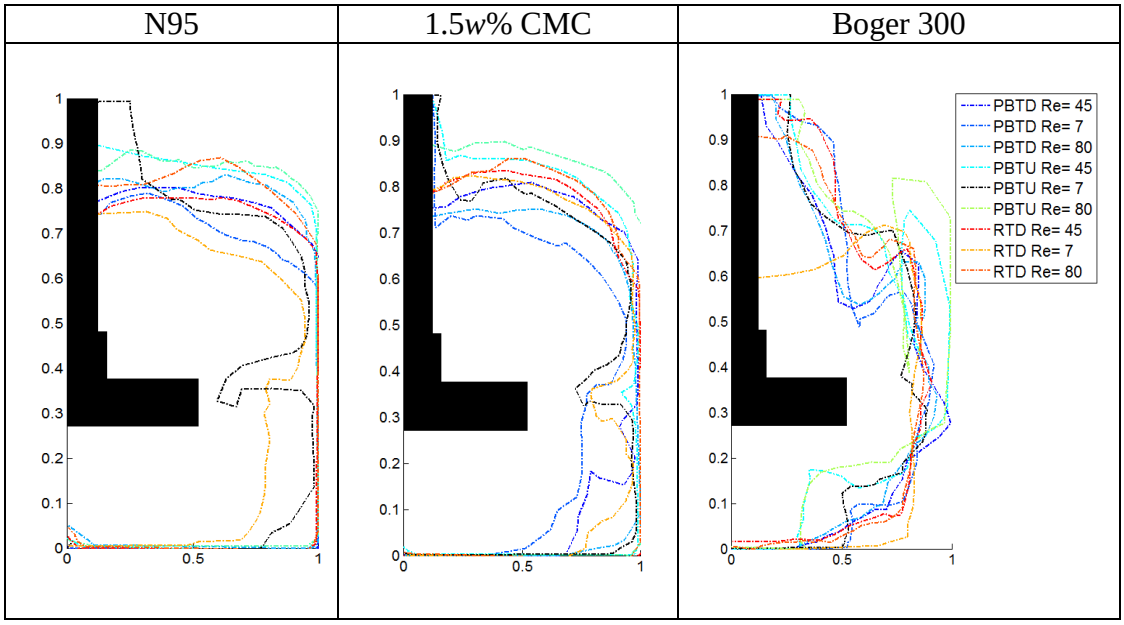

Figure 5.15. Pseudo-cavern boundaries for different impellers at three flow regimes: Re_{PL} = 7, Re_{PL} = 45, and Re_{PL} = 80.

5.4.5 Conclusions

By using two viscoelastic Boger fluids that exhibited different elasticity and constant viscosity, the effect of viscoelasticity on the flow fields of such viscoelastic fluids was investigated in a stirred tank. Two viscous Newtonian fluids and a shear-thinning fluid were used to identify the effect of elasticity on fluid mixing. The Particle Image Velocimetry (PIV) technique was employed in this study.

The results show a significant change in flow pattern of a Boger fluid compared to that of the Newtonian and shear-thinning fluids. The flow patterns in the viscoelastic fluid were highly dependent on the elasticity of the liquids, which was characterized by dimensionless number *Wi* (elasticity force/viscous forces) and the range of operation *Re*

(inertial force/viscous force). The dimensionless Elastic Number ($El=Wi/Re$) was applied to charcterize the strength of the fluid elasticity in a stirred tank and it was able to identify whether the flow was driven by inertia or elastic forces for each experimental condition. The Boger fluid 100PAA at a high Reynolds number of Re_{PL} = 80, with low elasticity (El = 0.019) and under the PBTD impeller configuration showed an anti-clockwise circulation loop above the impeller, similar to that seen in the examined Newtonian and shear-thinning fluids. However, under the PBTU configuration, the elasticity of the Boger fluid 100PAA caused the flow circulation loop to become reversed above and below the impeller. Under the RTD configuration the flow pattern of 100PAA broke into two regions. The flow close to the impeller area formed two circulation loops above and below the impeller, with a second reversed circulation loop being formed away from impeller. The formation of this second loop is undesirable as it leads to the reduction of mixing efficiency.

At lower flow regimes (Re_{PL} = 45, Re_{PL} = 7) the viscoelastic fluid behaves like the Newtonian fluid N93 and the shear-thinning fluid 1.5w% CMC under the RTD and PBD impeller configurations. The highly viscoelastic Boger fluid 300PAA revealed flow reversal in both circulations, below and above the impeller within the stirred tank, at all three flow regimes and under all three impeller types of this study. In this case, the elasticity force produced by the shearing flow is higher than the force due to fluid inertia, leading to a reversal of flow direction. The flow velocity is mostly in the tangential direction, and the time-averaged mean velocity acquired from the PIV data hardly reached $u_{rz} = 0.2\ U_{tip}$ in the 300PAA Boger fluid.

Chapter 6

CONCLUSIONS AND FUTURE WORK

The detailed conclusions for the work presented in this thesis can be found at the end of each results chapter. This final chapter presents a summary of the overall conclusions and also recommendations for further research in this area.

6.1 Conclusions

The rheological effects of complex fluids on mixing in a mechanically agitated stirred vessel were investigated by use of a two-dimensional visualisation technique. 2D Particle Image Velocimetry (PIV) was employed to characterize the flow fields of a thixotropic fluid and viscoelastic fluids under laminar and transitional regimes at three different Reynolds number. The Planar Laser Induced Fluorescence (PLIF) visualization technique was also applied to the thixotropic fluid in order to investigate in more detail the evolution of the cavern formation and mixing with time. Three different types of impeller were investigated in this study: Rushton turbine (RTD), and Pitch Blade Turbine (PBT) in up pumping mode (PBTU) and in down pumping mode (PBTD).

6.1.1 Effect of Thixotropy on Fluid Mixing in a Stirred Tank

The effects of time dependency were investigated for the mixing of a thixotropic liquid in a stirred vessel. To investigate only the effect of thixotropy on mixing, other rheological variables were fixed by choosing a time-independent reference fluid that had the same rheological properties as that of the thixotropic fluid, here being a transparent colloidal dispersion of 2.2*w*% Laponite. The reference fluid used in this work was a 1*w*%

Carbopol aqueous solution, a time-independent, shear-thinning fluid with a yield stress. Flow fields, flow patterns, normalized mean velocity and cavern growth in the vessel were characterized during mixing for the thixotropic fluid and the results were compared to the reference fluid under laminar and transitional regimes at three different Reynolds number (7, 61 and 158). The mixing efficiency of the impellers was analyzed in terms of size and growth of a cavern over time and impeller pumping efficiency. Mixing was performed for 300s.The results show that for both PBTD and PBTU the flow developed with time and reached a steady state condition almost in the middle of stirring (at t =138s). For the RTD impeller, the flow fields of the thixotropic fluid reached the steady state condition early, within t = 14s of mixing. Furthermore, the presence of baffles within the stirring vessel was also investigated for three impellers (PBTU, PBTD, and RTD). For the thixotropic fluid in a baffled vessel, the cavern size become larger and improved flow fields were obtained compared to an un-baffled case at Re_{HB} =158. For the viscoplastic fluid, the conventional baffled vessel reduced the mixing efficiency by minimizing cavern size and flow velocity. To conclude, at Re_{HB} =158 in a baffled vessel the yield stress and apparent viscosity of the studied thixotropic fluid appeared to decline with time during stirring, indicating that the energy supplied to the fluid is mostly consumed to divert the flow from a tangential direction to an axial one. For the viscoplastic fluid, the yield stress acted as a barrier to the fluid momentum.

6.1.2 The Effect Of Viscoelasticity In a Stirred Tank

The mixing of viscoelastic fluids is commonly carried out in stirred tanks in many industrial processes. To investigate the effect of viscoelasticity on mixing, a model fluid called Boger was used in this study. This model fluid exhibited constant viscosity over

shear, and was prepared by adding polyacrylamide to a viscous, Newtonian fluid. Hence, the effect of viscoelasticity can be studied in the absence of other rheological behaviors of most viscoelastic fluids, such as e.g. shear-thinning. The results were compared with those of a shear-thining fluid, 1.5w% CMC, and viscous Newtonian fluids (glycerin-water mixes), under laminar and transition regimes at three different Reynolds number (7, 45 and 80) for three type of impellers (PBTU, PBTD, and RTD).

The 2D Particle Image Velocimetry (PIV) technique was used to measure the flow velocity of the viscoelastic fluid in the mechanically agitated vessel. The flow patterns for this fluid were highly dependent on the elasticity of the liquid, the latter of which which was characterized by the dimensionless parameter called the elasticity force, *Wi*, and also by the range of operation, *Re* (inertial force/viscous force). The impeller type also impacts on the flow behaviour of a viscoelastic Boger fluid with low elasticity. Moreover, a different flow pattern was observed for each impeller and flow regime. However, for a viscoelastic Boger fluid with high elasticity a flow reversal was observed at the three flow regimes and for all three impeller types.

6.2 Future work

In this work, the effect of thixotropy on mixing in stirred vessel was investigated for a single phase fluid. In a thixotropic fluid the cavern grows with time and even at high transition Reynold's number the cavern completely fills the vessel, as opposed to what happesn with a time-independent fluid with yield stress. As such it is worth investigating the effect of particle suspensions in mixing of thixotropic fluids with different solid concentrations and compare results to a reference fluid, both experimentally and numerically. In addition, the same can be done for particle suspensions in viscoelastic

Boger fluids, owing to the fact that particle suspensions within such fluids are commonly observed in industrial mixing processes.

The behaviour of the viscoelastic Boger fluids used in the work presented here was investigated with the 2D PIV visualisation technique, in order to better understand the effect of viscoelasticity on mixing in a stirred vessel. As the flow of such fluids is observed moving extremely in the tangential direction, it is worth using a non-invasive technique (such as PEPT) for the analysis of a full 3D velocity field. Fianlly, the capability of modeling suspensions of particles in viscoelastic Boger fluids can be assessed in comparison with the PEPT and PIV measurements.

REFERENCES

Adams, L., Chiti, F., Guida, A., Jaffer, S., Nienow, A.W. and Barigou, M. (2008), Positron emission particle tracking caverns formed during mixing of an industrial slurry, Proceedings of International Symposium on Mixing in Industrial Processes VI, Niagara on the Lake, Niagara Falls, Ontario, Canada, Aug, 17-21.

Adams, L.W. (2009), Experimental and computational study of non-turbulent flow regimes and cavern formation of non-Newtonian fluids in a stirred tank, Ph.D. Thesis, University of Birmingham.

Adams, L.W. and Barigou, M. (2007), CFD analysis of caverns and pseudo-caverns developed during mixing of non-Newtonian fluids, Chemical Engineering Research and Design, 85 (A5), 598-604.

Adrian, R.J. (1991), Particle-Imaging Techniques for Experimental Fluid-Mechanics, Annu Rev Fluid Mech, 23(21), 261-304.

Alvarez-Hernández, M.M., Shinbrot, T., Zalc, J. and Muzzio, F.J. (2002), Practical chaotic mixing, Chem Eng Sci, 57(17), 3749-3753.

Amanullah, A., Hjorth, S.A., Nienow, A.W., (1997), Cavern sizes generated in highly shear thinning viscous fluids by SCABA 3SHP1 impellers, Transactions I.Chem.E. 75(C), 232-238.

Amanullah, A. H., S. A; Nienow, A.W. 1998. A new mathematical model to predict cavern dimaters in highly shear thining power law liquids using axial flow impellers. Chemical Enqmeering Science, 53.

Ameur, H. and Bouzit, M. (2012), Mixing in shear thinning fluids, Brazilian Journal Chemical Engineering, 29 (2), 349-358.

Ameur, H., Bouzit, M. and Helmaoui, M. (2011), Numerical study of fluid flow and power consumption in a stirred vessel with a SCABA 6SRGT impeller, Chemical Process Engineering, 32 (4), 351-366.

Armenante, P. M. and Nagamine, E. U. (1998), Effect of low off-bottom impeller clearance on the minimum agitation speed for complete suspension of solid in stirred tanks. Chemical Engineering Science, 53, 1757-1775.

Armenante, P.M., Luo, C.G., Chou, C.C., Fort, I. and Medek, J. (1997), Velocity profiles in a closed, unbaffled vessel: comparison between experimental LDV data and numerical CFD predictions, Chem Eng Sci, 52(20), 3483-3492.

Arratia, P. E., Kukura, J., Lacombe, J. & Muzzio, F. J. 2006. Mixing of shear-thinning fluids with yield stress in stirred tanks. AIChE Journal, 52**,** 2310-2322.

Aubin, J., Fletcher, D. F. and Xuereb, C. (2004), Modeling turbulent flow in stirred tank with CFD: the influence of the modelin approach, turbulence model and numerical scheme, Experimental Thermal and Fluid Science, 28, 431-445.

Aubin, J., Le Sauze, N., Bertrand, J., Fletcher, D.F. and Xuereb, C. (2004), PIV measurements of flow in an aerated tank stirred by a down- and an up-pumping axial flow impeller, Exp Therm Fluid Sci, 28(5), 447-456.

Aubin, J., Naude, I., Bertrand, J. and Xuereb, C. (2000), Blending of Newtonian and shear-thinning fluids in a tank stirred with a helical screw agitator, Chemical Engineering Research and Design, Trans IChenE, 78 (A8), 1105-1114.

Baird, Donald G. (2011). Flow behavior of viscoelastic fluids. In AccessScience. McGraw-Hill Education.

Bakker, A., Myers, K.J., Ward, R.W. and Lee, C.K. (1996), The laminar and turbulent flow pattern of a pitch blade turbine, Chemical Engineering Research and Design, 74 (A), 485-491.

Baldi, S. and Yianneskis, M. (2003), On the direct measurement of turbulence energy dissipation in stirred vessels with PIV, Industrial & Engineering Chemistry Research, 42, 7006-7016.
Barigou, M. (2004), Particle tracking in opaque mixing systems: An overview of the capabilities of PET and PEPT, Chem Eng Res Des, 82(A9), 1258-1267.

Barigou, M., Chiti, F., Pianko-Oprych, P., Guida, A., Adams, L.; Fan, X., Parker, D. J. and Nienow, A. W. (2009), Using Positron Emission Particle Tracking (PEPT) to study mixing in stirred vessels: validation and tackling unsolved problems in opaque systems. Journal of Chemical Engineering of Japan, 42, 829-846.

Barnes, H. (1997). Thixotropy—a review. Journal of Non-Newtonian Fluid Mechanics, 70(1-2), pp.1-33.

Barnes, H.A.; Hutton, J.F. and Walters, K. (1988) An introduction to rheology. Elsevier.

Brito-de la Fuente E., Choplin, L. and Tanguy, P. A. (1997), Mixing with helical ribbon impellers: effect of highly shear thinning behaviour and impeller geometry, Transaction IChemE, **75** (A), 45-52.

Bujalski, W., Nienow, A.W. and Liu, H.X. (1990), The Use of Upward Pumping 45-Degrees Pitched Blade Turbine Impellers in 3-Phase Reactors, Chem Eng Sci, 45(2), 415-421.

Boger, D. V. & Nguyen, H. 1978. A model viscoelastic fluid. Polymer Engineering & Science, 18**,** 1037-1043.

Bonn, D., Tanase, S., Abou, B., Tanaka, H. & Meunier, J. 2002. Laponite: Aging and Shear Rejuvenation of a Colloidal Glass. Physical Review Letters, 89.

Cabaret, F., Bonnot, S., Fradette, L. and Tanguy, P.A. (2007), Mixing time analysis using colorimetric methods and image processing, Ind Eng Chem Res, 46(14), 5032-5042.

Choplin, L. & Carreau, P. J. 1986. End effects for highly elastic-constant viscosity fluids. Rheologica Acta, 25**,** 95-101.

Chung, K.H.K. (2008), Mixing in high throughput experimentation reactors, Ph.D. Thesis, University of Birmingham.

Chung, K.H.K., Barigou, M. and Simmons, M.J.H. (2007), Reconstruction of 3-D flow field inside miniature stirred vessels using a 2-D PIV technique, Chemical Engineering Research and Design, 85 (A5), 560-567.

Chung, K.H.K., Simmons, M.J.H. and Barigou, M. (2009), Angle-resolved Particle Image Velocimetry measurements of flow and turbulence fields in small-scale stirred vessels of different mixer configurations, Ind Eng Chem Res, 48(2), 1008-1018.

Cronin, D.G., Nienow, A.W. and Moody, G.W. (1994), An experimental study of the mixing in a protofermenter agitated by dual Rushton turbines, Food Bioprod Process, 72(C1), 35-40.

Collias, D. J. & Prud'homme, R. K. 1985. The effect of fluid elasticity on power consumption and mixing times in stirred tanks. Chemical Engineering Science, 40**,** 1495--1505.

Couerbe, G., Fletcher, D. F., Xuereb, C. & Poux, M. 2008. Impact of thixotropy on flow patterns induced in a stirred tank: Numerical and experimental studies. Chemical Engineering Research and Design, 86**,** 545-553.

Coussot, P., Leonow, A. I. & Piau, J. M. 1993. Rheology of concentrated dispersed systems in a low molecular weight matrix. Journal of Non-Newtonian Fluid Mechanics, 46**,** 179-217.

Coussot, P., Nguyen, Q. D., Huynh, H. T. & Bonn, D. 2002. Avalanche Behavior in Yield Stress Fluids. Physical Review Letters, 88.

Cutter, L.A. (1966), Turbulence: The filtering approach, Journal of Fluid Mechanics, 238, 325-336.

Derksen, J. J. 2010. Agitation and mobilization of thixotropic liquids. AIChE Journal, 56(9), 2236-2247.

Edwards, M.F., Baker, M.R. and Godfrey, J.C. (1997), Laminar flow and distributive mixing, in: Harnby, N., Edwards, M.F., Nienow, A.W. (Eds), Mixing in the process industries, Butterworth-Heinemann: Oxford. Chapter 11, 200-224.

Ein-Mozaffari, F., Upreti, S.R. (2009), Using ultrasonic Doppler velocimetry and CFD modelling to investigate the mixing of non-Newtonian fluid possessing yield stress, Chemical Engineering Research and Design, 87, 515-523.

Escudié, R. and Liné, A. (2006), Analysis of turbulence anisotropy in a mixing tank, Chemical Engineering Science, 61 (9), 2771-2779.

Escudie, R., Bouyer, D., Line, A., 2004. Characterization of trailing vortices generated by a Rushton turbine. A.I.Ch.E. Journal 50, 75.

Fairhurst, P.G., Barigou, M., Fryer, P.J., Pain, J-P., Parker, D.J., (2001), Using positron emission particle tracking (PEPT) to study nearly neutrally buoyant particles in high solid fraction pipe flow, International Journal of Multiphase Flow, 27, 1881-1901.

Fangary, Y.S., Barigou, M., Seville, J.P.K. and Parker, D.J. (2000), Fluid trajectories in a stirred vessel of non-Newtonian liquid using Positron Emission Particle Tracking, Chemical Engineering Science, 55 (24), 5969-5979.

Fangary, Y.S., Barigou, M., Seville, J.P.K. and Parker, D.J. (2002), A Lagrangian study of solids suspension in a stirred vessel by Positron Emission Particle Tracking (PEPT), Chemical Engineering Technology, 25 (5), 521-528.

Fangary, Y.S., Seville, J.P.K. and Barigou, M. (1999), Flow studies in stirred tanks by positron emission particle tracking (PEPT), Institution of Chemical Engineers Symposium Series, 146, 23-24.

Gabriele, A., Nienow, A.W. and Simmons, M.J.H. (2009), Use of angle resolved PIV to estimate local specific energy dissipation rates for up- and down-pumping pitched blade agitators in a stirred tank, Chem Eng Sci, 64(1), 126-143.

Galindo, E. and Nienow, A. W. (1992), Mixing of highly viscous simulated Xanthan fermentation broths with the Lightinin A-315 impeller, Biotechnology Progress, 8, 233-239.

Galletti, C., Paglianti, A., Yianneskis, M., (2005), Observations on the significance of instabilities turbulence and intermittent motions on the fluid mixing processes in stirred reactors, Chemical Engineering Science, 60, 2317-2331.

Guida, A. (2010), Positron emission particle tracking applied to solid-liquid mixing in mechanically agitated vessels, Ph.D. Thesis, University of Birmingham.

Guida, A., Nienow, A. W. & Barigou, M. 2010. The effects of the azimuthal position of the measurement plane on the flow parameters determined by PIV within a stirred vessel. Chemical Engineering Science, 65**,** 2454-2463.

Guillard, F., Trägärdh, C. and Fuchs, L. (2000), A study of turbulent mixing in a turbine-agitated tank using a fluorescence technique, Experiments in Fluids, 28, 225-235.

Gunkel, A.A., Weber, M.E., 1975, Flow phenomena in stirred tanks, Part I. The impeller stream, A.I.Ch.E. Journal, 21(5), 931-948.

Hall, J.F., Barigou, M., Simmons, M.J.H. and Stitt, E.H. (2005a), Just because it's small doesn't mean it's well mixed: Ensuring good mixing in mesoscale reactors, Ind Eng Chem Res, 44(25), 9695-9704.

Hall, J.F., Barigou, M., Simmons, M.J.H. and Stitt, E.H. (2005b), Comparative study of different mixing strategies in small high throughput experimentation reactors, Chem Eng Sci, 60(8-9), 2355-2368.

Hall, J. J. 2005. Study of viscous and viscoelastic flows with reference to laminar stirred vessels. Ph.D. Thesis, University of London.

Hirata, Y. & Aoshima, Y. 1996. Formation and growth of cavern in yield stress fluids agitated under baffled and non-baffled conditions. Chemical engineering research & design, 74**,** 438-444.

James, D. F. 2009. Boger Fluids. Annual Review of Fluid Mechanics, 41**,** 129--142.

Jaworski, Z., Nienow, A.W., Koutsakos, E., Dyster, K. and Bujalski, W. (1991), An LDA study of turbulent flow in a baffled vessel agitated by a pitched blade turbine, Chemical Engineering Research and Design, 64 (A4), 313-320.

Khan, F. R. 2005. Investigation of turbulent flows and instabilities in a stirred vessel using particle image velocimetry, Ph.D. Thesis, Loughborough University.

Khan, F. R., Rielly, C. D. and Hargrave, G. D. (2004), A multi-block approach to obtain angle-resolved PIV measurements of the mean flow and turbulence fields in a stirred vessel, Chemical Engineering Technology, 27 (3), 264-269.

Khan, F.R., Rielly, C.D. and Brown, D.A.R. (2006), Angle-resolved stereo-PIV measurements close to a down-pumping pitched-blade turbine, Chemical Engineering Science, 61 (9), 2799-2806.

Kresta, S.M. and Wood, P.E. (1993), The flow field produced by a pitched blade turbine: characterization of the turbulence and estimation of the dissipation rate, Chemical Engineering Science, 48 (10), 1761–1774.

Kukura, J., Arratia, P.C., Szalai, E.S., Bittorf, K.J. and Muzzio, F.J. (2002), Understanding pharmaceutical flows, Pharmaceutical Technology, 48-72.

Lim, K. S. 2005. Studies of foam microstructure and rheology, Ph.D. Thesis, The University of Birmingham.

Liu, L. 2013. Computatinal fluid dynamics modeling of complex fluid flow in stirred vessels, Ph.D. Thesis, The University of Birmingham.

Lourenco, L.M., Krothopalli, A. and Smith, C.A. (1989), Particle image velocimetry, in: Gad-el-Hak, M. (Ed), Advances in fluid mechanics measurement, Springer-Verlag: Berlin. Chapter 4, 128-199.

Mackay, M. E. & Boger, D. V. 1987. An explanation of the rheological properties of Boger fluids. Journal of Non-Newtonian Fluid Mechanics, 22**,** 235-243.

Magda, J. J., Lou, J., Baek, S. G. & Devries, K. L. 1991. Second normal stress difference of a Boger fluid. Polymer, 32**,** 2000--2009.

Maingonnat, J.F., Muller, L., Leuliet, J.C., (2005), Modelling the build-up of a thixotropic fluid under viscosimetric and mixing conditions, Journal of Food Engineering, 3, 265-272.

Mavros, P., Xuereb, C. and Bertrand, J. (1996), Determination of 3-D flow fields in agitated vessels by laser-Doppler velocimetry: Effect of impeller type and liquid viscosity on liquid flow patterns, Chem Eng Res Des, **74**(A6), 658-668.

Mavros, P., Xuereb, C. and Bertrand, J. (1998), Determination of 3-D flow fields in agitated vessels by laser-Doppler velocimetry: Use and interpretation of RMS velocities, Chem Eng Res Des, **76**(A2), 223-233.

Metzner, A.B. and Otto, R.E. (1957), Agitation of Non-Newtonian Fluids, AIChE J, 3(1), 3-10.

Micheletti, M. and Yianneskis, M. (2004), Study of fluid velocity characteristics in stirred solid-liquid suspensions with a refractive index matching technique, Proceedings of the Institution of Mechanical Engineers, 218, 191-204.

Montante, G., Lee, K. C., Brucato, A. and Yianneskis, M. (1999), Double to single loop flow pattern transition in stirred vessels, The Canadian Journal of Chemical Engineering, 77, 649-659.

Montante, G., Paglianti, A. and Magelli, F. (2012), Analysis of dilute solid-liquid suspensions in turbulent stirred tanks, Chemical Engineering Research and Design, 90 (10), 1448-1456.

Nienow, A.W. (1968), Suspension of Solid Particles in Turbine Agitated Baffled Vessels, Chem Eng Sci, 23(12), 1453-1459.

Nienow, A.W. (1997a), On impeller circulation and mixing effectiveness in the turbulent flow regime, Chemical Engineering Science, 52 (15), 2557-2565.

Nienow, A.W. (1997b), The suspension of solids particles, in: Harnby, N., Edwards, M.F., Nienow, A.W. (Eds), Mixing in the process industries, Butterworth-Heinemann: Oxford. Chapter 16, 364-394.

Nouri, J. M. & Whitelaw, J. H. 1990. Flow characteristics of stirred reactors with newtonian and non-newtonian fluids. AIChE Journal, 36**,** 627-629.

Ochieng, A., Onyango, M.S., Kumar, A., Kiriamiti, K. and Musonged, P. (2008), Mixing in a tank stirred by a Rushton turbine at a low clearance, Chemical Engineering and Processing, 47, 842-851.

Özcan-Taskin, N. Gul (1993), On the Effects of Viscoelasticity in Stirred Tanks Ph.D. Thesis, University of Birmingham.

Özcan-Taskin, N. Gul, AW Nienow (1995), Mixing viscoelastic fluids flow with axial 'impellers: flow fields and power consumption, Food and Bioproducts Processing, 73**,** 49-56.

Papadopoulos, G. and Arik, E.B. (2004), Experimental Methods: Fundamental Flow Measurement, in: Paul, E.L., Atiemo-Obeng, V.A. and Kresta, S.M. (Eds), Handbook of industrial mixing: Science and practice, Wiley- Interscience: Hoboken, NJ. Chapter 4B, 202-256.

Parker, D.J., Broadbent, C.J., Fowles, P., Hawkesworth, M.R. and Mcneil, P. (1993), Positron Emission Particle Tracking - A technique for studying flow within engineering equipment, Nucl Instrum Methods Phys Res A, 326(3), 592-607.

Parker, D.J., Forster, R.N., Fowles, P. and Takhar, P.S. (2002), Positron Emission Particle Tracking using the new Birmingham positron camera, Nucl Instrum Methods Phys Res A, 477(1-3), 540-545.

Paul, E. L., Atiemo-Obeng, V. A. and Kresta, S. M. (2004), Hand book of industrial mixing: Science and practice, Wiley-Interscience: Hoboken, NJ.

Peters and Smith, (1962). Chemical Engineering Journal, Volume 8, pp-83.

Pianko-Oprych, P., Nienow, A.W. and Barigou, M. (2009), Positron emission particle tracking (PEPT) compared to particle image velocimetry (PIV) for studying the flow generated by a pitched-blade turbine in single phase and multi-phase systems, Chemical Engineering Science, 64 (23), 4955–4968.

Prajapati, P. and Ein-Mozaffari, F. (2009), CFD investigation of the mixing of yield-pseudoplastic fluid with anchor impeller, Chemical Engineering, Tecnology, 32 (8), 1211-1218.

Prilutski, G., Gupta, R. K., Sridhar, T. & Ryan, M. E. 1983. Model viscoelastic liquids. Journal of Non-Newtonian Fluid Mechanics, 12**,** 233-241.

Pryce-Jones, (1934, 1836, 1943). Journal of the Oil and Colour Chemists' Association. Wembley, Middlesex, 17 (1934) 305; 19 (1936) 395; 26 (1943) 3.

Rice, M., Hall, J., Papadakis, G. & Yianneskis, M. 2006. Investigation of laminar flow in a stirred vessel at low Reynolds numbers. Chemical Engineering Science, 61**,** 2762-2770.

Rutherford, K., Mahmoudi, S.M.S., Lee, K.C. and Yianneskis, M. (1996), The influence of Rushton impeller blade and disk thickness on the mixing characteristics of stirred vessels, Chemical Engineering Research and Design, 74 (A), 369-378.

Sano, Y. and Usui, H. (1985), Interrelations among mixing time, power number and discharge flow rate number in baffled mixing vessels, Journal of Chemical Engineering of Japan, 18 (1), 47-52.

Seyssiecq, I. & Tolofoudy 2003. Viscoelastic Liquids in Stirred Vessels– Part I: Power Consumption in Unaerated Vessels. Chemical Engineering \& Technology, 26**,** 1155--1165.

Schäfer, M., Yianneskis, M., Wächter, P., Durst, F., 1998, Trailing vortices around a 45° Pithced-blade impeller, AIChE Journal, **44** (6), 1233-1246.

Scott-Blair, G.W. (1943) A Survey of General and Applied Rheology, London, Pitman.
Seitzman, J.M. and Hanson, R.K. "Planar Fluorescence Imaging in Gases," in Experimental Methods for Flows With Combustion ed. A. Taylor. Academic Press, London (1993).

Sharp, K. V. and Adrian, R. J. (2001), PIV study of small-scale flow structure around a Rushton turbine, Fluid Mechanics and Transport Phenomena, 47 (4), 766-778.

Sheng, J., Meng, H. and Fox, R.O. (1998), Validation of CFD simulations of a stirred tank using particle image velocimetry data, The Canadian Journal of Chemical Engineering, 76, 611-625.

Skelland A.H.P. (1967) Non-Newtonian flow and heat transfer. John Wiley and Sons Inc. New York.

Stokes, J. R. 1998. swirling flow of viscoelstic fluids. Doctor of Philosophy, University of Melbourne.

Stokes, J. R., Graham, L. J. W., Lawson, N. J. & Boger, D. V. 2001. Swirling flow of viscoelastic fluids. Part 1. Interaction between inertia and elasticity. Journal of Fluid Mechanics, 429**,** 67--115.

Ulbrecht, J.J. and Carreau, P. (1985) Mixing of viscous non-Newtonian liquids (in 'Mixing of liquids by mechanical agitation' Gordon and Breach, New York. eds. ULBRECHT, J.J. and G.K. PATTERSON) p: 93- 135.

Szalai, E.S., Arratia, P., Johnson, K. and Muzzio, F.J. (2004), Mixing analysis in a tank stirred with Ekato Intermid®impellers, Chemical Engineering Science, 59, 3793-3805.

Thyagaraja, A., Fletcher, D. and Cook, I. (1987). One-dimensional calculations of two-phase mixing flows. International Journal for Numerical Methods in Engineering, 24(2), pp.459-469.Turbine Impellers in 3-Phase Reactors, Chem Eng Sci, 45(2), 415-421.

Unadkat, H., Rielly, C.D. and Hargrave, G.K. (2009), Application of fluorescent PIV and digital image analysis to measure turbulence properties of solid-liquid stirred suspensions, Chemical Engineering Research and Design, 87 (4), 573-586.

Weissenberg, K. (1948), "Abnormal Substances and Abnormal Phenomena of Flow," Proc. of First Intl. Cong. Rheol., North Holland, Amsterdam, I29.

Whelan, T. (1994), Polymer Technology Dictionary, Chapman & Hall, London.
Willert, C.E. and Gharib, M. (1991), Digital Particle Image Velocimetry, Exp Fluids, 10(4), 181-193.

Wu, H. and Patterson, G. K. (1989), Laser-Doppler measurements of turbulent-flow parameters in a stirred mixer, Chemical Engineering Science, **44** (10), 2207-2221.

Yianneskis, M., Popiolek, Z. and Whitelaw, J. H. (1987), An experimental study of the steady and unsteady flow characteristics of stirred reactors, Journal of Fluid Mechanics, 175,537-555.

Zalc, J. M., Alvarez, M. M., Muzzio, F. J. and Arik, B. E. (2001), Extensive validation of computed laminar flow in a stirred tank with three Rushton turbines, AIChE Journal, 47 (10), 2145-2154.

Zalc, J. M., Alvarez, M. M., Muzzio, F. J. and Arik, B. E. (2001), Extensive validation of computed laminar flow in a stirred tank with three Rushton turbines, AIChE Journal, 47 (10), 2145-2154.

Zhou, G. and Kresta, S. M. (1996), Impact of geometry on the maximum turbulence energy dissipation rate for various impellers, AIChE Journal, 42, 2476-2490.

Zlokarnik, M. (2001), Stirring: Theory and practice, Wiley-VCH: Weinheim.